

AWARD NUMBER: W81XWH-18-1-0198

TITLE: Antibiotic Tolerance and Therapeutic Failure in Diabetic Infections

PRINCIPAL INVESTIGATOR: Dr. Peter Belenky

CONTRACTING ORGANIZATION: Brown University, Providence, RI

REPORT DATE: June 2021

TYPE OF REPORT: Annual

PREPARED FOR: U.S. Army Medical Research and Materiel Command
Fort Detrick, Maryland 21702-5012

DISTRIBUTION STATEMENT: Approved for Public Release; Distribution Unlimited

The views, opinions and/or findings contained in this report are those of the author(s) and should not be construed as an official Department of the Army position, policy or decision unless so designated by other documentation.

| REPORT DOCUMENTATION PAGE | | | | Form Approved OMB No. 0704-0188 | |
|---|---------------------------------|----------------------------------|--|--|--|
| Public reporting burden for this collection of information is estimated to average 1 hour per response, including the time for reviewing instructions, searching existing data sources, gathering and maintaining the data needed, and completing and reviewing this collection of information. Send comments regarding this burden estimate or any other aspect of this collection of information, including suggestions for reducing this burden to Department of Defense, Washington Headquarters Services, Directorate for Information Operations and Reports (0704-0188), 1215 Jefferson Davis Highway, Suite 1204, Arlington, VA 22202-4302. Respondents should be aware that notwithstanding any other provision of law, no person shall be subject to any penalty for failing to comply with a collection of information if it does not display a currently valid OMB control number. PLEASE DO NOT RETURN YOUR FORM TO THE ABOVE ADDRESS. | | | | | |
| 1. REPORT DATE June 2021 | | 2. REPORT TYPE. Annual | | 3. DATES COVERED 01Jun2020-31May2021 | |
| 4. TITLE AND SUBTITLE Antibiotic Tolerance and Therapeutic Failure in Diabetic Infections | | | | 5a. CONTRACT NUMBER W81XWH-18-1-0198 | |
| | | | | 5b. GRANT NUMBER W81XWH-18-1-0198 | |
| | | | | 5c. PROGRAM ELEMENT NUMBER | |
| 6. AUTHOR(S) Dr. Peter Belenky E-Mail: peter.belenky@brown.edu | | | | 5d. PROJECT NUMBER | |
| | | | | 5e. TASK NUMBER | |
| | | | | 5f. WORK UNIT NUMBER | |
| 7. PERFORMING ORGANIZATION NAME(S) AND ADDRESS(ES) Brown University Providence, RI 02912 | | | | 8. PERFORMING ORGANIZATION REPORT NUMBER | |
| 9. SPONSORING / MONITORING AGENCY NAME(S) AND ADDRESS(ES) U.S. Army Medical Research and Materiel Command Fort Detrick, Maryland 21702-5012 | | | | 10. SPONSOR/MONITOR'S ACRONYM(S) | |
| | | | | 11. SPONSOR/MONITOR'S REPORT NUMBER(S) | |
| 12. DISTRIBUTION / AVAILABILITY STATEMENT Approved for Public Release; Distribution limited | | | | | |
| 13. SUPPLEMENTARY NOTES | | | | | |
| 14. ABSTRACT An important health problem affecting veterans and Americans with type 2 diabetes is the high rate of diabetic foot infection (DFI) and is most often caused by the bacterium <i>Staphylococcus aureus</i> . For people with diabetes, these infections are harder to treat and often result in antibiotic therapeutic failure, which can lead to antibiotic resistance. We hypothesize that the metabolic state of the host can impact bacterial metabolism and contribute to altered antibiotic susceptibility in the microbiome and in diabetic foot infections (DFI). The goal of this project is to define the antibiotic response of the total microbiome in the gut as well as <i>S. aureus</i> in the hindfoot infection in hyperglycemic mice. Over the past year, we have made progress in writing up the results of Aim 2 of the proposal. This manuscript was submitted to <i>Cell Reports</i> , and we are in the process of conducting experiments and revisions requested by the reviewers and editor. This work outlines our data on the impact of hyperglycemia on the murine microbiome with and without antibiotic exposure. Our new data indicate that hyperglycemia predisposes the microbiome to antibiotic-induced perturbation as well as post-antibiotic colonization with enteric pathogens. During the remaining time of the NCE we aim to finalize revisions to the Cell Reports manuscript and resubmit. During the past year, we have also published a related article in <i>MSystems</i> . | | | | | |
| 15. SUBJECT TERMS Microbiome, hyperglycemia, infection, diabetic foot infection, staphylococcus aureus, antibiotic, antibiotic resistance, and dysbiosis. | | | | | |
| 16. SECURITY CLASSIFICATION OF: U | | | 17. LIMITATION OF ABSTRACT Unclassified | 18. NUMBER OF PAGES 126 | 19a. NAME OF RESPONSIBLE PERSON USAMRMC |
| a. REPORT Unclassified | b. ABSTRACT Unclassified | c. THIS PAGE Unclassified | | | 19b. TELEPHONE NUMBER (include area code) |

Table of Contents

| | <u>Page</u> |
|---|-------------|
| 1. Introduction..... | 3 |
| 2. Keywords..... | 3 |
| 3. Accomplishments..... | 3 |
| 4. Impact..... | 5 |
| 5. Challenges/Problems | 5 |
| 6. Products | 6 |
| 7. Participants & other collaborating organizations..... | 6 |
| 8. Special reporting requirements | 7 |
| 9. Appendices..... | 7 |

1. INTRODUCTION:

An important health problem affecting veterans and Americans with type 2 diabetes is the high rate of diabetic foot infection (DFI) and is most often caused by the bacterium *Staphylococcus aureus*. For people with diabetes, these infections are harder to treat and often result in antibiotic therapeutic failure, which can lead to antibiotic resistance. We hypothesize that the metabolic state of the host can impact bacterial metabolism and contribute to altered antibiotic susceptibility in the microbiome and in diabetic foot infections (DFI). The goal of this project is to define the antibiotic response of the total microbiome in the gut as well as *S. aureus* in the hindfoot infection in hyperglycemic mice. Over the past year, we have made progress in writing up the results of Aim 2 of the proposal. This manuscript was submitted to *Cell Reports*, and we are in the process of conducting experiments and revisions requested by the reviewers and editor. This work outlines our data on the impact of hyperglycemia on the murine microbiome with and without antibiotic exposure. Our new data indicate that hyperglycemia predisposes the microbiome to antibiotic-induced perturbation as well as post-antibiotic colonization with enteric pathogens. During the remaining time of the NCE we aim to finalize revisions to the Cell Reports manuscript and resubmit. During the past year, we have also published a related article in *MSystems*.

2. KEYWORDS:

Microbiome, hyperglycemia, infection, diabetic foot infection, staphylococcus aureus, antibiotic, antibiotic resistance, and dysbiosis.

3. ACCOMPLISHMENTS:

- **What were the major goals of the project?**
 - We proposed to study the impacts of host hyperglycemia on antibiotic efficacy in pathogenic bacteria and the microbiome. This work is vital to understanding the high rate of infections and therapeutic failure among patients with diabetes mellitus, particularly diabetic veterans.
 - **Aim 1)** Determine the impacts of induced hyperglycemia on pathogen killing by bactericidal antibiotics and relate these results to the activity of metabolism-based tolerance mechanisms. This aim is divided into two parts Aim 1A and Aim 1B. The goal of Aim 1A is to utilize a bioluminescent strain of *S. aureus* to determine the impacts of hyperglycemia on antibiotic mediated clearance of a DFI infection while the goal for Aim 1B is to use a Tn-Seq library in *S. aureus* to identify genes responsible for hyperglycemia-induced tolerance.
 - **Aim 2)** Determine the impacts of induced hyperglycemia on the composition of the murine gut microbiome and its functional response to bactericidal antibiotics.
 - In addition, we proposed to submit an R01 at the one-year mark to continue funding of this project.
- **What was accomplished under these goals?**
 - Aim 1) During earlier cycles we reported significant progress on Aim 1; thus, in this past year of the work we have mostly focused on writing up the microbiome work completed for Aim 2.

- Aim 2) We have generated data that indicates that hyperglycemia impacts the structure of the microbiome and its response to amoxicillin (AMX). We also conducted metagenomics, metatranscriptomics, and metabolomics that link these taxonomic impacts to functional responses and metabolite availability during STZ induce hyperglycemia.
- In addition, our data indicated that after antibiotic treatment STZ mice have an overabundance of ethanolamines, that past studies have associated with *Salmonella* colonization susceptibility. To test if these conditions predispose mice to colonization STZ-treated and normoglycemic mice were challenged with *Salmonella enterica* serovar Typhimurium at infective doses between 1×10^2 and 1×10^6 colony forming units. We found that STZ treatment both lowered the threshold required to establish infection after AMX treatment and worsened disease outcomes as measured by lethality. Specifically, at all tested infection doses, hyperglycemia increased lethality by day 7 and significantly increases the total pathogenic load within the intestines.
- Over the past year, we have made progress in writing up the results of Aim 2 of the proposal. This manuscript was submitted to *Cell Reports*, and we are in the process of conducting experiments and revisions requested by the reviewers and editor. The initial submission is included in the appendix of this report. This work outlines our data on the impact of hyperglycemia on the murine microbiome with and without antibiotic exposure. Our new data indicate that hyperglycemia predisposes the microbiome to antibiotic-induced perturbation as well as post-antibiotic colonization with enteric pathogens. During the remaining time of the NCE we aim to finalize revisions to the Cell Reports manuscript and resubmit. During the past year, we have also published a related article in *MSystems*.

What opportunities for training and professional development has the project provided?

- "Nothing to Report."
- How were the results disseminated to communities of interest?

Publications

1. Cabral D.J, Wurster J.I, Korry B.J, Penumutthu S., **Belenky P.** "Consumption of a Western-Style Diet Modulates the Response of the Murine Gut Microbiome to Ciprofloxacin". **mSystems**. (2020) Jul 28;5(4):e00317-20. doi: 10.1128/mSystems.00317-20. PMID: 32723789; PMCID: PMC7394352 (Research paper)

Presentations describing this work

1. 2020 "Microbial Metabolism is a Determinant of Antibiotic-induced Disruption of the Gut Microbiome" **Microbiology and Immunology Dartmouth Medical School**, Hanover, NH
2. 2020 "Microbial Metabolism is a Determinant of Antibiotic-induced Disruption of the Gut Microbiome" **Bacteriology & the Biology Program University of Wisconsin Madison**, Madison, WI
3. 2020 "Host and Microbial Metabolism as Determinants of Antibiotic-induced Disruption in the Microbiome" **2020 North American Cystic Fibrosis Conference**, Phoenix (virtual), AZ
4. 2021 "Microbial metabolism is a modulator of antibiotic efficacy and dysbiosis in the microbiome" **Mayo Clinic MPET**, Rochester MN

- **What do you plan to do during the next reporting period to accomplish the goals?**
 - We will complete the revisions requested by Cell reports and resubmit.

4. IMPACT:

- **What was the impact on the development of the principal discipline(s) of the project?**
 - *So far, the key developmental impact from this work has been in demonstrating the capacity of metatranscriptomics to define the responses of bacteria to antibiotics in the microbiome. We envision that in the same way the RNA-seq has revolutionized in vitro microbiology this new capacity will revolutionize the study of bacteria in their natural environment.*
- **What was the impact on other disciplines?**
 - *I believe that the metatranscriptomics approach that we demonstrated is applicable outside of ID research as well.*
- **What was the impact on technology transfer?**
 - *"Nothing to Report."*
- **What was the impact on society beyond science and technology?**
 - *"Nothing to Report."*

5. CHANGES/PROBLEMS:

- **Changes in approach and reasons for change**
 - *Nothing to report*
- **Actual or anticipated problems or delays and actions or plans to resolve them**

Starting from March 9th 2020 the physical space of the Belenky lab has been largely shutdown due to the COVID19 crisis. In June 2020 the lab was partially reopened (approximately 20% capacity). Over the past year the situation has improved and the lab is currently at all most full capacity, However, it is important to note that the short- and long-term impact of this shutdown are still difficult to anticipate. For example, many reagents and supplies are still difficult to get and this reduces the rate at which we can complete key work.

Changes that had a significant impact on expenditures

- *The shutdown has significantly impacted or planed expenditures. While our personnel obligations remained unchanged we had to significantly reduced spending on supplies, animals, and services.*
- **Significant changes in use or care of human subjects, vertebrate animals, biohazards, and/or select agents**
 - *Nothing to report*

- Significant changes in use or care of human subjects
- Significant changes in use or care of vertebrate animals.
- Significant changes in use of biohazards and/or select agents

6. PRODUCTS:

- Publications, conference papers, and presentations
Report only the major publication(s) resulting from the work under this award.

Publications

1. Cabral D.J, Wurster J.I, Korry B.J, Penumutthu S., **Belenky P.** “Consumption of a Western-Style Diet Modulates the Response of the Murine Gut Microbiome to Ciprofloxacin”. **mSystems**. (2020) Jul 28;5(4):e00317-20. doi: 10.1128/mSystems.00317-20. PMID: 32723789; PMCID: PMC7394352 (Research paper)

Presentations describing this work

1. 2020 “Microbial Metabolism is a Determinant of Antibiotic-induced Disruption of the Gut Microbiome” **Microbiology and Immunology Dartmouth Medical School**, Hanover, NH
2. 2020 “Microbial Metabolism is a Determinant of Antibiotic-induced Disruption of the Gut Microbiome” **Bacteriology & the Biology Program University of Wisconsin Madison**, Madison, WI
3. 2020 “Host and Microbial Metabolism as Determinants of Antibiotic-induced Disruption in the Microbiome” **2020 North American Cystic Fibrosis Conference**, Phoenix (virtual), AZ
4. 2021 “Microbial metabolism is a modulator of antibiotic efficacy and dysbiosis in the microbiome” **Mayo Clinic MPET**, Rochester MN

7. PARTICIPANTS & OTHER COLLABORATING ORGANIZATIONS

- What individuals have worked on the project?

| | |
|--|---|
| Name: | <i>Rachael Nilson</i> |
| Project Role: | <i>Graduate Student</i> |
| Researcher Identifier (e.g. ORCID ID): | RNILSON |
| Nearest person month worked: | 1 month |
| Contribution to Project: | <i>Rachael assisted with mouse work in Aim2</i> |
| Funding Support: | this award |
| Name: | <i>Kathy Antosca</i> |
| Project Role: | Postdoctoral associate |
| Researcher Identifier (e.g. ORCID ID): | https://orcid.org/0000-0001-9027-9874 |
| Nearest person month worked: | 1 |

| | |
|--|---|
| Contribution to Project: | Kathy provided key guidance in computational analysis |
| Funding Support: | this award |
| Name: | Peter Belenky |
| Project Role: | PI |
| Researcher Identifier (e.g. ORCID ID): | BELENKYP |
| Nearest person month worked: | 0.3 |
| Contribution to Project: | Project leader |
| Funding Support: | this award |
| | |

- **Has there been a change in the active other support of the PD/PI(s) or senior/key personnel since the last reporting period?**
 - *"Nothing to Report."*
- **What other organizations were involved as partners?**
 - *"Nothing to Report."*

8. SPECIAL REPORTING REQUIREMENTS

- **COLLABORATIVE AWARDS:**
- **QUAD CHARTS:**

9. APPENDICES:

We have attached 2 manuscripts as Appendices for this report. These include a published *MSystems* manuscript and an unpublished but submitted *Cell Reports* manuscript.

PR172193: Antibiotic Tolerance and Therapeutic Failure in Diabetic Infections

PI: Peter Belenky, Brown University

Budget: 321,422.00 **Topic Area:** FOCUS AREA OR DISEASE AREA **Mechanism:** FUNDING

OPPORTUNITY

Research Area: Refer to Scientific Classification System (SCS codes) **Award Status:** 01 June 2018 – 30 November 2020

Study Goals:

We propose to study the impacts of host hyperglycemia on antibiotic efficacy in pathogenic bacteria and the microbiome. This work is vital to understanding the high rate of infections and therapeutic failure among patients with diabetes mellitus, particularly diabetic veterans.

Specific Aims:

Aim 1) Determine the impacts of induced hyperglycemia on pathogen killing by bactericidal antibiotics and relate these results to the activity of metabolism-based tolerance mechanisms.

Aim 2) Determine the impacts of induced hyperglycemia on the composition of the murine gut microbiome and its functional response to bactericidal antibiotics.

Key Accomplishments:

Publications:

1. Cabral D.J, Wurster J.I, Korry B.J, Penumutchu S., Belenky P. "Consumption of a Western-Style Diet Modulates the Response of the Murine Gut Microbiome to Ciprofloxacin". mSystems. (2020) Jul 28;5(4):e00317-20. doi: 10.1128/mSystems.00317-20. PMID: 32723789; PMCID: PMC7394352 (Research paper)

Patents: Nothing to report

Funding Obtained:

Project / Proposal Title: Relating impacts of antibiotics on the gut metabolome and microbiome to host physiology and weight

Source of Support: NIH NIDK

Total Award Amount: \$2,536,655 Total Award Period Covered: 08/01/20-05/31/25



Consumption of a Western-Style Diet Modulates the Response of the Murine Gut Microbiome to Ciprofloxacin

Damien J. Cabral,^{a*} Jenna I. Wurster,^a Benjamin J. Korry,^a Swathi Penumutthu,^a  Peter Belenky^a

^aDepartment of Molecular Microbiology and Immunology, Brown University, Providence, Rhode Island, USA

Damien J. Cabral and Jenna I. Wurster contributed equally to this work. Author order was determined both by seniority and by involvement in study planning.

ABSTRACT Dietary composition and antibiotic use have major impacts on the structure and function of the gut microbiome, often resulting in dysbiosis. Despite this, little research has been done to explore the role of host diet as a determinant of antibiotic-induced microbiome disruption. Here, we utilize a multi-omic approach to characterize the impact of Western-style diet consumption on ciprofloxacin-induced changes to gut microbiome structure and transcriptional activity. We found that Western diet consumption dramatically increased *Bacteroides* abundances and shifted the community toward the metabolism of simple sugars and mucus glycoproteins. Mice consuming a Western-style diet experienced a greater expansion of *Firmicutes* following ciprofloxacin treatment than those eating a control diet. Transcriptionally, we found that ciprofloxacin reduced the abundance of tricarboxylic acid (TCA) cycle transcripts on both diets, suggesting that carbon metabolism plays a key role in the response of the gut microbiome to this antibiotic. Despite this, we observed extensive diet-dependent differences in the impact of ciprofloxacin on microbiota function. In particular, at the whole-community level we detected an increase in starch degradation, glycolysis, and pyruvate fermentation following antibiotic treatment in mice on the Western diet, which we did not observe in mice on the control diet. Similarly, we observed diet-specific changes in the transcriptional activity of two important commensal bacteria, *Akkermansia muciniphila* and *Bacteroides thetaiotaomicron*, involving diverse cellular processes such as nutrient acquisition, stress responses, and capsular polysaccharide (CPS) biosynthesis. These findings demonstrate that host diet plays a role in determining the impacts of ciprofloxacin on microbiome composition and microbiome function.

IMPORTANCE Due to the growing incidence of disorders related to antibiotic-induced dysbiosis, it is essential to determine how our “Western”-style diet impacts the response of the microbiome to antibiotics. While diet and antibiotics have profound impacts on gut microbiome composition, little work has been done to examine their combined effects. Previous work has shown that nutrient availability, influenced by diet, plays an important role in determining the extent of antibiotic-induced disruption to the gut microbiome. Thus, we hypothesize that the Western diet will shift microbiota metabolism toward simple sugar and mucus degradation and away from polysaccharide utilization. Because of bacterial metabolism’s critical role in antibiotic susceptibility, this change in baseline metabolism will impact how the structure and function of the microbiome are impacted by ciprofloxacin exposure. Understanding how diet modulates antibiotic-induced microbiome disruption will allow for the development of dietary interventions that can alleviate many of the microbiome-dependent complications of antibiotic treatment.

KEYWORDS diet, antibiotics, metagenomics, metatranscriptomics, dysbiosis


Citation Cabral DJ, Wurster JI, Korry BJ, Penumutthu S, Belenky P. 2020. Consumption of a Western-style diet modulates the response of the murine gut microbiome to ciprofloxacin. *mSystems* 5:e00317-20. <https://doi.org/10.1128/mSystems.00317-20>.

Editor Lawrence A. David, Duke University

Copyright © 2020 Cabral et al. This is an open-access article distributed under the terms of the [Creative Commons Attribution 4.0 International license](https://creativecommons.org/licenses/by/4.0/).

Address correspondence to Peter Belenky, peter_belenky@brown.edu.

* Present address: Damien J. Cabral, Exploratory Science Center, Merck & Co., Inc., Cambridge, Massachusetts, USA.

 You are what you eat: consumption of a Western-style diet alters the microbiota’s metabolic activity and exacerbates the negative impacts of antibiotic treatment

Received 16 April 2020

Accepted 8 July 2020

Published 28 July 2020

The gut microbiome includes the trillions of largely commensal bacteria, archaea, and fungi that inhabit the gastrointestinal tract (1–3). These communities play an important role in numerous biological processes such as digestion, neurological development, colonization resistance, and immune function (4–17). Consequently, it is unsurprising that disruption of microbial homeostasis, termed dysbiosis, has numerous harmful impacts to the host. The gut microbiome is highly sensitive to perturbations such as broad-spectrum antibiotic usage. Within hours of treatment, antibiotics induce dramatic reductions in both bacterial load and diversity within the microbiome, both of which are common indicators of dysbiosis (18, 19).

While compositional changes are typically transient and recover following the cessation of a perturbation, oftentimes the structure and diversity of the microbiota never return to their original levels. The resulting dysbiosis often has numerous acute and chronic impacts on host health. In the case of antibiotic usage, this may increase the risk of infection with opportunistic fungal and bacterial pathogens by reducing colonization resistance (1, 4, 5, 17, 20–24). Most notably, broad-spectrum antibiotic treatment is a major risk factor in *Clostridioides difficile* infection (20, 22, 25, 26). Persistent dysbiosis is correlated with many chronic conditions with considerable morbidity and mortality, such as asthma, obesity, and inflammatory bowel disease (6–9, 11, 13, 14, 17, 26).

Interestingly, antibiotic-induced disruption of the microbiome may be influenced by the metabolic environment of the gut. A large body of *in vitro* data indicates that the rate of metabolic activity for bacteria correlates positively with antimicrobial susceptibility, such that metabolically active, ATP-producing processes such as respiration promote toxicity, whereas less efficient or quiescent metabolism induces tolerance (27–29). A similar trend is observed in the context of bacteria responding to antibiotics in the gut microbiome, where nutrient availability and bacterial metabolism are closely linked to host diet. Recent work has demonstrated that antibiotic exposure changes both the composition of the gut microbiome and its metabolic capacity, such that the surviving microbiome is overall less metabolically active (19). Further, amoxicillin treatment was shown to increase the expression of polysaccharide utilization genes, while simultaneously decreasing the abundance of transcripts involved in simple sugar utilization (19). Reflecting these changes, amoxicillin also decreased the total concentration of glucose within the ceca of mice (19). These transcriptional changes have significant impacts on the response of specific bacteria to the treatment. In the case of *Bacteroides thetaiotaomicron*, polysaccharide utilization promoted tolerance to amoxicillin, and simple sugar utilization increased toxicity. Accordingly, the response of the microbiota to antibiotics can be impacted by dietary nutrient modulation (30). For example, Cabral et al. found that glucose supplementation impacts the response of the total community and reduces the absolute abundance of bacteria, particularly *B. thetaiotaomicron*, following amoxicillin treatment in mice (19). Together these findings suggest that dietary composition may act as an additional perturbation that drives the severity of the microbiome's response to antibiotic treatment.

Dietary composition is known to have a profound impact on microbiome diversity and overall gut health (31–37). Diets high in fat and simple sugars, typically referred to as “Western” diets, have been associated with a number of negative health states including obesity, diabetes mellitus, allergies, and inflammatory bowel disease (36–46). Such diets have very low levels of microbiota-accessible carbohydrates (MACs), which are typically found in complex plant polysaccharides and are indigestible and unabsorbable by the host (40, 44, 47–49). MACs are typically fermented by the colonic microbiota to produce short-chain fatty acids (SCFAs), which play important roles in regulating energy homeostasis and inflammation within the host (40, 45, 50–55). High-MAC diets have also been shown to increase microbial diversity, a classic benchmark for gut microbiota health. Conversely, low-MAC diets are known to reduce both microbiome diversity and SCFA production (44, 46, 49, 56). MAC starvation enriches for muciniphilic microbes that are capable of degrading the mucosal lining of the gut, such as *Akkermansia muciniphila* (40, 42, 48, 57). Degradation of the mucosal layer over time

may result in compromised gut barrier function and lead to increased inflammation, colitis, and susceptibility to infection by enteric pathogens (57).

Individually, antibiotic usage and the consumption of Western-style diets are known to negatively impact the microbiota, impacting host health. Despite this, little work has explored the impact of diet on the response of the microbiota to antibiotics. Previous work has suggested that dietary composition may play an important role in determining the extent of antibiotic-induced microbiome disruption (19). Thus, we hypothesize that the consumption of a Western-style diet will significantly modify the metabolic activity of the microbiome toward simple sugar and mucus glycoprotein degradation rather than dietary polysaccharide utilization. This will be characterized by differential utilization of carbohydrate-active enzymes (CAZymes) along with changes in respiratory activity and central carbon metabolism. Given that respiratory activity plays a key role in drug susceptibility *in vitro*, when this community is treated with a bactericidal antibiotic like ciprofloxacin, its compositional and functional responses to the drug would be different due to the altered metabolic state. Overall, we anticipate that the diet-related metabolic state of the microbiome before treatment will have a larger impact on drug disruption than the metabolic changes that are induced during the drug exposure. In this study, we use a combined metagenomic and metatranscriptomic approach to characterize the impact of a Western-style diet on the taxonomic and functional disruption of the microbiome during ciprofloxacin treatment. Using shotgun metagenomics, we found that ciprofloxacin elicited differential impacts on community composition in mice at both the phylum and species level in a diet-dependent manner. Using metatranscriptomics, we observed that consumption of a Western diet induced profound transcriptional changes within the gut microbiomes of mice. Furthermore, consumption of this diet modulated the transcriptional response of these communities to antibiotic treatment. Specifically, dietary composition had a major impact on the abundance of transcripts containing key metabolic genes. Lastly, we were able to detect unique species-specific transcriptional changes in response to both diet and ciprofloxacin treatment in two important commensal bacteria, *A. muciniphila* and *B. thetaiotaomicron*.

RESULTS

To determine the impact of dietary composition and antibiotic exposure on the structure and function of the murine gut microbiome, female C57BL/6J mice were randomly assigned to either a high-fat, high-sugar “Western”-style (Western) diet or a low-fat control diet for 7 days in multiple cages. At this point, mice from each diet were again randomly split between ciprofloxacin and vehicle control groups and treated for 24 h in multiple cages ($n = 8$ to 12 per group). Previously it has been shown that 24 h of ciprofloxacin treatment was sufficient to induce changes in community structure and transcriptional activity (19). This time frame also allowed for profiling the acute response of the microbiota to ciprofloxacin exposure, rather than characterizing a post-antibiotic state of equilibrium. Following treatment, the mice were sacrificed to harvest their cecal contents for taxonomic profiling and transcriptional analysis (Fig. 1A). Overall, we found that diet and ciprofloxacin treatment had a significant impact on gut microbiome structure (Fig. 1B to D; see also Fig. S1 in the supplemental material).

We first assessed the effects that diet and ciprofloxacin have on the diversity of the gut microbiome using 16S rRNA sequencing. Mice consuming the Western diet had significantly less diverse gut microbiomes than those fed the control diet (Fig. S1A). Interestingly, we also observed that the Western diet was associated with a reduction in alpha diversity during ciprofloxacin treatment (Fig. S1A). Next, we performed Principal Coordinate Analysis (PCoA) using Bray-Curtis dissimilarity paired with permutational multivariate analysis of variance (PERMANOVA) to profile the degree of dissimilarity between our samples and the significance of this distance. Our samples formed four distinct clusters driven by both diet and ciprofloxacin treatment (Fig. 1B).

Due to the limited phylogenetic resolution provided by 16S rRNA sequencing and

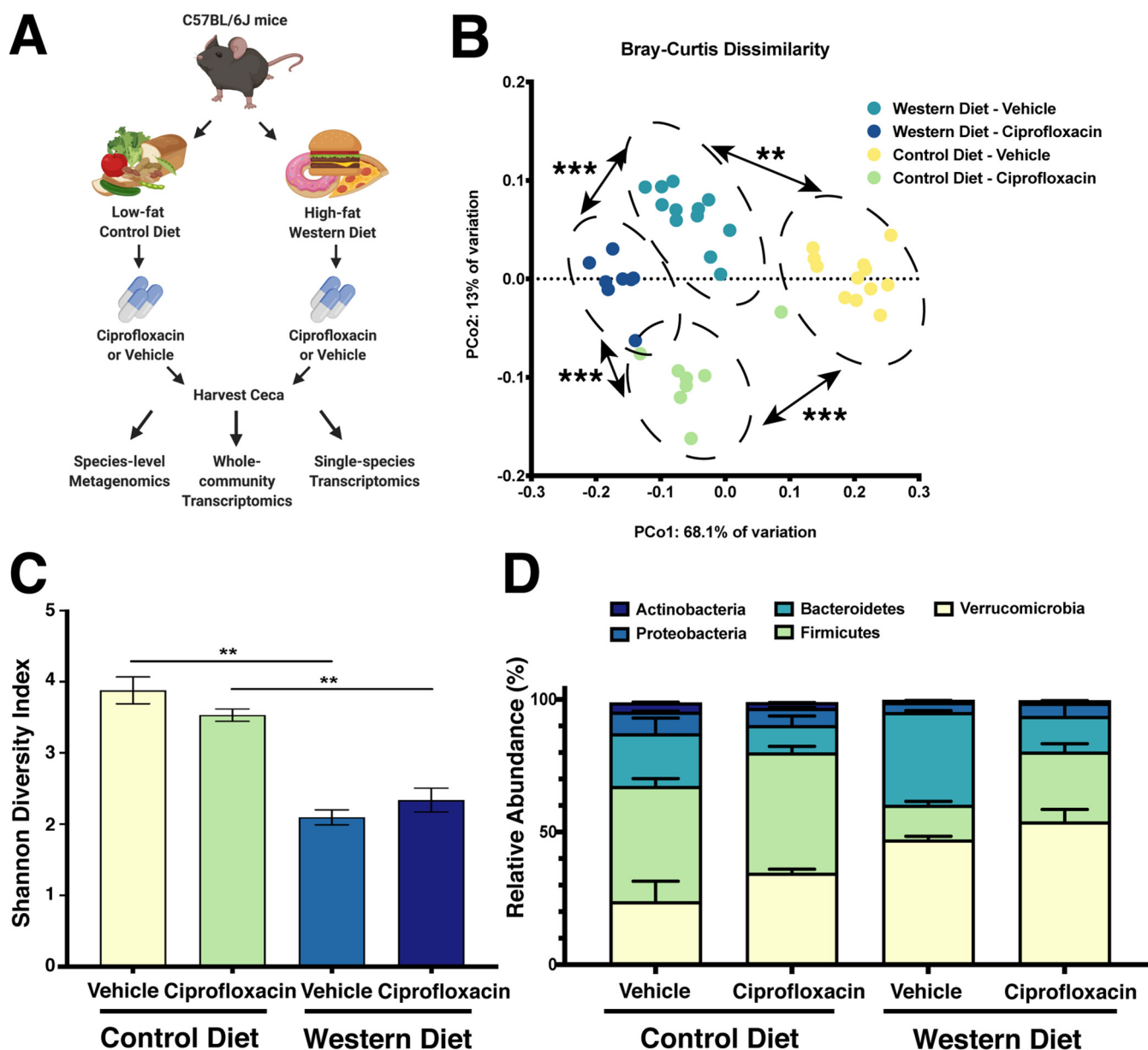


FIG 1 Impact of diet and ciprofloxacin administration on murine gut microbiome composition. (A) Experimental workflow used in this study. Figure was created with BioRender.com (BioRender, Toronto, Canada). (B) Principal Coordinate Analysis of experimental groups as measured by Bray-Curtis dissimilarity of 16S rRNA amplicons. (**, $P < 0.01$; ***, $P < 0.001$, permutational ANOVA). (C) Alpha diversity of experimental groups as measured by the Shannon diversity index. Data are represented as mean \pm standard error of the mean (SEM) (**, $P < 0.01$, Welch ANOVA with Dunnett T3 test for multiple hypothesis testing). (D) Stacked bar plot of the five most abundant bacterial phyla in our data set. Data are represented as mean \pm SEM for each phylum. For 16S rRNA amplicons, $n = 8$ to 12. For metagenomics, $n = 4$.

inability to provide functional information about sequenced communities, we opted to perform shotgun metagenomic and metatranscriptomic analyses on a subset of our samples, representing mice from multiple cages ($n = 4$ per treatment group) (19, 58–61). Interestingly, we observed that Western diet consumption reduced community diversity while ciprofloxacin did not have a statistically significant impact on the alpha diversity of the community (Fig. 1C). However, the metagenomic data exhibited a similar trend in unique taxonomic structures being associated with each treatment group, supporting a model wherein diet and antibiotic treatment are distinct perturbations (Fig. 1D). However, to evaluate if diet modifies the response to ciprofloxacin, we had to untangle diet-induced changes from antibiotic-induced changes. First, we characterized the impact of the Western diet consumption.

Consumption of a Western diet modifies the metabolic activity of the microbiome. Mice fed a Western diet displayed elevated levels of the phyla *Verrucomicrobia* and *Bacteroidetes* and a reduction of *Firmicutes* (Fig. 1D). At the species level, these shifts appear to be largely driven by an expansion of members of the *Bacteroides* genus (Fig. 2A, Fig. S1B, and Data Set S1). Additionally, the Western diet-fed mice displayed an elevated abundance of several species from the *Proteobacteria* phylum, suggestive of dysbiosis (62). Two important bacterial species found in the gut microbiomes of both mice and humans, *B. thetaiotaomicron* and *A. muciniphila*, were observed at significantly elevated levels in the mice fed a Western diet (Fig. 2A and Fig. S1B). Notably, both species are known to utilize host-produced mucins; thus, this observation is consistent with earlier studies suggesting that the consumption of a low-MAC Western diet enriches for muciniphilic bacteria (40, 42, 48).

Given this expansion, we anticipated that the transcriptional activity of these communities would exhibit an increased capacity for mucus degradation and simple sugar utilization. Due to the potential limitations of using a single pipeline, we analyzed our metatranscriptomic data set with SAMSA2 in parallel with HUMAnN2 (63, 64). The SAMSA2 pipeline generates unnormalized transcript abundances and thus is representative of overall transcript levels (63). SAMSA2 is advantageous in its capacity for annotation against multiple databases and enables differential abundance testing of individual transcripts in addition to pathway- and subsystem-level analysis (63). Conversely, the HUMAnN2 pipeline normalizes the abundance of RNA transcripts against their corresponding gene abundance in the metagenomic data set, thus normalizing for differences in community composition between experimental groups and facilitating comparisons of metabolic pathway expression at the whole-community level (64). When paired, these pipelines facilitate a more robust examination of microbiome transcriptional activity.

We observed an increased abundance of transcripts related to respiration at the SEED subsystem level in the microbiota of the mice consuming the Western diet, which was mirrored in our HUMAnN2 data set as increased tricarboxylic acid (TCA) cycle expression (Fig. 2B, Fig. S2A, and Data Sets S2 and S3). The Western diet-fed mouse microbiota also displayed increased abundance of transcripts involving fatty acid metabolism and terpenoid biosynthesis, likely reflecting altered nutrient availability and increased respiratory activity, respectively (Fig. 2B and Data Set S3) (65, 66). Interestingly, we also detected large increases in the abundance of two different sialidase transcripts, which play a key role in the utilization of host-produced mucins (Fig. S2B and Data Set S4) (67). While other studies have shown that the consumption of a Western diet enriches for muciniphilic taxa, this observation suggests that this diet also increases transcriptional activity related to mucin degradation within the microbiome (40, 42).

Additionally, the Western diet-fed mouse microbiota had reduced expression of nucleotide biosynthesis, glycolysis, gluconeogenesis, starch degradation, and pyruvate fermentation compared to control diet-fed mice (Fig. S2A and Data Set S2). We also observed relative reduction in the expression of the *Bifidobacterium* shunt, which is known to play a role in SCFA production and may provide mechanistic insight into the reduced SCFA levels observed on the Western diet in other studies (Fig. S2A and Data Set S2) (40, 51).

Examination of CAZyme activity provided further evidence of significant transcriptional reprogramming in response to diet. Specifically, we observed that Western diet consumption decreased transcript abundances of multiple enzymes involved in polysaccharide breakdown (Fig. 2C and Data Set S5) (68–71). Simultaneously, there was a significant increase in α -amylases, lysozyme C, and α -lactalbumin breakdown (Fig. 2C and Data Set S5) (72, 73). Given the content of the Western diet, a shift toward utilization of these carbon sources was not unexpected. However, the robust loss of complex polysaccharide breakdown was surprising and complements the SEED and HUMAnN2 data sets. Together these data suggest that Western diet alone is sufficient

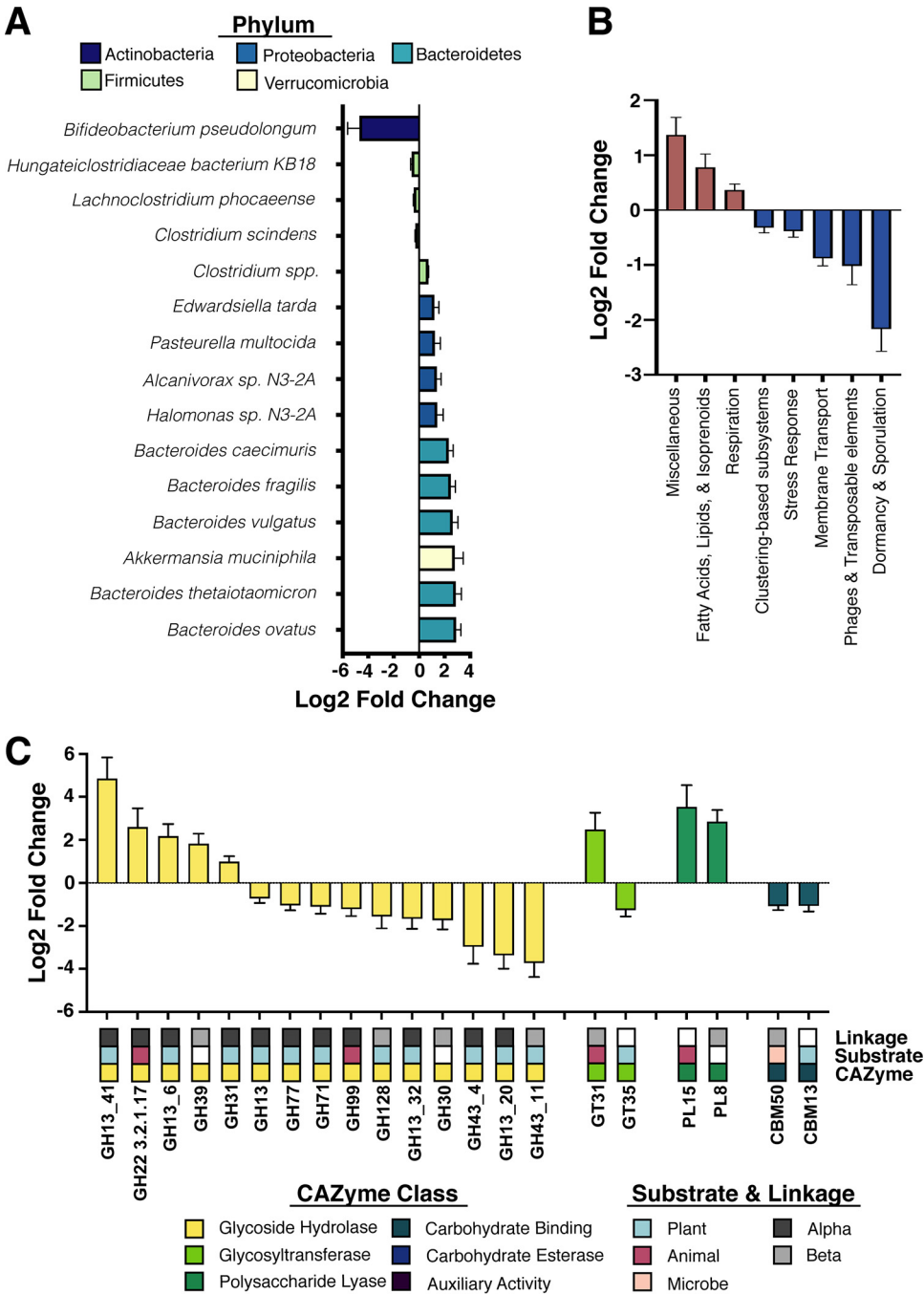


FIG 2 Consumption of a Western diet induces broad taxonomic and transcriptional changes at the community level. (A) Differentially abundant (Benjamini-Hochberg-adjusted P value < 0.05) bacterial species (within the 45 most abundant taxa) as detected in mice consuming the Western diet. Data are represented as \log_2 fold change relative to control diet \pm standard error. Bar color and top legend denote phylum-level taxonomic classification (yellow, *Verrucomicrobia*; green, *Firmicutes*; teal, *Bacteroidetes*; blue, *Proteobacteria*; navy, *Actinobacteria*). See Data Set S1 for full results. (B) Differentially expressed (Benjamini-Hochberg-adjusted P value < 0.05) level 1 SEED subsystems in the murine cecal metatranscriptome of mice consuming the Western diet. Data are represented as \log_2 fold change relative to control diet \pm standard error. Only features with a base mean of ≥ 100 were plotted. See Data Set S3 for full results. (C) Differentially expressed (Benjamini-Hochberg-adjusted P value < 0.05) CAZyme transcripts in the murine cecal metatranscriptome in mice consuming the Western diet. Data are represented as \log_2 fold change relative to control diet \pm standard error. CAZyme class (yellow, glycoside hydrolase; lime, glycosyltransferase; green, polysaccharide lyase; teal, carbohydrate binding modules; blue, carbohydrate esterase; purple, auxiliary activity), source of the target substrate (blue, plant derived; magenta, animal derived; peach, microbially derived), and linkages targeted by the CAZyme (dark gray, alpha; light gray, beta) are listed below the data and color coded. White values represent either a lack of singular substrate/linkage or a lack of enough information available to make a definitive call. See Data Set S5 for full results. For all analyses, $n = 4$.

to restructure the metabolic activity of the gut microbiome, due to significant changes in nutrient availability.

Ciprofloxacin elicits unique shifts in gene expression on Western and control diets. Given the significant body of literature that links microbial metabolism with antimicrobial susceptibility both *in vitro* and within the microbiome, we hypothesized that the metabolic restructuring induced by the Western diet would result in differential susceptibility to ciprofloxacin (19, 27–29). Although ciprofloxacin did not induce a significant reduction in alpha diversity in the time frame tested, we found that diet drove differential community composition following antibiotic exposure (Fig. 1C and D). At the phylum level, we observed a significant expansion in the relative abundance of *Firmicutes* following ciprofloxacin treatment on the Western diet (adjusted *P* value = 0.0388) but not on the control diet (adjusted *P* value = 0.8718) (Fig. 1D and Fig. S1B). To determine which species displayed a differential response to ciprofloxacin on the Western and control diets, we utilized DESeq2 to analyze the interaction between diet and antibiotic treatment to determine which species displayed differential responses to ciprofloxacin between the diets (74). While most species responded similarly to ciprofloxacin therapy on both diets, there were several notable exceptions. For example, the expansion of several *Clostridium* species (such as *Clostridium saccharolyticum*, *Clostridium sphenoides*, and *Clostridium scindens*) following ciprofloxacin was higher on the Western diet than the control (positive interaction values, Fig. 3A and Data Set S1). Conversely, the reduction of several *Bacteroides* species following antibiotic treatment tended to be exacerbated on the Western diet (negative interaction values, Fig. 3A and Data Set S1).

We detected clear differences in ciprofloxacin susceptibility between the two diets and hypothesized that diet-induced differences in metabolism would both alter susceptibility and be reflected in unique transcriptional signatures. An all-by-all comparison of experimental groups demonstrated that the microbiota of Western diet-consuming mice displayed elevated expression of TCA cycle and fatty acid degradation pathways in both vehicle and ciprofloxacin treatments, likely reflective of the increased fat and sugar content of this diet (Fig. 3B and Data Set S2). Additionally, we found elevated expression of glycogen degradation genes that was specific to Western diet-fed mice receiving ciprofloxacin (Fig. 3B and Data Set S2). Conversely, the microbiota of control diet-consuming mice had elevated expression of amino acid biosynthesis pathways (isoleucine, aspartate, asparagine, lysine, and histidine) regardless of antibiotic treatment (Fig. 3B and Data Set S2). We also observed elevated levels of several different nucleotide biosynthesis pathways in the vehicle-treated control diet mice while the Western diet mice displayed elevated levels of adenosine and guanosine nucleotide degradation (Fig. 3B and Data Set S2). Overall, these data support that our experimental groups could be characterized by unique transcriptional signatures.

We found key differences in the overall transcriptional profiles in response to ciprofloxacin on each diet. On the Western diet, ciprofloxacin treatment was associated with an increased abundance of transcripts from glycogen and starch degradation, glycolysis, and pyruvate fermentation (Fig. S3C and Data Set S2). Notably, the expression of glycogen degradation was elevated in vehicle-treated samples on the control diet, suggesting that the utilization of this pathway during ciprofloxacin treatment is diet dependent (Fig. S3C and Data Set S2). We observed that TCA cycle expression was reduced in ciprofloxacin-treated mice compared to the vehicle treatment—the lone commonality between diets (Fig. S3C and Data Set 2). Previous work has demonstrated that TCA cycle elevation increases sensitivity to bactericidal antibiotics (27–29, 75). Thus, this result suggests that TCA cycle activity may play a key role in the response of the microbiota to ciprofloxacin treatment *in vivo*, though more work is required to understand its impact.

Interestingly, comparatively few subsystems were changed following ciprofloxacin treatment on either diet (Fig. 3C and D and Data Set S3), suggesting that the pretreatment metabolic state affects the antibiotic response more than the drug-induced transcriptional changes. Most notably, we observed a decrease in transcripts related to

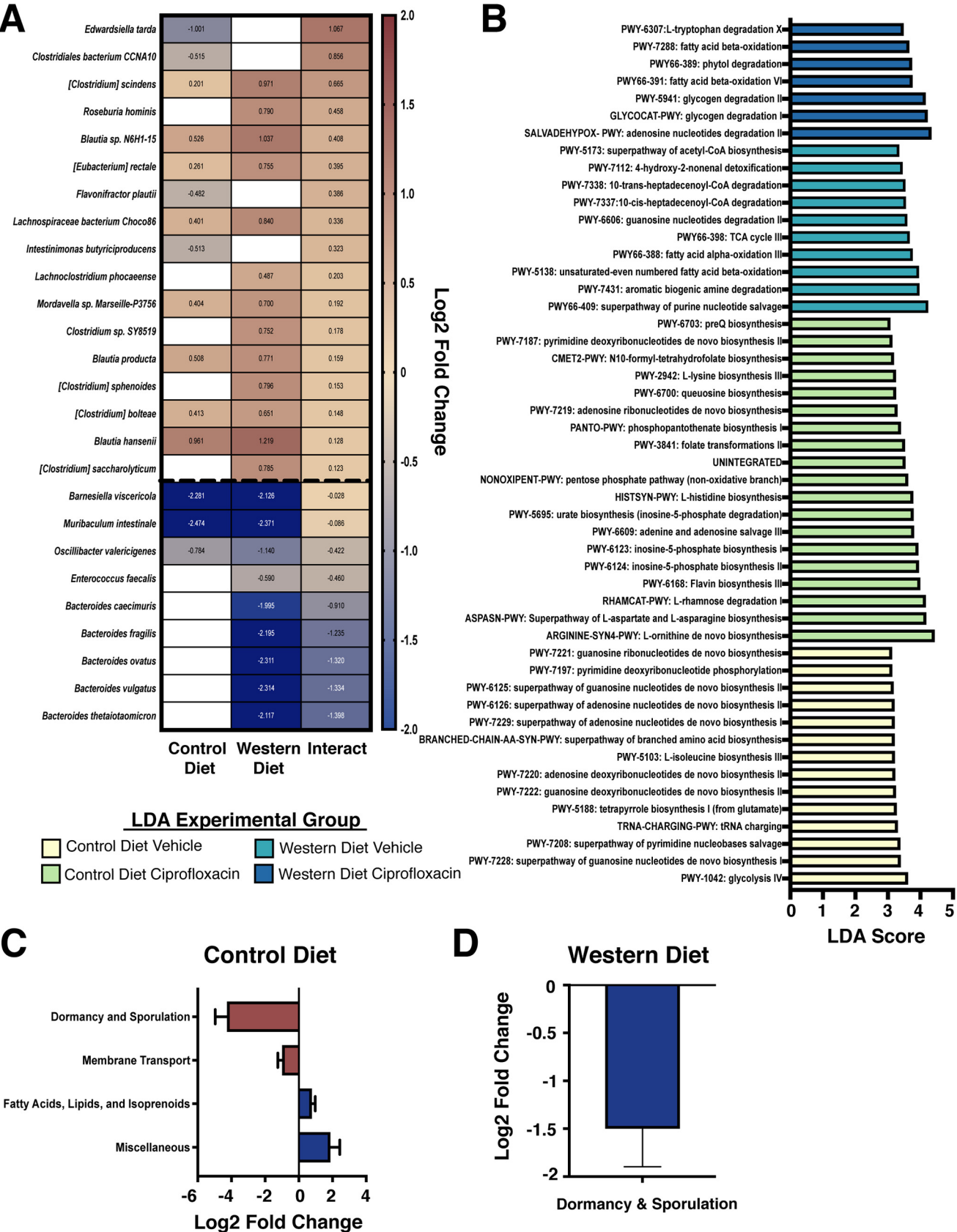


FIG 3 Ciprofloxacin elicits unique shifts in gene expression on Western and control diets at the community level. (A) Heatmap of the change in abundance of the top 45 bacterial species in response to ciprofloxacin on control and Western diets. The Interact column represents the interaction term generated (Continued on next page)

dormancy and sporulation in response to ciprofloxacin on both diets (Fig. 3C and D and Data Set S3). A similar finding was observed in a recent study, suggesting that these transcripts may play a key role in the response of the microbiota to this antibiotic (19). Furthermore, ciprofloxacin increased the abundance of sialidase transcripts in mice on the control diet, suggesting that this effect may be exacerbated by antibiotic treatment (Fig. S3A and Data Set S4). Reflecting the overall reduction in sporulation seen at the subsystem level, we found that several sporulation-related transcripts were reduced on the control diet following ciprofloxacin treatment (Fig. S3A and Data Set S4).

We also examined the interaction of diet and antibiotic treatment on transcript abundance within the microbiome. Notably, we found that several sporulation genes were significantly higher on the Western diet than the control following ciprofloxacin treatment (Data Set S4), which was reflected in the SEED subsystem level (Fig. 3C and D). Additionally, transcripts encoding phosphotransferase system (PTS) transporters of various substrates were also found to be higher on the Western diet following ciprofloxacin treatment (Data Set S4). Conversely, Western diet consumption significantly reduced the change in transcript abundance of both pectate lyase and a hemin receptor following ciprofloxacin therapy. Together, these findings demonstrate that dietary composition significantly impacts the transcriptional response of the microbiome to ciprofloxacin.

Recent studies have shown CAZyme activity to be a significant component of the microbiome's response to antibiotic stress (19). In our study, over 75 CAZymes exhibited differential abundance during ciprofloxacin treatment (Data Set S5). Interestingly, these changes were exclusive to the control diet-fed microbiota, as the Western diet-fed communities displayed no significant difference in CAZyme abundance (Data Set S5). The microbiota of mice on the control diet exhibited increases in CAZymes involved in starch, glycogen, xylose, pectin, rhamnogalacturonan, and arabinofuranose degradation (Data Set S5) (76, 77). Additionally, these communities exhibited a significant increase in trehalose phosphorylase and synthase activity, both of which have been associated with transient antibiotic tolerance in pathogenic species (Data Set S5) (78, 79). Loss of these CAZyme shifts may be directly involved in the increased toxicity of ciprofloxacin on the Western diet; however, more work is required to elucidate the mechanism. These data, in conjunction with our SEED and HUMAnN2 data sets, provide evidence for unique transcriptional signatures during ciprofloxacin challenge that are diet dependent. Overall, this supports a model in which diet-driven differences in baseline metabolism directly impact taxonomic and functional responses to ciprofloxacin treatment.

Diet and ciprofloxacin alter gene expression within *B. thetaiotaomicron* and *A. muciniphila*. Next, we sought to profile how diet and drug treatment impacted the transcriptional response of individual species within the microbiota. In order to have sufficient genome coverage and sequencing depth, we ranked all taxa that were differentially abundant in the Western diet by average RNA reads, further analyzing only those with 500,000 or greater (Data Set S6). With this criterion, we used a previously published pipeline to interrogate the impact of diet and antibiotic treatment on three individual species: *B. thetaiotaomicron*, *A. muciniphila*, and *C. scindens* (19, 80).

FIG 3 Legend (Continued)

by DESeq2, denoting the impact of diet on the change in abundance of each species to ciprofloxacin compared to vehicle control. Cell color denotes \log_2 fold change of a particular species in response to ciprofloxacin (white represents failure to meet statistical significance: Benjamini-Hochberg-adjusted P value < 0.05). Heatmap rows were sorted by interaction term value from highest to lowest, and taxa with no differential abundance (failure to meet statistical significance) in either group were removed. See Data Set S1 for full DESeq2 results. (B) Linear discriminant analysis (LDA) of MetaCyc pathways that were differentially associated with each experimental group. Bar size indicates LDA score, and color indicates the experimental group that a MetaCyc pathway was significantly associated with. All LDA scores were generated using LEfSe on unstratified pathway outputs from HUMAnN2. For full pathway names and statistics, see Data Set S2. (C) Differentially expressed (Benjamini-Hochberg-adjusted P value < 0.05) level 1 SEED subsystems in the murine cecal metatranscriptome after ciprofloxacin treatment in mice consuming the control diet. Data are represented as \log_2 fold change relative to vehicle controls \pm standard error. Only features with a base mean of ≥ 100 were plotted. See Data Set S3 for full results. (D) Differentially expressed (Benjamini-Hochberg-adjusted P value < 0.05) level 1 SEED subsystems in the murine cecal metatranscriptome after ciprofloxacin treatment in mice consuming the Western diet. Data are represented as \log_2 fold change relative to vehicle controls \pm standard error. Only features with a base mean of ≥ 100 were plotted. See Data Set S3 for full results. For all analyses, $n = 4$.

We focused on these bacteria because they are known human gut commensals, were found at relatively high levels in all samples analyzed, and were differentially abundant in a diet-dependent manner. Unfortunately, *C. scindens* had relatively few transcriptional changes across all comparisons, and those genes that were differentially regulated were almost exclusively hypothetical proteins (Data Set S6).

The Western diet significantly elevated the relative abundance of *A. muciniphila* (Fig. 4A). Interestingly, on this diet *A. muciniphila* displayed increased expression of several known stress response genes: catalase HPII, ATP-dependent chaperone ClpB, a universal stress protein, superoxide dismutase, and a UvrB/UvrC protein (Fig. 4B and Data Set S7). Additionally, we observed numerous changes in respiration and central carbon metabolism, including increased terminal oxidases, TCA cycle, glycolysis, and pyruvate metabolism, suggesting broad metabolic changes in response to the Western diet (Fig. 4B and Data Set 7). No CAZymes were differentially expressed on this diet, suggesting that the changes in *A. muciniphila* that facilitate its expansion are not driven by CAZyme activity (Data Set S7).

Ciprofloxacin treatment had a relatively minor impact on *A. muciniphila* gene expression (Data Set S7), likely due to the relatively low impact on the relative abundance of *A. muciniphila* (Fig. 4A). In total, ciprofloxacin significantly altered the expression of 2 and 17 genes on the control and Western diets, respectively (Data Set S7). On the control diet, *A. muciniphila* increased the expression of the molecular chaperone protein DnaK, which is known to play a role in stress responses (81–84). On the Western diet, several genes related to tryptophan biosynthesis and metabolism were elevated following ciprofloxacin treatment; however, their biological significance is unclear at this time (Data Set S7). Additionally, ciprofloxacin induced the differential expression of a sole chitin or lysozyme glycoside hydrolase, and only on the control diet (Fig. S3F and Data Set S7). Lastly, an examination of the interaction between diet and ciprofloxacin treatment indicated that only three genes were significantly altered. Overall, these data suggest that diet does not have a major impact on the response of this bacterium to ciprofloxacin within the microbiome (Data Set 7).

In contrast to *A. muciniphila*, diet had a relatively minor impact on *B. thetaiotaomicron* gene expression while ciprofloxacin induced extensive changes. Of note, *B. thetaiotaomicron* bloomed in response to the Western diet and was significantly perturbed by ciprofloxacin on this diet but not on the control (Fig. 4C). In total, 42 genes were altered in *B. thetaiotaomicron* in response to Western diet consumption (Data Set S7). Of note, this diet increased the expression of an aminoglycoside efflux pump and a hemin receptor. However, more than half of the genes (52.4%) that changed in response to diet are of unknown function and are classified as “hypothetical proteins,” making interpretation difficult. Interestingly, *B. thetaiotaomicron* did not exhibit robust changes in CAZyme transcription in response to the Western diet. Like *A. muciniphila*, *B. thetaiotaomicron* did not exhibit any differentially abundant CAZymes, suggesting that carbohydrate utilization does not drive the diet-induced changes in *B. thetaiotaomicron* abundance (Data Set S7). Ultimately, a description of this change will be dependent on improved functional annotations going forward.

On the control diet, we observed an increased abundance of transcripts encoding proteins involved in capsular polysaccharide (CPS) biosynthesis and export (Fig. 4D and Data Set S7). Within *B. thetaiotaomicron*, CPS production is encoded by a total of 182 genes distributed among eight loci (typically termed *cps1* to -8) (85, 86). It is hypothesized that an individual bacterium expresses one of these CPS configurations at any given time and that these structures play key roles in processes such as nutrient acquisition and immune evasion (86). Additionally, the two genes with the greatest increase in expression during ciprofloxacin treatment encoded UDP-glucose 6-dehydrogenase, which plays a key role in the biosynthesis of glycan precursors that are essential for capsule production in other bacteria (87–89). Together, these findings may suggest a role for CPS state as a determinant of ciprofloxacin susceptibility *in vivo*.

On the Western diet, ciprofloxacin elicited profound changes in transcriptional activity, altering the expression of 278 different genes (Fig. 4E and Data Set S7), and this

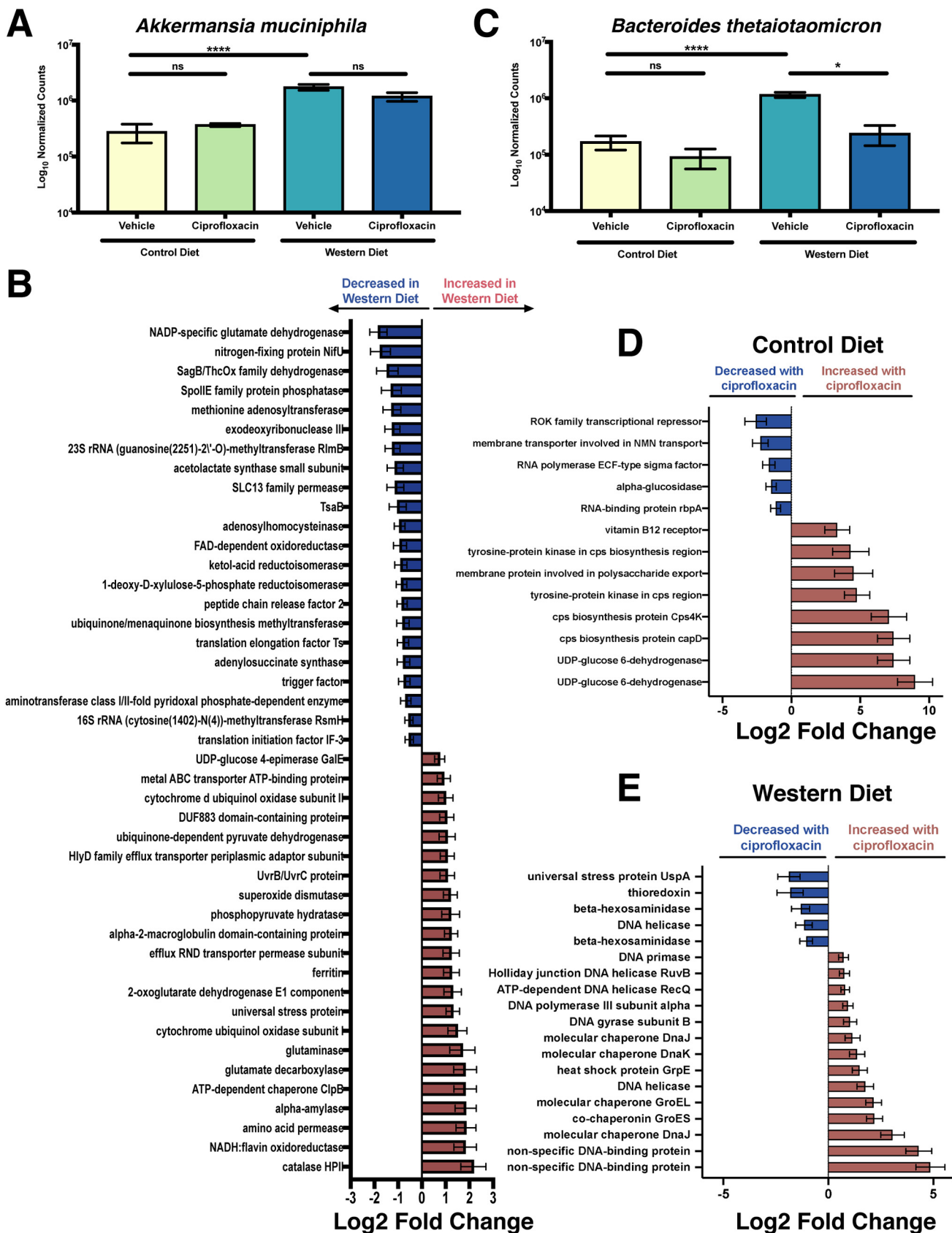


FIG 4 Diet and ciprofloxacin alter gene expression within *B. thetaiotaomicron* and *A. muciniphila*. (A) Normalized counts of *A. muciniphila* in each experimental group. Data are represented as mean \pm SEM. Normalized counts were generated with DESeq2 and subsequently used to perform differential (Continued on next page)

robust response may be related to the reduction in *B. thetaiotaomicron* under this condition (Fig. 4C). Interestingly, expression of many genes involved in the utilization of host-derived carbohydrates (sialic acid-specific 9-*O*-acetyltransferase, endo-beta-*N*-acetylglucosaminidase F1, beta-hexosaminidase) and stress responses (universal stress protein UspA, thioredoxin) was reduced, mirroring changes seen at the whole-community level (Fig. 4E and Data Set S7) in response to ciprofloxacin. Conversely, we observed increased expression of several genes that encode molecular chaperones or are involved in DNA replication or damage repair (Fig. 4E and Data Set S7). Ciprofloxacin triggers DNA damage via inhibition of DNA gyrase and topoisomerase IV. Thus, these changes in gene expression may be reflective of the primary mechanism of action of this antibiotic, are consistent with previously published data, and serve as a validation for our analysis (19).

Diet appears to have a significant impact on ciprofloxacin-induced transcriptional changes in *B. thetaiotaomicron*, modulating the response of 71 genes (Data Set S7). Of note, Western diet consumption in the context of ciprofloxacin treatment had a negative impact on several genes involved in the acquisition of nutrients, such as vitamin B₁₂ and hemin receptors, and transporters of glucose/galactose, hexuronate, arabinose, and Na⁺ (Data Set S7). Thus, it is likely that the availability of nutrients within the gut plays a role in the response of these bacteria to antibiotics. Lastly, we examined the impact that nutrient availability has on the response of *B. thetaiotaomicron* CAZyme abundance to ciprofloxacin. We observed notable differences in CAZyme levels between the diets as well as differences in substrate targets (Fig. S3D and E and Data Set S7). On the control diet, *B. thetaiotaomicron* exhibits an increase in polysaccharide CAZymes, including those targeting pectin, rhamnogalacturonan, β -glucans, and hemicelluloses, with a simultaneous decrease in β -fucosidases (Fig. S3D and Data Set S7). On the Western diet, *B. thetaiotaomicron* exhibits an increase in lipopolysaccharide (LPS) biosynthesis and heparan degradation (Fig. S3E and Data Set S7). While interesting, more work will be required to elucidate mechanisms driving these phenotypes.

DISCUSSION

Previous work has demonstrated that host diet, particularly with respect to sugar and fiber content, plays a major role in antibiotic-induced microbiome disruption (19, 30). In Western societies, many people consume a diet high in added sugars and fat but low in host-indigestible fiber. Such a composition is thought to promote the development of metabolic syndrome, heart disease, diabetes, and a number of other chronic conditions (36–46). Furthermore, broad-spectrum antibiotic use and resulting microbiome dysbiosis have been associated with a number of similar comorbidities along with increased susceptibility to opportunistic infections (1, 4, 5, 17, 20–22, 24, 25). Despite this connection, little work has been done examining how host dietary composition impacts the response of the microbiota to antibiotic perturbation. Nutrient availability and metabolic state are known to be major determinants of antibiotic susceptibility of bacteria *in vitro* (19, 27–29, 75, 90–95). Thus, modulating diet and subsequently nutrient availability to the microbiota would likely alter the sensitivity of bacteria in these communities to antibiotic therapy.

Using a combined metagenomic and metatranscriptomic approach, we demonstrate that diet composition has a major impact on the response of the murine gut

FIG 4 Legend (Continued)

abundance testing. (*, $P < 0.05$; ****, $P < 0.0001$; Wald test with Benjamini and Hochberg correction). See Data Set S1 for full results. (B) Select differentially expressed (Benjamini-Hochberg-adjusted P value < 0.05) genes of interest in *A. muciniphila* within the cecum of vehicle-treated mice consuming the Western diet. Data are represented as log₂ fold change relative to control diet \pm standard error. See Data Set S7 for full results. (C) Normalized counts of *B. thetaiotaomicron* in each experimental group. Data are represented as mean \pm SEM. Normalized counts were generated with DESeq2 and subsequently used to perform differential abundance testing. (*, $P < 0.05$; ****, $P < 0.0001$; Wald test with Benjamini and Hochberg correction). See Data Set S1 for full results. (D) Select differentially expressed (Benjamini-Hochberg-adjusted P value < 0.05) genes of interest in *B. thetaiotaomicron* within the cecum of ciprofloxacin-treated mice consuming the control diet. Data are represented as log₂ fold change relative to vehicle-treated controls \pm standard error. See Data Set S7 for full results. (E) Select differentially expressed (Benjamini-Hochberg-adjusted P value < 0.05) genes of interest in *B. thetaiotaomicron* within the cecum of ciprofloxacin-treated mice consuming the Western diet. Data are represented as log₂ fold change relative to vehicle-treated controls \pm standard error. See Data Set S7 for full results. For all analyses, $n = 4$. ns, not significant.

microbiome to ciprofloxacin therapy. By utilizing these tools in parallel, we are able to link transcriptional changes to observed shifts in community structure on each diet. Using metagenomics, we observed that ciprofloxacin had a differential impact on community composition in a diet-dependent manner. Specifically, we observed a significant expansion of the *Firmicutes* phylum following ciprofloxacin treatment only on the Western diet. Metatranscriptomic data showed decreased abundance of transcripts from the TCA cycle after antibiotic treatment in both diets, suggesting that this response is diet independent, which is consistent with previous *in vitro* findings that demonstrate a key role for bacterial respiration as a determinant of fluoroquinolone susceptibility (27, 28, 77, 94, 96–98). Conversely, the impact of ciprofloxacin on the abundance of various iron and mucin utilization transcripts differed between diets. Lastly, we detected species-specific transcriptional changes in two important commensal bacteria, *B. thetaiotaomicron* and *A. muciniphila*. In addition to detecting changes in transcript levels that were reflective of stress responses, we also observed differential expression in transcripts involved in diverse cellular processes such as nutrient acquisition, carbon metabolism, and capsular polysaccharide (CPS) biosynthesis. Together, our findings supported our hypothesis that the Western diet would modify the metabolic capacity of the gut microbiome and that this change would directly translate to differential activity in response to ciprofloxacin treatment.

Despite the advantages of a multi-omic approach, there are several drawbacks to these techniques that complicate interpretation of the results. First, our study was performed only in female mice. It is now understood that sex-dependent differences exist in diet metabolism, mucosal immunity, and gut microbiome antibiotic responses, and as such our findings may not be generalizable to males (96, 99, 100). Another critical drawback is that the analytical pipelines used to analyze microbiome data are reliant on existing databases that are largely incomplete: approximately half of all genes within the human gut microbiome are hypothesized to have no functional annotation, limiting the ability to accurately profile the transcriptional activity of these communities (101). Additionally, inferring biological significance of taxonomic changes is often difficult in many microbiome analyses. 16S amplicon sequencing and shotgun metagenomics are inherently limited to reporting relative abundances and thus may fail to fully characterize changes in absolute abundance. Thus, we cannot comment on how diet or antibiotics change the total number of bacteria found in the gut, nor can we determine if the bloom in *Firmicutes* is a result of an increase in colony-forming units or a reduction of other bacteria relative to *Firmicutes*. Due to the complex nature of these communities, it is challenging to ascertain if the observed transcriptional changes are the result of the direct action of the antibiotic or the indirect effect of changes in host physiology, nutrient availability, or the disruption of ecological networks within the microbiome. For example, our transcriptional analysis of *B. thetaiotaomicron* showed that this bacterium differentially expressed receptors for both heme and vitamin B₁₂, which may suggest that these nutrients play a role in ciprofloxacin toxicity. Alternatively, it is possible that these transcriptional changes are reflective of increased availability of these nutrients due to decreased competition from other members of the microbiota. Further, dietary composition could play a significant role in antibiotic absorption or sequestration in the gut, which in turn would impact the extent of the damage caused to the microbiota.

This study builds on recent work that demonstrates that the availability of metabolites plays an important role in determining the extent of antibiotic-induced microbiome disruption (19). Taken together, these results demonstrate the need to consider dietary composition in the design and interpretation of experiments focused on understanding the impact of antibiotics on the microbiota. Previous studies have demonstrated that dietary changes induce rapid shifts in gut microbiome composition (32, 34, 43, 56, 97, 98, 102, 103). Therefore, in the long term, dietary modulation could represent an attractive strategy to reduce the collateral damage to commensal bacteria and the resulting complications from dysbiosis caused by clinical therapy. Despite these promising applications, considerable work is required before these findings have direct

clinical relevance. In particular, the considerable differences in physiology, microbiome composition, and diet between humans and rodents complicate the direct clinical relevance of these findings. Furthermore, it is unclear whether short-term dietary modulation has any long-term consequences on either the host or the microbiome. Thus, additional research is warranted to fully elucidate how host diet impacts antibiotic-induced microbiome disruption in humans and how specific dietary formulation will impact these disruptions.

MATERIALS AND METHODS

Animal procedures. All animal work was approved by Brown University's Institutional Animal Care and Use Committee (IACUC) under protocol number 1706000283. Four-week-old female C57BL/6J mice were purchased from Jackson Laboratories (Bar Harbor, ME, USA) and given a 2-week habituation period immediately following arrival at Brown University's Animal Care Facility. After habituation, mice were switched from standard chow (Laboratory Rodent Diet 5001; St. Louis, MO, USA) to either a Western diet (D12079B; Research Diets Inc., New Brunswick, NJ, USA) or a macronutrient-defined control diet (D12450B; Research Diets Inc., New Brunswick, NJ, USA) for 1 week (see Data Set S7, Sheet 41, in the supplemental material). On the 8th day of dietary intervention, mice were given acidified ciprofloxacin (12.5 mg/kg of body weight/day), or a pH-adjusted vehicle, via filter-sterilized drinking water *ad libitum* for 24 h ($n = 8$ to 12 per treatment group). Water consumption was monitored to ensure equal consumption across cages. Mice were then sacrificed and dissected in order to collect cecal contents. Cecal contents were immediately transferred to ZymoBIOMICS DNA/RNA Miniprep kit (Zymo Research, Irvine, CA, USA) collection tubes containing DNA/RNA Shield. Tubes were processed via vortexing at maximum speed for 5 min to homogenize cecal contents and then placed on ice until permanent storage at -80°C .

Nucleic acid extraction and purification. Total nucleic acids (DNA and RNA) were extracted from samples using the ZymoBIOMICS DNA/RNA Miniprep kit from Zymo Research (R2002; Irvine, CA, USA) using the parallel extraction protocol per the manufacturer's instructions. Total RNA and DNA were eluted in nuclease-free water and quantified using the dsDNA-HS and RNA-HS kits on a Qubit 3.0 fluorometer (Thermo Fisher Scientific, Waltham, MA, USA) before use in library preparations.

16S rRNA amplicon preparation and sequencing. The 16S rRNA V4 hypervariable region was amplified from total DNA using the barcoded 518F forward primer and the 816Rb reverse primers from the Earth Microbiome Project (104). Amplicons were generated using 5 \times Phusion high-fidelity DNA polymerase under the following cycling conditions: initial denaturation at 98°C for 30 s, followed by 25 cycles of 98°C for 10 s, 57°C for 30 s, and 72°C for 30 s, and then a final extension at 72°C for 5 min. After amplification, samples were pooled in equimolar amounts and visualized via gel electrophoresis. The pooled amplicon library was submitted to the Rhode Island Genomics and Sequencing Center at the University of Rhode Island (Kingston, RI, USA) for sequencing on the Illumina MiSeq platform. Amplicons were pair-end sequenced (2×250 bp) using the 500-cycle kit with standard protocols. We obtained an average of $106,135 \pm 49,789$ reads per sample.

Analysis of 16S rRNA sequencing reads. Raw 16S rRNA reads were subjected to quality filtering, trimming, denoising, and merging using the DADA2 package (version 1.8.0) in R (version 3.5.0). Ribosomal sequence variants were assigned taxonomy using the RDP Classifier algorithm with RDP Training set 16 using the *assignTaxonomy* function in DADA2 (105). Alpha diversity (Shannon) and beta diversity (Bray-Curtis dissimilarity) were calculated using the phyloseq package (version 1.24.2) in R (version 3.5.0).

Metagenomic and metatranscriptomic library preparation. Metagenomic libraries were prepared from DNA (100 ng) using the NEBNext Ultra II FS DNA library prep kit (New England BioLabs, Ipswich, MA, USA) >100-ng input protocol per the manufacturer's instructions. This yielded a pool of 200- to 1,000-bp fragments where the average library was 250 to 500 bp. Metatranscriptomic libraries were prepared from total RNA using the NEBNext Ultra II Directional RNA sequencing prep kit (New England BioLabs, Ipswich, MA, USA) in conjunction with the NEBNext rRNA depletion kit for human/mouse/rat (New England BioLabs, Ipswich, MA, USA) and the MICROBExpress kit (Invitrogen, Carlsbad, CA, USA). First, up to 1 μg of total RNA was treated with recombinant DNase I (rDNase I) and subsequently depleted of bacterial rRNAs using MICROBExpress per the manufacturer's instructions. This depleted RNA was then used to prepare libraries with the NEBNext Ultra II Directional RNA sequencing prep and rRNA depletion kits per the manufacturer's instructions. This yielded libraries that averaged between 200 and 450 bp. Once library preparation was complete, both metagenomic and metatranscriptomic libraries were sequenced as paired-end 150-bp reads on an Illumina HiSeq X Ten. We sequenced an average of 2,278,948,631 ($\pm 2,309,494,556$) bases per metagenomic sample and 14,751,606,319 ($\pm 3,089,205,166$) bases per metatranscriptomic sample. One metagenomic sample from the Western diet + vehicle group had an abnormally low number of bases sequenced (165,000 bp) and was excluded from all subsequent analyses. Following the removal of this sample, we obtained an average of 2,430,867,540 ($\pm 2,306,317,898$) bases per metagenomic sample.

Processing of raw metagenomic and metatranscriptomic reads. Raw metagenomic reads were trimmed and decontaminated using the kneaddata utility (version 0.6.1) (106). In brief, reads were first trimmed to remove low-quality bases and Illumina TruSeq3 adapter sequences using Trimmomatic (version 0.36) using a SLIDINGWINDOW value of 4:20 and an ILLUMINACLIP value of 2:20:10, respectively (107). Trimmed reads shorter than 75 bases were discarded. Reads passing quality control were

subsequently decontaminated by removing those that mapped to the genome of C57BL/6J mice using bowtie2 (version 2.2) (108). Additionally, preliminary work by our group detected high levels of reads mapping to two murine retroviruses found in our animal facility: murine mammary tumor virus (MMTV, accession [NC_001503](#)) and murine osteosarcoma viruses (MOV, accession [NC_001506.1](#)) (19). Raw metatranscriptomic reads were trimmed and decontaminated using the same parameters. However, in addition to removing reads that mapped to the C57BL/6J, MMTV, and MOV genomes, we also decontaminated sequences that aligned to the SILVA 128 LSU and SSU Parc rRNA databases (109).

Taxonomic classification of metagenomic reads. Trimmed and decontaminated metagenomic reads were taxonomically classified against a database containing all bacterial and archaeal genomes found in NCBI RefSeq using Kraken2 (version 2.0.7-beta) with a default k-mer length of 35 (110). Phylum- and species-level abundances were subsequently calculated from Kraken2 reports using Bracken (version 2.0.0) with default settings (111). The phyloseq package (version 1.28.0) in R (version 3.6.0) was used to calculate alpha diversity using the Shannon diversity index (112). Metagenomic data were not subsampled prior to analysis.

To perform differential abundance testing, species-level taxonomic output was first filtered to remove taxa that were not observed in >1,000 reads (corresponding to approximately 0.1% of all reads) in at least 20% of all samples using phyloseq in R. Differential abundance testing was subsequently performed on filtered counts using the DESeq2 package (version 1.24.0) using default parameters (74). All *P* values were corrected for multiple hypothesis testing using the Benjamini-Hochberg method (113).

Annotation of metatranscriptomic reads using SAMSA2. Trimmed and decontaminated metatranscriptomic reads were annotated using a modified version of the Simple Annotation of Metatranscriptomes by Sequence Analysis 2 (SAMSA2) pipeline as described previously (19, 63, 114). First, the Paired-End Read Merger (PEAR) utility was used to merge forward and reverse reads (115). Merged reads were then aligned to databases containing entries from the RefSeq, SEED Subsystems, and CAZyme databases using DIAMOND (version 0.9.12) (116–118). The resulting alignment counts were subsequently analyzed using DESeq2 (version 1.24.0) using the Benjamini-Hochberg method to perform multiple hypothesis testing correction (19, 63, 113). Features with an adjusted *P* value of less than 0.05 were considered to be statistically significant.

Metatranscriptomic analysis using HUMAnN2. To determine the impact of dietary modulation and ciprofloxacin treatment on gene expression within the gut microbiome, we used the HMP Unified Metabolic Analysis Network 2 (HUMAnN2, version 0.11.1) pipeline (64). First, metagenomic reads were taxonomically annotated using MetaPhlan2 (version 2.6.0) and functionally annotated against the UniRef90 database to generate gene family and MetaCyc pathway-level abundances. To ensure consistent assignment between paired samples, the taxonomic profile generated from the metagenomic reads was supplied to the HUMAnN2 algorithm during the analysis of the corresponding metatranscriptomic reads. Metatranscriptomic reads were subsequently annotated as done for metagenomic reads. The resulting gene family and pathway-level abundance data from the metatranscriptomic reads were normalized against the metagenomic data from the corresponding sample and smoothed using the Witten-Bell method (119). Lastly, the resulting RPKM (reads per kilobase per million) values were unstratified to obtain whole-community level data, converted into relative abundances, and analyzed using LEfSe (version 1) hosted on the Galaxy web server (120).

Transcriptional analysis of *A. muciniphila* and *B. thetaiotaomicron*. A modified version of a previously published pipeline from Deng et al. was utilized to perform transcriptional analysis of individual species within the murine microbiome during dietary modulation and antibiotic treatment (19, 80). First, Kraken2 (version 2.0.7-beta) was used to identify the 50 most prevalent bacterial species present within the metatranscriptomic samples (110). Next, the BBSplit utility within the BBMap package (version 37.96) was used to extract reads within our metatranscriptomic data set that mapped to these 50 most abundant species (121). Reads from *B. thetaiotaomicron*, *A. muciniphila*, and *C. scindens* were subsequently aligned to their corresponding reference genomes using the BWA-MEM algorithm (version 0.7.15) (122). Lastly, the featureCounts command within the subread program (version 1.6.2) was used to analyze the resulting alignment files to generate a count table for differential expression analysis with DESeq2 (74). All *P* values were corrected for multiple hypothesis testing with the Benjamini-Hochberg method (113). Features with an adjusted *P* value of less than 0.05 were considered to be statistically significant.

Data availability. The data sets generated and analyzed during this study are available from the NCBI Sequence Read Archive (SRA) under BioProject accession numbers [PRJNA563913](#) (metagenomics and metatranscriptomics) and [PRJNA594642](#) (16S rRNA amplicon sequences). Any additional information is available from the corresponding author upon request.

SUPPLEMENTAL MATERIAL

Supplemental material is available online only.

FIG S1, PDF file, 0.2 MB.

FIG S2, PDF file, 0.5 MB.

FIG S3, PDF file, 0.4 MB.

DATA SET S1, XLS file, 0.05 MB.

DATA SET S2, XLS file, 0.1 MB.

DATA SET S3, XLS file, 0.04 MB.

DATA SET S4, XLS file, 5.5 MB.

DATA SET S5, XLS file, 0.4 MB.

DATA SET S6, XLS file, 1.8 MB.

DATA SET S7, XLS file, 4.5 MB.

ACKNOWLEDGMENTS

D.J.C., J.I.W., B.J.K., and S.P. were supported by the Graduate Research Fellowship Program from the National Science Foundation under award number 1644760. P.B. was supported by the U.S. Department of Defense through the Peer Reviewed Medical Research Program under award number W81XWH-18-1-0198, by the National Center for Complementary & Integrative Health of the NIH under award number R21AT010366, and by institutional development awards P20GM121344 and P20GM109035 received from the National Institute of General Medical Sciences. The funding agencies had no role in the design of the study or the collection, analysis, and interpretation of data.

We specifically thank Caroline D. Keroack for her thoughtful feedback during the editing process.

We declare that we have no competing interests.

D.J.C. planned the study, performed mouse experiments, extracted nucleic acids from cecal samples, conducted analysis of 16S rRNA amplicon, metagenomic, and metatranscriptomic data, and cowrote the manuscript. J.I.W. assisted with mouse experiments, prepared DNA and RNA into sequencing libraries for metagenomics and metatranscriptomics, conducted analysis of metatranscriptomic data, assisted in the interpretation of results, and cowrote the manuscript. B.J.K. assisted with the analysis of metatranscriptomic data. S.P. assisted in the interpretation of results. P.B. conceptualized and planned the study, contributed to the writing of the manuscript, and secured funding. All authors have read and approved of the final manuscript.

REFERENCES

- Rowan-Nash AD, Korry BJ, Mylonakis E, Belenky P. 2019. Cross-domain and viral interactions in the microbiome. *Microbiol Mol Biol Rev* 83: 51–63. <https://doi.org/10.1128/MMBR.00044-18>.
- Gilbert JA, Blaser MJ, Caporaso JG, Jansson JK, Lynch SV, Knight R. 2018. Current understanding of the human microbiome. *Nat Med* 24: 392–400. <https://doi.org/10.1038/nm.4517>.
- Ursell LK, Metcalf JL, Parfrey LW, Knight R. 2012. Defining the human microbiome. *Nutr Rev* 70:S38–S44. <https://doi.org/10.1111/j.1753-4887.2012.00493.x>.
- Mukherjee PK, Chandra J, Retuerto M, Sikaroodi M, Brown RE, Jurevic R, Salata RA, Lederman MM, Gillevet PM, Ghannoum MA. 2014. Oral mycobiome analysis of HIV-infected patients: identification of *Pichia* as an antagonist of opportunistic fungi. *PLoS Pathog* 10:e1003996. <https://doi.org/10.1371/journal.ppat.1003996>.
- Peleg AY, Hogan DA, Mylonakis E. 2010. Medically important bacterial-fungal interactions. *Nat Rev Microbiol* 8:340–349. <https://doi.org/10.1038/nrmicro2313>.
- De Luca F, Shoenfeld Y. 2019. The microbiome in autoimmune diseases. *Clin Exp Immunol* 195:74–85. <https://doi.org/10.1111/cei.13158>.
- Dickerson F, Severance E, Yolken R. 2017. The microbiome, immunity, and schizophrenia and bipolar disorder. *Brain Behav Immun* 62:46–52. <https://doi.org/10.1016/j.bbi.2016.12.010>.
- Foster JA, Neufeld K-A. 2013. Gut-brain axis: how the microbiome influences anxiety and depression. *Trends Neurosci* 36:305–312. <https://doi.org/10.1016/j.tins.2013.01.005>.
- Hartstra AV, Bouter KEC, Bäckhed F, Nieuwdorp M. 2015. Insights into the role of the microbiome in obesity and type 2 diabetes. *Diabetes Care* 38:159–165. <https://doi.org/10.2337/dc14-0769>.
- Leong KSW, Derraik JGB, Hofman PL, Cutfield WS. 2018. Antibiotics, gut microbiome and obesity. *Clin Endocrinol (Oxf)* 88:185–200. <https://doi.org/10.1111/cen.13495>.
- Lynch SV, Boushey HA. 2016. The microbiome and development of allergic disease. *Curr Opin Allergy Clin Immunol* 16:165–171. <https://doi.org/10.1097/ACI.0000000000000255>.
- Riiser A. 2015. The human microbiome, asthma, and allergy. *Allergy Asthma Clin Immunol* 11:35. <https://doi.org/10.1186/s13223-015-0102-0>.
- Rogers MB, Firek B, Shi M, Yeh A, Brower-Sinning R, Aveson V, Kohl BL, Fabio A, Carcillo JA, Morowitz MJ. 2016. Disruption of the microbiota across multiple body sites in critically ill children. *Microbiome* 4:66. <https://doi.org/10.1186/s40168-016-0211-0>.
- Tremlett H, Bauer KC, Appel-Cresswell S, Finlay BB, Waubant E. 2017. The gut microbiome in human neurological disease: a review. *Ann Neurol* 81:369–382. <https://doi.org/10.1002/ana.24901>.
- Vieira SM, Pagovich OE, Kriegel MA. 2014. Diet, microbiota and autoimmune diseases. *Lupus* 23:518–526. <https://doi.org/10.1177/0961203313501401>.
- Stiemsma LT, Michels KB. 2018. The role of the microbiome in the developmental origins of health and disease. *Pediatrics* 141:e20172437. <https://doi.org/10.1542/peds.2017-2437>.
- Blaser M. 2011. Antibiotic overuse: stop the killing of beneficial bacteria. *Nature* 476:393–394. <https://doi.org/10.1038/476393a>.
- Dethlefsen L, Relman DA. 2011. Incomplete recovery and individualized responses of the human distal gut microbiota to repeated antibiotic perturbation. *Proc Natl Acad Sci U S A* 108(Suppl 1):4554–4561. <https://doi.org/10.1073/pnas.1000087107>.
- Cabral DJ, Penumatchu S, Reinhart EM, Zhang C, Korry BJ, Wurster JI, Nilson R, Guang A, Sano WH, Rowan-Nash AD, Li H, Belenky P. 2019. Microbial metabolism modulates antibiotic susceptibility within the murine gut microbiome. *Cell Metab* 30:800–823.e7. <https://doi.org/10.1016/j.cmet.2019.08.020>.
- Chang JY, Antonopoulos DA, Kalra A, Tonelli A, Khalife WT, Schmidt TM, Young VB. 2008. Decreased diversity of the fecal microbiome in recurrent *Clostridium difficile*-associated diarrhea. *J Infect Dis* 197:435–438. <https://doi.org/10.1086/525047>.
- Preidis GA, Versalovic J. 2009. Targeting the human microbiome with antibiotics, probiotics, and prebiotics: gastroenterology enters the metagenomics era. *Gastroenterology* 136:2015–2031. <https://doi.org/10.1053/j.gastro.2009.01.072>.
- Theriot CM, Bowman AA, Young VB. 2016. Antibiotic-induced alterations of the gut microbiota alter secondary bile acid production and allow for *Clostridium difficile* spore germination and outgrowth in the large intestine. *mSphere* 1:e00045-15. <https://doi.org/10.1128/mSphere.00045-15>.
- Rea MC, Dobson A, O'Sullivan O, Crispie F, Fouhy F, Cotter PD, Shana-

- han F, Kiely B, Hill C, Ross RP. 2011. Effect of broad- and narrow-spectrum antimicrobials on *Clostridium difficile* and microbial diversity in a model of the distal colon. *Proc Natl Acad Sci U S A* 108:4639–4644. <https://doi.org/10.1073/pnas.1001224107>.
24. Rafii F, Sutherland JB, Cerniglia CE. 2008. Effects of treatment with antimicrobial agents on the human colonic microflora. *Ther Clin Risk Manag* 4:1343–1357. <https://doi.org/10.2147/tcr.m.s4328>.
 25. Lessa FC, Mu Y, Bamberg WM, Beldavs ZG, Dumyati GK, Dunn JR, Farley MM, Holzbauer SM, Meek JI, Phipps EC, Wilson LE, Winston LG, Cohen JA, Limbago BM, Fridkin SK, Gerding DN, McDonald LC. 2015. Burden of *Clostridium difficile* infection in the United States. *N Engl J Med* 372:825–834. <https://doi.org/10.1056/NEJMoa1408913>.
 26. Hryckowian AJ, Van Treuren W, Smits SA, Davis NM, Gardner JO, Bouley DM, Sonnenburg JL. 2018. Microbiota-accessible carbohydrates suppress *Clostridium difficile* infection in a murine model. *Nat Microbiol* 3:662–669. <https://doi.org/10.1038/s41564-018-0150-6>.
 27. Belenky P, Ye JD, Porter CBM, Cohen NR, Lobritz MA, Ferrante T, Jain S, Korry BJ, Schwarz EG, Walker GC, Collins JJ. 2015. Bactericidal antibiotics induce toxic metabolic perturbations that lead to cellular damage. *Cell Rep* 13:968–980. <https://doi.org/10.1016/j.celrep.2015.09.059>.
 28. Lobritz MA, Belenky P, Porter CBM, Gutierrez A, Yang JH, Schwarz EG, Dwyer DJ, Khalil AS, Collins JJ. 2015. Antibiotic efficacy is linked to bacterial cellular respiration. *Proc Natl Acad Sci U S A* 112:8173–8180. <https://doi.org/10.1073/pnas.1509743112>.
 29. Dwyer DJ, Belenky PA, Yang JH, MacDonald IC, Martell JD, Takahashi N, Chan CTY, Lobritz MA, Braff D, Schwarz EG, Ye JD, Pati M, Vercruysse M, Ralifo PS, Allison KR, Khalil AS, Ting AY, Walker GC, Collins JJ. 2014. Antibiotics induce redox-related physiological alterations as part of their lethality. *Proc Natl Acad Sci U S A* 111:E2100–E2109. <https://doi.org/10.1073/pnas.1401876111>.
 30. Schnitzlein MK, Vendrov KC, Edwards SJ, Martens EC, Young VB. 2020. Dietary xanthan gum alters antibiotic efficacy against the murine gut microbiota and attenuates *Clostridioides difficile* colonization. *mSphere* 5:e00708-19. <https://doi.org/10.1128/mSphere.00708-19>.
 31. Smits SA, Leach J, Sonnenburg ED, Gonzalez CG, Lichtman JS, Reid G, Knight R, Manjurova A, Chagalucha J, Elias JE, Dominguez-Bello MG, Sonnenburg JL. 2017. Seasonal cycling in the gut microbiome of the Hadza hunter-gatherers of Tanzania. *Science* 357:802–806. <https://doi.org/10.1126/science.aan4834>.
 32. Bisanz JE, Upadhyay V, Turnbaugh JA, Ly K, Turnbaugh PJ. 2019. Meta-analysis reveals reproducible gut microbiome alterations in response to a high-fat diet. *Cell Host Microbe* 26:265–272.e4. <https://doi.org/10.1016/j.chom.2019.06.013>.
 33. Ley RE, Backhed F, Turnbaugh P, Lozupone CA, Knight RD, Gordon JL. 2005. Obesity alters gut microbial ecology. *Proc Natl Acad Sci U S A* 102:11070–11075. <https://doi.org/10.1073/pnas.0504978102>.
 34. Turnbaugh PJ, Ridaura VK, Faith JJ, Rey FE, Knight R, Gordon JL. 2009. The effect of diet on the human gut microbiome: a metagenomic analysis in humanized gnotobiotic mice. *Sci Transl Med* 1:6ra14. <https://doi.org/10.1126/scitranslmed.3000322>.
 35. Xu Z, Knight R. 2015. Dietary effects on human gut microbiome diversity. *Br J Nutr* 113:S1–S5. <https://doi.org/10.1017/S0007114514004127>.
 36. Argueta DA, DiPatrizio NV. 2017. Peripheral endocannabinoid signaling controls hyperphagia in western diet-induced obesity. *Physiol Behav* 171:32–39. <https://doi.org/10.1016/j.physbeh.2016.12.044>.
 37. Kanoski SE, Hsu TM, Pennell S. 2014. Obesity, Western diet intake, and cognitive impairment, p 57–62. In Watson RR, De Meester F (ed), *Omega-3 fatty acids in brain and neurological health*. Elsevier, San Diego, CA.
 38. Sami W, Ansar T, Butt NS, Hamid M. 2017. Effect of diet on type 2 diabetes mellitus: a review. *Int J Health Sci* 11:65–71.
 39. Qi L, Cornelis MC, Zhang C, van Dam RM, Hu FB. 2009. Genetic predisposition, Western dietary pattern, and the risk of type 2 diabetes in men. *Am J Clin Nutr* 89:1453–1458. <https://doi.org/10.3945/ajcn.2008.27249>.
 40. Sonnenburg ED, Sonnenburg JL. 2014. Starving our microbial self: the deleterious consequences of a diet deficient in microbiota-accessible carbohydrates. *Cell Metab* 20:779–786. <https://doi.org/10.1016/j.cmet.2014.07.003>.
 41. Sonnenburg ED, Sonnenburg JL. 2019. The ancestral and industrialized gut microbiota and implications for human health. *Nat Rev Microbiol* 17:383–390. <https://doi.org/10.1038/s41579-019-0191-8>.
 42. Sonnenburg JL, Xu J, Leip DD, Chen C-H, Westover BP, Weatherford J, Buhler JD, Gordon JL. 2005. Glycan foraging in vivo by an intestine-adapted bacterial symbiont. *Science* 307:1955–1959. <https://doi.org/10.1126/science.1109051>.
 43. Turnbaugh PJ. 2017. Microbes and diet-induced obesity: fast, cheap, and out of control. *Cell Host Microbe* 21:278–281. <https://doi.org/10.1016/j.chom.2017.02.021>.
 44. Trompette A, Gollwitzer ES, Yadava K, Sichelstiel AK, Sprenger N, Ngom-Bru C, Blanchard C, Junt T, Nicod LP, Harris NL, Marsland BJ. 2014. Gut microbiota metabolism of dietary fiber influences allergic airway disease and hematopoiesis. *Nat Med* 20:159–166. <https://doi.org/10.1038/nm.3444>.
 45. Arpaia N, Campbell C, Fan X, Dikiy S, van der Veen J, deRoos P, Liu H, Cross JR, Pfeffer K, Coffey PJ, Rudensky AY. 2013. Metabolites produced by commensal bacteria promote peripheral regulatory T-cell generation. *Nature* 504:451–455. <https://doi.org/10.1038/nature12726>.
 46. Cotillard A, Kennedy SP, Kong LC, Prifti E, Pons N, Le Chatelier E, Almeida M, Quinquis B, Levenez F, Galleron N, Gougis S, Rizkalla S, Batto J-M, Renault P, ANR MicroObes consortium, Doré J, Zucker J-D, Clément K, Ehrlich SD. 2013. Dietary intervention impact on gut microbial gene richness. *Nature* 500:585–588. <https://doi.org/10.1038/nature12480>.
 47. Walker AW, Ince J, Duncan SH, Webster LM, Holtrop G, Ze X, Brown D, Stares MD, Scott P, Bergerat A, Louis P, McIntosh F, Johnstone AM, Lobley GE, Parkhill J, Flint HJ. 2011. Dominant and diet-responsive groups of bacteria within the human colonic microbiota. *ISME J* 5:220–230. <https://doi.org/10.1038/ismej.2010.118>.
 48. Fischbach MA, Sonnenburg JL. 2011. Eating for two: how metabolism establishes interspecies interactions in the gut. *Cell Host Microbe* 10:336–347. <https://doi.org/10.1016/j.chom.2011.10.002>.
 49. Kashyap PC, Marcobal A, Ursell LK, Smits SA, Sonnenburg ED, Costello EK, Higginbottom S, Domino SE, Holmes SP, Relman DA, Knight R, Gordon JL, Sonnenburg JL. 2013. Genetically dictated change in host mucus carbohydrate landscape exerts a diet-dependent effect on the gut microbiota. *Proc Natl Acad Sci U S A* 110:17059–17064. <https://doi.org/10.1073/pnas.1306070110>.
 50. Yatsunenkov T, Rey FE, Manary MJ, Trehan I, Dominguez-Bello MG, Contreras M, Magris M, Hidalgo G, Baldassano RN, Anokhin AP, Heath AC, Warner B, Reeder J, Kuczynski J, Caporaso JG, Lozupone CA, Lauber C, Clemente JC, Knights D, Knight R, Gordon JL. 2012. Human gut microbiome viewed across age and geography. *Nature* 486:222–227. <https://doi.org/10.1038/nature11053>.
 51. Wong JMW, de Souza R, Kendall CWC, Emam A, Jenkins D. 2006. Colonic health: fermentation and short chain fatty acids. *J Clin Gastroenterol* 40:235–243. <https://doi.org/10.1097/00004836-200603000-00015>.
 52. Topping DL, Clifton PM. 2001. Short-chain fatty acids and human colonic function: roles of resistant starch and nonstarch polysaccharides. *Physiol Rev* 81:1031–1034. <https://doi.org/10.1152/physrev.2001.81.3.1031>.
 53. Macfarlane S, Macfarlane GT. 2003. Regulation of short-chain fatty acid production. *Proc Nutr Soc* 62:67–72. <https://doi.org/10.1079/PNS2002207>.
 54. Cani PD, Van Hul M, Lefort C, Depommier C, Rastelli M, Everard A. 2019. Microbial regulation of organismal energy homeostasis. *Nat Metab* 1:34–46. <https://doi.org/10.1038/s42255-018-0017-4>.
 55. Chambers ES, Preston T, Frost G, Morrison DJ. 2018. Role of gut microbiota-generated short-chain fatty acids in metabolic and cardiovascular health. *Curr Nutr Rep* 7:198–206. <https://doi.org/10.1007/s13668-018-0248-8>.
 56. David LA, Maurice CF, Carmody RN, Gootenberg DB, Button JE, Wolfe BE, Ling AV, Devlin AS, Varna Y, Fischbach MA, Biddinger SB, Dutton RJ, Turnbaugh PJ. 2014. Diet rapidly and reproducibly alters the human gut microbiome. *Nature* 505:559–563. <https://doi.org/10.1038/nature12820>.
 57. Desai MS, Seekatz AM, Koropatkin NM, Kamada N, Hickey CA, Wolter M, Pudlo NA, Kitamoto S, Terrapon N, Muller A, Young VB, Henrissat B, Wilmes P, Stappenbeck TS, Núñez G, Martens EC. 2016. A dietary fiber-deprived gut microbiota degrades the colonic mucus barrier and enhances pathogen susceptibility. *Cell* 167:1339–1353.e21. <https://doi.org/10.1016/j.cell.2016.10.043>.
 58. Poretsky R, Rodriguez-R LM, Luo C, Sementzi D, Konstantinidis KT. 2014. Strengths and limitations of 16S rRNA gene amplicon sequencing in revealing temporal microbial community dynamics. *PLoS One* 9:e93827. <https://doi.org/10.1371/journal.pone.0093827>.
 59. Ranjan R, Rani A, Metwally A, McGee HS, Perkins DL. 2016. Analysis of the microbiome: advantages of whole genome shotgun versus 16S amplicon sequencing. *Biochem Biophys Res Commun* 469:967–977. <https://doi.org/10.1016/j.bbrc.2015.12.083>.

60. Clooney AG, Fouhy F, Sleator RD, O'Driscoll A, Stanton C, Cotter PD, Claessens MJ. 2016. Comparing apples and oranges?: next generation sequencing and its impact on microbiome analysis. *PLoS One* 11: e0148028. <https://doi.org/10.1371/journal.pone.0148028>.
61. Tessler M, Neumann JS, Afshinnekoo E, Pineda M, Hersch R, Velho LFM, Segovia BT, Lansac-Toha FA, Lemke M, DeSalle R, Mason CE, Brugler MR. 2017. Large-scale differences in microbial biodiversity discovery between 16S amplicon and shotgun sequencing. *Sci Rep* 7:6589. <https://doi.org/10.1038/s41598-017-06665-3>.
62. Shin N-R, Whon TW, Bae J-W. 2015. Proteobacteria: microbial signature of dysbiosis in gut microbiota. *Trends Biotechnol* 33:496–503. <https://doi.org/10.1016/j.tibtech.2015.06.011>.
63. Westreich ST, Treiber ML, Mills DA, Korf I, Lemay DG. 2018. SAMSA2: a standalone metatranscriptome analysis pipeline. *BMC Bioinformatics* 19:175. <https://doi.org/10.1186/s12859-018-2189-z>.
64. Franzosa EA, McIver LJ, Rahnavard G, Thompson LR, Schirmer M, Weingart G, Lipson KS, Knight R, Caporaso JG, Segata N, Huttenhower C. 2018. Species-level functional profiling of metagenomes and metatranscriptomes. *Nat Methods* 15:962–968. <https://doi.org/10.1038/s41592-018-0176-y>.
65. Odom AR. 2011. Five questions about non-mevalonate isoprenoid biosynthesis. *PLoS Pathog* 7:e1002323. <https://doi.org/10.1371/journal.ppat.1002323>.
66. Gill SR, Pop M, DeBoy RT, Eckburg PB, Turnbaugh PJ, Samuel BS, Gordon JL, Relman DA, Fraser-Liggett CM, Nelson KE. 2006. Metagenomic analysis of the human distal gut microbiome. *Science* 312: 1355–1359. <https://doi.org/10.1126/science.1124234>.
67. Corfield AP, Wagner SA, Clamp JR, Kriaris MS, Hoskins LC. 1992. Mucin Degradation in the human colon: production of sialidase, sialate O-acetyltransferase, N-acetylneuraminidase, arylesterase, and glycosyltransferase activities by strains of fecal bacteria. *Infect Immun* 60: 3971–3978. <https://doi.org/10.1128/IAI.60.10.3971-3978.1992>.
68. Knoch E, Dilokpimol A, Geshi N. 2014. Arabinogalactan proteins: focus on carbohydrate active enzymes. *Front Plant Sci* 5:198–199. <https://doi.org/10.3389/fpls.2014.00198>.
69. Kaur R, Sharma M, Ji D, Xu M, Agyei D. 2020. Structural features, modification, and functionalities of beta-glucan. *Fibers* 8:1. <https://doi.org/10.3390/fib8010001>.
70. Eckardt NA. 2008. Role of xyloglucan in primary cell walls. *Plant Cell* 20:1421–1422. <https://doi.org/10.1105/tpc.108.061382>.
71. Hii SL, Tan JS, Ling TC, Ariff AB. 2012. Pullulanase: role in starch hydrolysis and potential industrial applications. *Enzyme Res* 2012: 921362. <https://doi.org/10.1155/2012/921362>.
72. Zhou J, Xiong X, Yin J, Zou L, Wang K, Shao Y, Yin Y. 2019. Dietary lysozyme alters sow's gut microbiota, serum immunity, and milk metabolite profile. *Front Microbiol* 10:177. <https://doi.org/10.3389/fmicb.2019.00177>.
73. Layman DK, Lönnérda B, Fernstrom JD. 2018. Applications for α -lactalbumin in human nutrition. *Nutr Rev* 76:444–460. <https://doi.org/10.1093/nutrit/nuy004>.
74. Love MI, Huber W, Anders S. 2014. Moderated estimation of fold change and dispersion for RNA-seq data with DESeq2. *Genome Biol* 15:550. <https://doi.org/10.1186/s13059-014-0550-8>.
75. Meylan S, Porter CBM, Yang JH, Belenky P, Gutierrez A, Lobritz MA, Park J, Kim SH, Moskowitz SM, Collins JJ. 2017. Carbon sources tune antibiotic susceptibility in *Pseudomonas aeruginosa* via tricarboxylic acid cycle control. *Cell Chem Biol* 24:195–206. <https://doi.org/10.1016/j.chembiol.2016.12.015>.
76. Mäkelä MR, DiFalco M, McDonnell E, Nguyen TTM, Wiebenga A, Hildén K, Peng M, Grigoriev IV, Tsang A, de Vries RP. 2018. Genomic and exoproteomic diversity in plant biomass degradation approaches among aspergilli. *Stud Mycol* 91:79–99. <https://doi.org/10.1016/j.simyco.2018.09.001>.
77. Lapébie P, Lombard V, Drula E, Terrapon N, Henrissat B. 2019. Bacteroidetes use thousands of enzyme combinations to break down glycans. *Nat Commun* 10:2043. <https://doi.org/10.1038/s41467-019-10068-5>.
78. Collins J, Robinson C, Danhof H, Knetsch CW, van Leeuwen HC, Lawley TD, Auchtung JM, Britton RA. 2018. Dietary trehalose enhances virulence of epidemic *Clostridium difficile*. *Nature* 553:291–294. <https://doi.org/10.1038/nature25178>.
79. Lee JJ, Lee S-K, Song N, Nathan TO, Swarts BM, Eum S-Y, Ehrst S, Cho S-N, Eoh H. 2019. Transient drug-tolerance and permanent drug-resistance rely on the trehalose-catalytic shift in *Mycobacterium tuberculosis*. *Nat Commun* 10:2928. <https://doi.org/10.1038/s41467-019-10975-7>.
80. Deng Z-L, Sztajer H, Jarek M, Bhujji S, Wagner-Döbler I. 2018. Worlds apart—transcriptome profiles of key oral microbes in the periodontal pocket compared to single laboratory culture reflect synergistic interactions. *Front Microbiol* 9:124. <https://doi.org/10.3389/fmicb.2018.00124>.
81. Susin MF, Baldini RL, Gueiros-Filho F, Gomes SL. 2006. GroES/GroEL and DnaK/DnaJ have distinct roles in stress responses and during cell cycle progression in *Caulobacter crescentus*. *J Bacteriol* 188:8044–8053. <https://doi.org/10.1128/JB.00824-06>.
82. Anglès F, Castanié-Cornet M-P, Slama N, Dinclaux M, Cirinesi A-M, Portais J-C, Létisse F, Genevaux P. 2017. Multilevel interaction of the DnaK/DnaJ(HSP70/HSP40) stress-responsive chaperone machine with the central metabolism. *Sci Rep* 7:41341. <https://doi.org/10.1038/srep41341>.
83. Ogata Y, Mizushima T, Kataoka K, Kita K, Miki T, Sekimizu K. 1996. DnaK heat shock protein of *Escherichia coli* maintains the negative supercoiling of DNA against thermal stress. *J Biol Chem* 271:29407–29414. <https://doi.org/10.1074/jbc.271.46.29407>.
84. Wong KS, Houry WA. 2012. Novel structural and functional insights into the MoxR family of AAA+ ATPases. *J Struct Biol* 179:211–221. <https://doi.org/10.1016/j.jsb.2012.03.010>.
85. Coyne MJ, Comstock LE. 2008. Niche-specific features of the intestinal Bacteroidales. *J Bacteriol* 190:736–742. <https://doi.org/10.1128/JB.01559-07>.
86. Porter NT, Canales P, Peterson DA, Martens EC. 2017. A subset of polysaccharide capsules in the human symbiont *Bacteroides thetaiotaomicron* promote increased competitive fitness in the mouse gut. *Cell Host Microbe* 22:494–506.e8. <https://doi.org/10.1016/j.chom.2017.08.020>.
87. Petit C, Rigg GP, Pazzani C, Smith A, Sieberth V, Stevens M, Boulnois G, Jann K, Roberts IS. 1995. Region 2 of the *Escherichia coli* K5 capsule gene cluster encoding proteins for the biosynthesis of the K5 polysaccharide. *Mol Microbiol* 17:611–620. <https://doi.org/10.1111/j.1365-2958.1995.mmi.17040611.x>.
88. van Selm S, Kolkman MAB, van der Zeijst BAM, Zwaagstra KA, Gastra V, van Putten J. 2002. Organization and characterization of the capsule biosynthesis locus of *Streptococcus pneumoniae* serotype. *Microbiology* 148:1747–1755. <https://doi.org/10.1099/00221287-148-6-1747>.
89. Dougherty BA, van de Rijn I. 1993. Molecular characterization of hasB from an operon required for hyaluronic acid synthesis in group A streptococci. *J Biol Chem* 268:7118–7124.
90. Cabral D, Wurster J, Belenky P. 2018. Antibiotic persistence as a metabolic adaptation: stress, metabolism, the host, and new directions. *Pharmaceuticals* 11:14–19. <https://doi.org/10.3390/ph11010014>.
91. Allison KR, Brynildsen MP, Collins JJ. 2011. Metabolite-enabled eradication of bacterial persisters by aminoglycosides. *Nature* 473:216–220. <https://doi.org/10.1038/nature10069>.
92. Kohanski MA, Dwyer DJ, Hayete B, Lawrence CA, Collins JJ. 2007. A common mechanism of cellular death induced by bactericidal antibiotics. *Cell* 130:797–810. <https://doi.org/10.1016/j.cell.2007.06.049>.
93. Chittesham Thomas V, Kinkead LC, Janssen A, Schaeffer CR, Woods KM, Lindgren JK, Peaster JM, Chaudhari SS, Sadykov M, Jones J, Mohamadi AbdelGhani SM, Zimmerman MC, Bayles KW, Somerville GA, Fey PD. 2013. A dysfunctional tricarboxylic acid cycle enhances fitness of *Staphylococcus epidermidis* during β -lactam stress. *mBio* 4:e00437-13. <https://doi.org/10.1128/mBio.00437-13>.
94. Adolfsen KJ, Brynildsen MP. 2015. Futile cycling increases sensitivity toward oxidative stress in *Escherichia coli*. *Metab Eng* 29:26–35. <https://doi.org/10.1016/j.ymben.2015.02.006>.
95. Cho H, Uehara T, Bernhardt TG. 2014. Beta-lactam antibiotics induce a lethal malfunctioning of the bacterial cell wall synthesis machinery. *Cell* 159:1300–1311. <https://doi.org/10.1016/j.cell.2014.11.017>.
96. Elderman M, Hugenholtz F, Belzer C, Boekschoten M, van Beek A, de Haan B, Savelkoul H, de Vos P, Faas M. 2018. Sex and strain dependent differences in mucosal immunology and microbiota composition in mice. *Biol Sex Differ* 9:26. <https://doi.org/10.1186/s13293-018-0186-6>.
97. Singh RK, Chang H-W, Yan D, Lee KM, Ucmak D, Wong K, Abrouk M, Farahnik B, Nakamura M, Zhu TH, Bhutani T, Liao W. 2017. Influence of diet on the gut microbiome and implications for human health. *J Transl Med* 15:73. <https://doi.org/10.1186/s12967-017-1175-y>.
98. Johnson AJ, Vangay P, Al-Ghalith GA, Hillmann BM, Ward TL, Shields-Cutler RR, Kim AD, Shmagel AK, Syed AN, Walter J, Menon R, Koecher K, Knights D, Personalized Microbiome Class Students. 2019. Daily sampling reveals personalized diet-microbiome associations in humans. *Cell Host Microbe* 25:789–802.e5. <https://doi.org/10.1016/j.chom.2019.05.005>.
99. Gao H, Shu Q, Chen J, Fan K, Xu P, Zhou Q, Li C, Zheng H. 2019.

- Antibiotic exposure has sex-dependent effects on the gut microbiota and metabolism of short-chain fatty acids and amino acids in mice. *mSystems* 4:e00048-19. <https://doi.org/10.1128/mSystems.00048-19>.
100. Ingvorsen C, Karp NA, Lelliott CJ. 2017. The role of sex and body weight on the metabolic effects of high-fat diet in C57BL/6N mice. *Nutr Diabetes* 7:e261. <https://doi.org/10.1038/nutd.2017.6>.
 101. The Human Microbiome Project Consortium. 2012. A framework for human microbiome research. *Nature* 486:215–221. <https://doi.org/10.1038/nature11209>.
 102. Turnbaugh PJ, Ley RE, Mahowald MA, Magrini V, Mardis ER, Gordon JL. 2006. An obesity-associated gut microbiome with increased capacity for energy harvest. *Nature* 444:1027–1031. <https://doi.org/10.1038/nature05414>.
 103. Turnbaugh PJ, Bäckhed F, Fulton L, Gordon JL. 2008. Diet-induced obesity is linked to marked but reversible alterations in the mouse distal gut microbiome. *Cell Host Microbe* 3:213–223. <https://doi.org/10.1016/j.chom.2008.02.015>.
 104. Thompson LR, Sanders JG, McDonald D, Amir A, Ladau J, Locey KJ, Prill RJ, Tripathi A, Gibbons SM, Ackermann G, Navas-Molina JA, Janssen S, Kopylova E, Vázquez-Baeza Y, González A, Morton JT, Mirarab S, Zech Xu Z, Jiang L, Haroon MF, Kanbar J, Zhu Q, Jin Song S, Kosciulek T, Bokulich NA, Lefler J, Brislawn CJ, Humphrey G, Owens SM, Hampton-Marcell J, Berg-Lyons D, McKenzie V, Fierer N, Fuhrman JA, Clausen A, Stevens RL, Shade A, Pollard KS, Goodwin KD, Jansson JK, Gilbert JA, Knight R, The Earth Microbiome Project Consortium. 2017. A communal catalogue reveals Earth's multiscale microbial diversity. *Nature* 551:457–463. <https://doi.org/10.1038/nature24621>.
 105. Wang Q, Garrity GM, Tiedje JM, Cole JR. 2007. Naive Bayesian classifier for rapid assignment of rRNA sequences into the new bacterial taxonomy. *Appl Environ Microbiol* 73:5261–5267. <https://doi.org/10.1128/AEM.00062-07>.
 106. Mclver LJ, Abu-Ali G, Franzosa EA, Schwager R, Morgan XC, Waldron L, Segata N, Huttenhower C. 2018. bioBakery: a meta'omic analysis environment. *Bioinformatics* 34:1235–1237. <https://doi.org/10.1093/bioinformatics/btx754>.
 107. Bolger AM, Lohse M, Usadel B. 2014. Trimmomatic: a flexible trimmer for Illumina sequence data. *Bioinformatics* 30:2114–2120. <https://doi.org/10.1093/bioinformatics/btu170>.
 108. Langmead B, Salzberg SL. 2012. Fast gapped-read alignment with Bowtie 2. *Nat Methods* 9:357–359. <https://doi.org/10.1038/nmeth.1923>.
 109. Pruesse E, Quast C, Knittel K, Fuchs BM, Ludwig W, Peplies J, Glockner FO. 2007. SILVA: a comprehensive online resource for quality checked and aligned ribosomal RNA sequence data compatible with ARB. *Nucleic Acids Res* 35:7188–7196. <https://doi.org/10.1093/nar/gkm864>.
 110. Wood DE, Salzberg SL. 2014. Kraken: ultrafast metagenomic sequence classification using exact alignments. *Genome Biol* 15:R46. <https://doi.org/10.1186/gb-2014-15-3-r46>.
 111. Lu J, Breitwieser FP, Thielen P, Salzberg SL. 2017. Bracken: estimating species abundance in metagenomics data. *PeerJ Comput Sci* 3:e104. <https://doi.org/10.7717/peerj-cs.104>.
 112. McMurdie PJ, Holmes S. 2013. phyloseq: an R package for reproducible interactive analysis and graphics of microbiome census data. *PLoS One* 8:e61217. <https://doi.org/10.1371/journal.pone.0061217>.
 113. Benjamini Y, Hochberg Y. 1995. Controlling the false discovery rate: a practical and powerful approach to multiple testing. *J R Stat Soc* 57:289–300. <https://doi.org/10.1111/j.2517-6161.1995.tb02031.x>.
 114. Westreich ST, Korf I, Mills DA, Lemay DG. 2016. SAMSA: a comprehensive metatranscriptome analysis pipeline. *BMC Bioinformatics* 17:399. <https://doi.org/10.1186/s12859-016-1270-8>.
 115. Zhang J, Kobert K, Flouri T, Stamatakis A. 2014. PEAR: a fast and accurate Illumina Paired-End reAd mergeR. *Bioinformatics* 30:614–620. <https://doi.org/10.1093/bioinformatics/btt593>.
 116. Overbeek R, Olson R, Pusch GD, Olsen GJ, Davis JJ, Disz T, Edwards RA, Gerdes S, Parrello B, Shukla M, Vonstein V, Wattam AR, Xia F, Stevens R. 2014. The SEED and the Rapid Annotation of microbial genomes using Subsystems Technology (RAST). *Nucleic Acids Res* 42:D206–D214. <https://doi.org/10.1093/nar/gkt1226>.
 117. Buchfink B, Xie C, Huson DH. 2015. Fast and sensitive protein alignment using DIAMOND. *Nat Methods* 12:59–60. <https://doi.org/10.1038/nmeth.3176>.
 118. Cantarel BL, Coutinho PM, Rancurel C, Bernard T, Lombard V, Henrissat B. 2009. The Carbohydrate-Active EnZymes database (CAZy): an expert resource for glycogenomics. *Nucleic Acids Res* 37:D233–D238. <https://doi.org/10.1093/nar/gkn663>.
 119. Witten IH, Bell TC. 1991. The zero-frequency problem: estimating the probabilities of novel events in adaptive text compression. *IEEE Trans Inf Theory* 37:1085–1094. <https://doi.org/10.1109/18.87000>.
 120. Segata N, Izard J, Waldron L, Gevers D, Miropolsky L, Garrett WS, Huttenhower C. 2011. Metagenomic biomarker discovery and explanation. *Genome Biol* 12:R60. <https://doi.org/10.1186/gb-2011-12-6-r60>.
 121. Bushnell B. 2014. BBMap: a fast, accurate, splice-aware aligner. Conf 9th Annu Genomics Energy Environ Meet, Walnut Creek, CA.
 122. Li H, Durbin R. 2010. Fast and accurate long-read alignment with Burrows-Wheeler transform. *Bioinformatics* 26:589–595. <https://doi.org/10.1093/bioinformatics/btp698>.

Host Hyperglycemia Alters the Cecal Metabolome and Exacerbates Antibiotic-Induced Dysbiosis

Jenna I. Wurster¹, Rachel L. Peterson¹, Douglas V. Guzior^{2,3}, Kerri Neugebauer³, Swathi Penumutthu¹, Claire E. Brown¹, William H. Sano⁴, Robert A. Quinn^{2,3}, Peter Belenky^{1,5,*}

¹Department of Molecular Microbiology and Immunology, Brown University, Providence, RI 02906, USA

²Department of Microbiology and Molecular Genetics, Michigan State University, East Lansing, MI 48824, USA

³Department of Biochemistry and Molecular Biology, Michigan State University, East Lansing, MI 48824, USA

⁴Department of Biology, University of Washington, Seattle, WA 98195, USA

⁵Lead Contact

*Correspondence: peter_belenky@brown.edu

Summary

It is well established in the microbiome field that antibiotic use and metabolic disease both impact the structure and function of the gut microbiome. But how host and microbial metabolism interacts with antibiotic susceptibility to affect the resulting dysbiosis remains poorly understood. We used a combined metagenomic, metatranscriptomic, and metabolomic approach to profile host hyperglycemia-related changes in microbiome taxonomic composition, transcriptional activity, and metabolite abundance both pre- and post-antibiotic challenge. We found that hyperglycemia did not significantly change microbial community structure but modified microbiome metabolism and increased susceptibility to amoxicillin. Hyperglycemia exacerbated the drug-induced dysbiosis and increased both PTS system activity and energy catabolism compared to controls. Finally, STZ and amoxicillin dual treatment increased pathogen susceptibility and reduced survival in a *Salmonella enterica* infection model. Our data demonstrate that changes in host metabolism are sufficient to modify microbial metabolism, worsen the severity of antibiotic dysbiosis, and decrease colonization resistance.

Introduction

Exposure to broad-spectrum antibiotics is one of the most significant microbiome perturbations. Antibiotic-induced dysbiosis occurs within hours of treatment, characterized by rapid loss in total bacterial load and taxonomic diversity, and significant transcriptional reprogramming (Cabral et al., 2019; 2020; Dethlefsen and Relman, 2011). This consequentially alter the intestinal metabolome, placing the host at an increased risk for opportunistic infections (Bäumler and Sperandio, 2016; Buffie et al., 2012; Chang et al., 2008; Croswell et al., 2009; Kaiko and Stappenbeck, 2014; Rivera-Chávez et al., 2016; Theriot et al., 2015; Theriot and Young, 2015). Understanding the mechanistic activity of antibiotics within the gut and the external factors that dictate susceptibility is critical given the severity of antibiotic toxicity, downstream impacts on the microbiome, and the nearly ubiquitous use of these drugs.

Microbial metabolism is a critical determinant of the severity of antibiotic toxicity (Stokes et al., 2019a). Microbes performing metabolically-permissive processes that generate ATP, such as aerobic respiration, have increased bactericidal drug sensitivity and experience a lethal respiratory burst during drug challenge *in vitro* (Adolfson and Brynildsen, 2015; Belenky et al., 2015; Dwyer et al., 2014; Kohanski et al., 2007; Lam et al., 2020; Lobritz et al., 2015). Meanwhile, inefficient fermentation, diversion away from tricarboxylic acid (TCA) cycle activity, or overall reduction in metabolism can confer drug tolerance in some species (Ahn et al., 2016; Conlon et al., 2016; Lobritz et al., 2015; Meylan et al., 2017; Thomas et al., 2013). We recently showed that this trend holds true within the context of the gut microbiome, where antibiotic exposure dramatically reduces the overall metabolic capacity of the community (Cabral et al., 2019). Surviving taxa such

as *Bacteroides thetaiotaomicron* can survive amoxicillin (AMX) exposure by transcriptional reprogramming that prioritizes polysaccharide fermentation over the more-permissive utilization of simple sugars (Cabral et al., 2019). When considering mechanisms of *in vivo* antibiotic activity, the impact of available nutrients on microbial metabolism is important to consider. For the microbiome, host diet is likely one of the largest factors shaping the nutrient pool. Diet alone has been demonstrated to perturb microbiome diversity and activity, and thus may directly impact antibiotic susceptibility (Albenberg and Wu, 2014; Bisanz et al., 2019; Collins et al., 2018; David et al., 2014; Ley, 2014; Smits et al., 2017; Tanes et al., 2021). Consistent with this, we observed that dietary glucose supplementation exacerbates AMX toxicity within the murine cecum and reduces both the total bacterial load and tolerance phenotype of *B. thetaiotaomicron* (Cabral et al., 2019). This trend also occurs with the bactericidal drug ciprofloxacin, where consumption of a high fat/sugar diet increases mucus glycoprotein and simple sugars consumption within the gut, subsequently increasing the abundance of starch utilization, glycolysis, and pyruvate fermentation transcripts. Ultimately this increase in metabolic activity enhances the microbiota's susceptibility to ciprofloxacin (Cabral et al., 2020). These data bolster the hypothesis that the local nutrient pool can drive the severity of the microbiome's response to antibiotic pressure by modulating how metabolically permissive the resident taxa are.

Dietary composition is not the sole determinant of the gut nutrient pool. Host-derived molecules and pancreaticobiliary secretions can alter macronutrient breakdown within the small intestine (SI) and impact the gut microbiome (Shin et al., 2019). For example, the host controls the concentration of sugars that progress to the colon through

a combination of SI transporter expression, gastric emptying speed, and enteroendocrine function (L. Chen et al., 2016; Holst et al., 2016; Koepsell, 2020; Holst et al., 2016; Ussar et al., 2017). Macronutrient breakdown is thus an interconnected metabolic system. Disruptions of host metabolism, like digestive and metabolic disorders, are correlated with microbial dysbiosis (Brestoff and Artis, 2013; Nikita Lomis, 2015; Noor et al., 2017; Qin et al., 2012; Sabatino et al., 2017). For example, patients with dysglycemia demonstrate bacterial infiltration of the epithelial mucosa that is unrelated to dietary intake or body mass index, suggesting dysglycemia triggers an inflammatory intestinal phenotype and prompts microbial breakdown of mucus glycoproteins (Chassaing et al., 2017).

Host hyperglycemia may lead to potent modulation of the gut metabolic environment. Currently, the relationship between perturbations in host metabolism and the severity of antibiotic-induced dysbiosis remains relatively understudied. *We hypothesize that changes in host metabolism related to hyperglycemia will alter the microbiota-accessible cecal metabolite pool and place the community in a metabolically permissive state that increases toxicity to bactericidal antibiotics.* To test this, we chose to use the single-dose STZ model rather than a diet- or genetically-induced model of glucose dysregulation (Deeds et al., 2011; Kobayashi et al., 2000; C.-Y. Wang and Liao, 2011). The benefit of STZ is the selective destruction of pancreatic beta-cells which induces rapid and irreversible hyperglycemia without potentially microbiome-confounding factors like diet and host genetics (Deeds et al., 2011; Xiao et al., 2017; Yang et al., 2019). Existing research on glucose dysregulation and the microbiome is confounded by the use of metabolic animal models that require dietary modification such as the high-fat diet-induced diabetes mouse model (Fujisaka et al., 2016). In this study we used a multi-omic

approach that profiled the taxonomic composition, transcriptional activity, and small molecule repertoire of the cecum to characterize the impact of hyperglycemia on microbiome disruption during AMX exposure. We then assessed the impact of hyperglycemia on AMX-induced pathogen susceptibility by challenging mice with *Salmonella enterica*. Together, our data demonstrate that changes in host metabolism are sufficient to directly modulate the metabolic function of the gut microbiota and increase the susceptibility to antibiotic-induced dysbiosis and worsen a dysbiosis-related complication.

Results

To examine the combined impact of hyperglycemia and antibiotics on the structure and function of the cecal microbiome, male C57BL/6J mice were given an intraperitoneal injection of either STZ or sham vehicle (control). Mice were assessed for hyperglycemia 48 hours post-injection then randomized. The next day, animals were given AMX or vehicle for 24 hours *ad libitum*. This time frame is sufficient to profile the acute response of the microbiota to antimicrobial stress, without encountering significant extinctions resulting from prolonged drug exposure (Cabral et al., 2020; 2019). After AMX exposure, mice were sacrificed and cecal contents were harvested for multi-omic profiling (Figure 1A).

STZ caused significant and irreversible hyperglycemia (Figure 1B). Utilizing 16S rRNA sequencing, we found that hyperglycemia and AMX caused significant changes to the composition of the gut microbiome (Figure 1C). Because 16S sequencing has limited phylogenetic resolution, we conducted the remaining analyses with WMGS to gain

species-level resolution (Cabral et al., 2020; 2019; Clooney et al., 2016; Poretsky et al., 2014; Ranjan et al., 2016). We found that STZ did not impact microbiome alpha diversity, but exacerbated the reduction in diversity caused by AMX (Figure 1D). We propose that hyperglycemia sets up a transcriptional and metabolic environment that alters the microbiome's response to antibiotic exposure. Thus, we assessed the impact of host hyperglycemia on the activity of the pre-antibiotic community, then examined the impact of AMX on microbiome function.

Hyperglycemia Minimally Impacts Microbiome Composition but Modifies the Metabolome and Metatranscriptome. Unlike many dietary models of diabetes (Xiao et al., 2017; Yang et al., 2019), acute STZ had minimal impact on taxonomic composition (Figure 1D, 1E), and caused one significant phylum-level change: the expansion of Verrucomicrobia (Figure 1E, Figure 6G). We performed differential abundance testing and confirmed that the expansion was driven by *Akkermansia muciniphila* (Figure 2A, Figure 6Q) (Love et al., 2014). *A. muciniphila* forages carbon from epithelial mucins and has been proposed to breakdown gut lining integrity under dysbiotic conditions like polysaccharide starvation (Cabral et al., 2020; Desai et al., 2016; T. Zhang et al., 2019). Degradation of the mucosa by *A. muciniphila* could trigger imbalances in the local carbon pool and have downstream impacts on microbial cross-feeding networks (Belzer et al., 2017).

We observed a 17-fold reduction in the abundance of *Blautia* sp. YL58 in response to STZ (Figure 2A). Members of the *Blautia* genus are documented short-chain fatty acid (SCFA) producers that use mucin as a carbon substrate (Bui et al., 2019; Oliphant and

Allen-Vercoe, 2019; Rey et al., 2010; Vacca et al., 2020), and the differential abundance of two muciniphilic species may indicate STZ disrupts carbon syntrophy. Because of the compositional similarity prior to AMX exposure, we postulated that the disparity in drug susceptibility was due to modifications in metabolic and transcriptional activity that directly impacts toxicity.

Given the significant dysregulation of blood glucose metabolism in STZ-treated mice (Figure 1B), and insulin's involvement in maintaining proper intestinal glucose absorption (Ussar et al., 2017), we wondered if AMX susceptibility was related to cecal glucose levels. However, we found no significant difference without antibiotic perturbation (Figure 1F). We subsequently assessed the cecal metabolome divergence using Principal Coordinate Analysis, and found that the metabolomes of hyperglycemic and normoglycemic communities were distinct from each other (Figure 1G). We identified the most significant Q-TOF-MS features via differential abundance testing (Love et al., 2014) and pathway-level projection (Aggio et al., 2010), and LC-MS/MS features using random forest classification (Figure 2B, Figure 2C, Figure S2A, Table S1, Table S2). 454 Q-TOF-MS metabolites were differentially abundant and we characterized the top-50 most influential LC-MS/MS metabolite clusters in our machine learning model (Figure 2B, Figure 2C, Figure S1D, Figure S2A, Table S1, Table S2, Table S3). We paired these findings with community-level and species-level transcriptomics to better characterize the functional capacity of the microbiome prior to antibiotic introduction.

Despite consuming identical diets, hyper- and normoglycemic communities had different levels of plant-based fiber and polyphenols that suggested disturbed polysaccharide processing. We observed STZ-specific enrichment of the flavones

apigenin, schaftoside, and daidzein (Figure 2C, Table S1) and significant reductions in major metabolites from apigenin breakdown such as 3-(3-hydroxyphenyl)propanoate (Figure 2C, Table S1). Flavonol degradation can generate either hydroxyphenylacetic acids or phenolic intermediates that are converted to SCFAs by Firmicutes (Braune and Blaut, 2016), and loss of this degradation may partially explain how reduced polysaccharide processing impacts SCFA levels. We observed that STZ-treatment reduced transcription of phytate degradation and multiple plant polysaccharide-related carbohydrate-active enzymes (CAZymes), and reduced the abundance of the SCFA valerate (Figure 2C, Figure S1B, Table S1, Table S4). We also identified that polysaccharide-fermenting taxa like *B. thetaiotaomicron* (Martens et al., 2008; Sonnenburg et al., 2005) reduced the expression of loci for targeted polysaccharide import (Figure 2E: BT3086, BT3087, BT3090, and BT4581, Table S5). These data suggest diminished microbial breakdown of dietary fiber, and that STZ causes shifts in polysaccharide-derived carbon sources levels.

Amino acids are another significant bacterial carbon source (X. Wang et al., 2019). STZ treatment greatly modified amino acid metabolism by the cecal microbiota. Multiple metabolites associated with aromatic amino acid generation (AAA), including 3-(3-hydroxyphenyl)propanoic acid and phenylethyl alcohol were reduced by STZ (Figure 2C, Table S1). We also observed accumulation of shikimate pathway intermediates like 3-dehydroquinate, 3-dehydroshikimate, and shikimate, likely caused by a block in the terminal component of the pathway and exemplified by reduced transcription of both AAA and chorismate synthesis (Figure 2C, Figure 2D, Table S1, Table S6). Because the shikimate pathway feeds directly into AAA generation via chorismate synthesis, reduced

transcription and accumulation of metabolic intermediates could suggest a shift from anabolic to catabolic amino acid metabolism.

The shikimate pathway is also involved in B-vitamin generation and impacts the availability of energy carriers like coenzyme A (CoA) (Tzin and Galili, 2010). To that end, we observed enrichment of metabolites involved in pantothenate and CoA biosynthesis coupled with reduced pathway transcription (Figure 2D, Figure S1E, Table S3, Table S6). STZ also increased microbial expression of thiazole biosynthesis, which is critical for the generation of vitamin B1- and thus key metabolic enzymes like pyruvate dehydrogenase and decarboxylase, and α -ketoglutarate dehydrogenase (Andersen et al., 2015) (Figure 2D, Table S6). The link between energy carriers and primary metabolism prompted us to look for changes in TCA activity and glycolysis (Allaway et al., 2020; Yoshii et al., 2019). We observed increased pyruvate metabolism, glycolysis, and gluconeogenesis-related metabolites, including glutamine and glycerol-3-phosphate (Figure S1D, Figure S1E). Finally, we observed an increase in transcripts such as ATPases, phosphoenolpyruvate hydratase, and succinate dehydrogenase (Figure S1C, Table S8), that, in conjunction increased inosine and tRNA processing activity (Figure 2D, Table S1), may suggest increased respiration and translation by some of the microbiome (Figure S1E, Table S3).

These data indicate that STZ has robust impacts on both the metabolic and transcriptional activity of the gut microbiota without major modifications to its taxonomic composition. We also observed metabolites associated with increased translational demand, which likely requires higher metabolic flux from the gut microbiota. However, these data do not reveal directional information about these reactions and biochemical pathways. Additionally, we must consider that these processes likely occur

simultaneously within multiple compartments of the microbiome. Additionally, there is redundancy in species function and in substrate utilization across biochemical pathways (Tian et al., 2020). Thus, rather than a single disruption increasing drug susceptibility, it is likely that the summation of large-scale disruption places the STZ-treated community in a more metabolically permissive state. In concert, the observed changes to gut microbiome function ultimately may put increased metabolic demand on the community which may lead to increased AMX susceptibility.

Hyperglycemia Exacerbates Antibiotic Dysbiosis and Shifts Microbial Metabolism.

Given the connection between microbial metabolism and antibiotic susceptibility (Belenky et al., 2015; Cabral et al., 2019; Lobritz et al., 2015; Stokes et al., 2019b), we hypothesized that STZ-induced metabolic disruption would enhance susceptibility to AMX. Accordingly, STZ exacerbated the AMX-induced caused significant divergence in taxonomic, metabolite and transcriptional profiles (Figure 1E, Figure 1G, Figure 6A). The majority of detected responses were highly divergent between hyper- and normoglycemic mice. First, fatty acid metabolism was differentially regulated during drug challenge and may represent a core STZ-driven difference in AMX responses. Hyperglycemic animals had a unique loss of phosphatidylserines and tiglylcarnitines (Table S1) but had enrichment for multiple N-acyl ethanolamines (Figure 4A: positive interaction value, Table S1). Higher concentrations of ethanolamines may suggest increased fatty acid epoxidation within the gut and localized inflammation that has been associated with gut dysbiosis (Ormsby et al., 2019; Thiennimitr et al., 2011a).

To highlight host-dependent changes in CAZyme expression, we calculated the interaction between glycemia and AMX exposure for the CAZyme repertoire (Figure 3A, Table S4). Hyperglycemic animals do not have the same reduction in glycoside hydrolase (GH) 43 as controls, which suggests modified polysaccharide binding capacity, as GH43 is primarily assumed to be involved in xylan and arabinose binding (Figure 3A, Table S4) (Mewis et al., 2016). Despite increased GH43-related transcripts, we observed decreased GH transcripts at the SEED subsystem level, and an overall greater reduction in GH abundance relative to controls (Figure 3B, Figure 3D, Table S4, Table S7). Given the reduction in polysaccharide foraging in the STZ baseline, it is possible that the hyperglycemic microbiota is unable to adapt its CAZyme expression in response to AMX. Accordingly, we observed STZ-specific accumulation of polyphenols and polysaccharides, providing further support for host-dependent modifications in polysaccharide metabolism (Figure 4A: positive interaction, Table S1). STZ communities had accumulation of multiple phenylpropanoids, phenylacetic acids, polyphenols, alkaloids, flavonoids, and isoprenoids (Figure 4A, Table S1) as well as pathway-level enrichment of metabolites related to flavonoid/isoflavonoid synthesis after AMX treatment (Table S3). As with the pre-AMX baseline, hyperglycemia resulted in a diminished capacity for fiber and polyphenol metabolism by the gut which may directly contribute to the severity of AMX-induced dysbiosis.

Hyperglycemia also modified mucus foraging by the microbiota after AMX challenge. In our CAZyme dataset, STZ-treated communities had reduction (negative interaction value) of GHs that target the chitobiose core of mucins (GH115), and did not upregulate GH84, GH129, and GH89 which target N-acetylglucosamine, class-III mucins,

and mucus glycoproteins (Figure 3A, Table S4). Simultaneously, STZ- and AMX treatment downregulated expression of the Leloir pathway, which plays a role in foraging mucus galactose residues (Figure 3E, Table S6) (Tang et al., 2016). Additionally, hyperglycemic mice did not exhibit an enrichment of the sialic acid residue N-acetylneuraminic acid (NAN) that occurred in normoglycemic animals after AMX exposure (Table S1). Because NAN is liberated by mucus degradation of the epithelium (Croston et al., 2016), this suggests reduced mucinophilic activity by STZ-treated communities during AMX challenge. Changes in host-dependent polysaccharide and mucus metabolism were also true at the species level for *B. thetaiotaomicron* (See Supplementary Results). Ultimately, STZ-related modifications in glycan foraging occur both before and after AMX exposure, suggesting that host glycemia directly impacts the composition of the cecal carbon pool, and this may in turn modify bacterial metabolism during drug challenge.

Although AMX reduced cecal glucose concentrations in both hosts, hyperglycemic animals had significantly higher glucose levels than controls (Figure 1F). Accordingly, we observed that the expression of phosphotransferase system (PTS) transcripts and the abundance of PTS metabolites like mannitol 1-phosphate were elevated in hyperglycemic mice after AMX treatment (Figure 3D, Figure 4A, Table S1, Table S7). Elevated glucose and PTS activity likely increased catabolism. To that end, we observed STZ-specific increases in pyruvate fermentation (Figure 3E, Table S6) and higher concentrations of acetylated sugars like acetyl-maltose relative to controls (Table S1). STZ-treated mice had specific metabolic enrichment of catabolism and catabolism-supporting pathways including 2-oxocarboxylic acid metabolism (pyruvate), glycolysis, starch/sucrose utilization, nicotinate/nicotinamide generation, and propanoate generation (Table S3).

The enrichment of nicotinate/nicotinamide and propanoate generation-related metabolites likely impacts the abundance of energy carriers (Belenky et al., 2007), and accordingly in our LC-MS/MS dataset we saw that STZ-treated communities had a unique enrichment in riboflavin (Figure 4C: Cluster 699, Figure S2C, Table S2) (Steinert et al., 2020).

Hyperglycemia Modifies the Composition of Bacteroidetes and Firmicutes after Amoxicillin Challenge. The large metabolic changes observed after AMX translate to a highly divergent impact on microbial composition. We found that hyperglycemia enhanced the AMX-induced reduction in alpha diversity (Figure 1D). Hyperglycemic mice had a unique reduction in Verrucomicrobia, however this is potentially due to the baseline expansion of *A. muciniphila* in response to STZ treatment (Figure 1E, Figure 6A, Figure 6G, Figure 6Q). Interestingly, the phylum-level community changes that we anticipated in response to AMX (Cabral et al., 2019) were exacerbated in hyperglycemic mice. Specifically, there were greater reductions in Actinobacteria and Firmicute abundances and a significant increase in the AMX-induced bloom of Bacteroidetes (Figure 1E, Figure 6C-F). Consistent with our previous work (Cabral et al., 2019), the Bacteroidetes bloom was driven by expansion of *B. thetaiotaomicron* in both normo- and hyperglycemic mice (Figure 6A, Figure 6H).

To examine species-level AMX responses, we calculated the interaction of host metabolism and AMX treatment (Love et al., 2014). In addition to *B. thetaiotaomicron*, many members of the *Bacteroides* genus increased after AMX, but their abundances were significantly higher in hyperglycemic mice (positive interaction) (Figure 5A, Figure

6B). Meanwhile, the species with reduced abundance in STZ mice after AMX treatment (negative interaction) were primarily within the order Clostridiales. This includes *Intestinimonas butyriciproducens*, *Oscillibacter valericigenes*, *Oscillibacter* sp. PEA192, *Clostridium innocuum*, and *Erysipelotrichaceae* bacterium I46 (Figure 5A, Figure 6N-P). These taxa are key starch degraders and SCFA producers, and their reduction speaks to the increased dysbiotic state of STZ and AMX co-treated animals (Bui et al., 2016a; Iino et al., 2007; Kazemian et al., 2020; Newman et al., 2018). Overall, these data suggest that the metabolic shifts that occur in the gut microbiome via STZ exacerbates the post-AMX bloom of Bacteroidetes while significantly increasing the collapse of key SCFA-producing Firmicutes. This likely impacts the local metabolome and metatranscriptome, and thus AMX susceptibility, given the syntrophic nature of *Bacteroides* and Firmicute metabolism (Fischbach and Sonnenburg, 2011).

Hyperglycemia and Amoxicillin Dual-Treatment Increases Susceptibility to *Salmonella enterica* Infection. We observed STZ-specific enrichment of ethanolamines (Figure 4A: positive interaction, Table S1), and the ethanolamine precursor phosphatidylethanolamine after AMX treatment (Figure S3A, Table S1). Ethanolamines are naturally generated by phosphatidylethanolamine breakdown during cell turnover; however, the majority of the microbiota is unable to ferment ethanolamines and that any microbial use is strictly associated with pathogenic contexts (Garsin, 2010). Interestingly, ethanolamines have been characterized to increase both the colonization and virulence of multiple enteric pathogens (Anderson et al., 2018; Christopher J Anderson, 2015; Nawrocki et al., 2018; Rowley et al., 2018). Specifically, some *Enterobacteriaceae* are

enriched for the genetic machinery required to use ethanolamines, and can funnel its breakdown products into both nitrogen metabolism and respiration (Christopher J Anderson, 2015; Garsin, 2010; Srikumar and Fuchs, 2010; Thiennimitr et al., 2011b). In *Salmonella*, exogenous ethanolamine signals a cascade of metabolic and virulence genes that promote intestinal colonization (Anderson and Kendall, 2016). Antibiotic-induced dysbiosis is also associated with increased *S. enterica* colonization, likely through the induction of a respiratory-favorable environment and disruption of the endogenous microbiota (M. Y. Yoon and S. S. Yoon, 2018; Zeng et al., 2017). Thus, we asked if STZ and AMX treatment would increase infection susceptibility by challenging hyper- and normoglycemic mice with *S. enterica* (Figure 7A). AMX increased susceptibility to *S. enterica* even at low infective doses regardless of host glycemia. Lower infective doses were required to establish infection in STZ- and AMX-treated mice and these animals experience a higher total pathogen burden (Figure 7B).

At all tested infection doses, hyperglycemia increased lethality by day 7. We observed that 100 percent of control mice receiving the AMX sham survived the infection course, while AMX-treated mice from the 1×10^4 and 1×10^5 dosing groups had 75 and 50 percent survival, respectively (Figure 7C). The first lethality event in control mice did not occur until 72 hours post-infection (Figure 7C), while the first lethality event in hyperglycemic mice was at 24 hours (Figure 7D). Hyperglycemic mice receiving the AMX sham had reduced survival at the infective doses of 1×10^5 and 1×10^6 (75 and 40 percent, respectively) (Figure 7D). AMX-treated hyperglycemic mice experienced lethality events at all infective doses, and had overall lower survival rates. The 1×10^5 and 1×10^6 dosing groups had 80 percent lethality within 24 hours, and exhibited no survival after 7 days

(Figure 7D). Meanwhile, the 1×10^4 , 1×10^3 , and 1×10^2 doses exhibited survival rates between 25 and 50 percent (Figure 7D). Together, these data suggest that the combination of STZ and AMX severely reduces the probability of survival after *S. enterica* challenge, likely due to increased pathogen burden relative to controls. It is possible that the enrichment of favorable metabolites in STZ and AMX-treated communities promotes the expansion and virulence of *S. enterica*, although more work is required to confirm this hypothesis.

Discussion

Recent estimates of dysglycemia's global prevalence suggest that metabolic disruption occurs in approximately ten percent of individuals, with incidence increasing annually (Saeedi et al., 2019). Thus, understanding how host metabolism impacts the severity of antibiotic-induced dysbiosis is key to the development of informed therapeutic strategies to mitigate microbiome damage during antibiotic administration. To address this knowledge gap, we used an integrated multi-omic strategy to examine how STZ-induced hyperglycemia modifies the microbiome's response to AMX challenge. Specifically, we combined WMGS, metatranscriptomics, and Q-TOF-MS- and LC-MS/MS-based metabolomics to examine glycemia-related differences in microbiome taxonomic composition and metabolic function both pre- and post-antibiotic treatment.

STZ treatment initiated a cascade of changes to fiber and polyphenol foraging and SCFA generation. Although STZ did not have major implications on the taxonomic structure of the gut, it did reduce the abundance of SCFA-producing Firmicutes such as *Blautia* sp. YL58 that participate in syntrophy with carbohydrate-fermenting members of

the microbiota (Bui et al., 2016b; Oliphant and Allen-Vercoe, 2019; Rey et al., 2010; Vacca et al., 2020). One possible but untested explanation for this taxonomic shift is that changes in the abundance of muciniphilic species like *A. muciniphila* modifies the balance of favorable metabolites for *Blautia* sp. to initiate SCFA fermentation. Alternatively, STZ-induced changes to the cecal metabolome may alter the behavior of polysaccharide-foraging species, which would initiate a cascade of metabolic changes that enrich for muciniphile expansion, loss of SCFA production, and could generate a dysbiotic state. Given the overall shifts in polysaccharide metabolism in the STZ-treated gut, our data suggests that the latter is more likely.

A major indicator of perturbed polysaccharide metabolism in our datasets was the altered abundance of polyphenol substrates and metabolites. Bacteria can coopt plant-based phenylpropanoid intermediates for various enzymatic reactions and are capable of liberating sugars from these compounds for use in their own metabolic activity (Fraser and Chapple, 2011; Braune and Blaut, 2016; Moore et al., 2002). In fact, some microbiota-associated taxa can directly utilize flavones as a carbon source and fuel flavone metabolites into their respiratory cycle (Burlingame and Chapman, 1983). Thus, shifts in the abundance of dietary-derived polyphenols could modify microbial metabolism in the cecum. Reduced dietary intake of fiber and polyphenols has been recognized as a perturbation to the microbiota and, increases susceptibility to bactericidal antibiotics by modifying microbial metabolism (Cabral et al., 2020; 2019; Makki et al., 2018; Ng et al., 2019). We propose that a similar disruption of the microbiome is occurring in our study.

Reduced fiber use by the microbiota may be partially explained by a side-effect of STZ treatment. In rodents receiving a multiple low-dose regime (i.e. 50 mg/kg/day for 5

days) of STZ, treatment is correlated with an initial reduction in food consumption (Motyl and McCabe, 2009). However animals eventually exhibit hyperphagia after 1 week post-injection (Motyl and McCabe, 2009; M. Zhang et al., 2008). It is possible that our experimental time point for AMX administration and sample collection (3 and 4 days-post injection, respectively) are also associated with reduced food intake. This would reduce the availability of fiber for fermentation by the microbiota. The STZ-related shifts in amino acid metabolism that we observed may be explained by the fact that, in addition to SCFAs, reduced fiber use impacts the production of several amino acid-based metabolites by members of the Firmicutes phylum (Neis et al., 2015; Tanes et al., 2021). Interestingly, studies have correlated spikes in both aromatic and branched-chain amino acids to be predictive biomarkers of type-2 diabetes (Neis et al., 2015), suggesting an intrinsic link between metabolic dysregulation and shifts in gut amino acid metabolism. Broad changes in amino acid metabolism are also a biomarker of vancomycin-induced dysbiosis (Tanes et al., 2021), thus, reductions in amino acid generation may represent a generalized stress response to antibiotic challenge (Cabral et al., 2019). Because Firmicutes have been characterized to perform a bulk of amino acid, nitrogen, and sulfur metabolism reactions within the gut, it is possible that these changes in our datasets indicate disruption to Clostridial Firmicute metabolism rather than whole-community perturbation (Bernal et al., 2007; Böttcher et al., 2014; Gao et al., 2018; Meadows and Wargo, 2015). It is possible that the increased AAA catabolism in the STZ-treated microbiome places a higher metabolic demand on Firmicutes, which in turn places them in a more antibiotic-susceptible state. This could explain the increased sensitivity of these taxa to AMX in STZ-treated mice, but more work is needed to confirm this hypothesis.

A key consideration of any ecological network is its taxonomic composition (Coyte and Rakoff-Nahoum, 2019). Polymicrobial interactions are a significant component of the microbiome's ecology and changes to taxonomic structure will directly impact the functional capacity of a given polymicrobial network (Coyte and Rakoff-Nahoum, 2019; Layeghifard et al., 2017) (Boon et al., 2014). Our results contrast with existing work examining STZ-related microbial taxonomic changes in rats, but this may be indicative of inherent differences between mice and rats, differences in dosing regimens and sample collection, sequencing depth, or use of a diet in combination with and STZ versus the single-dose model (S. Liu et al., 2019; Ma et al., 2020; Patterson et al., 2014; Yin et al., 2020). Interestingly, the relatively minor taxonomic shifts we observed were correlated with significant modifications in both the cecal metatranscriptome and metabolome (Figure 2) as well as significant taxonomic restructuring after antibiotic challenge (Figure 6). Because STZ-treatment impacted total alpha diversity and the abundance of every major phyla tested compared to normoglycemic controls after antibiotic treatment, it stands to reason that changes in the transcriptional and metabolic function are the driving force behind the disparities in post-antibiotic taxonomic composition of the microbiome. Overall, these data make a very strong argument for the degree of control that changes in baseline functional capacity have on the compositional restructuring of the microbiome after an external perturbation.

Lastly, we examined if the increased severity of AMX toxicity in hyperglycemic animals would increase their susceptibility to acute complications of dysbiosis such as enteric infection. Overall, STZ- and AMX-treated animals exhibited both increased susceptibility to *S. enterica* and reduced overall survival after one-week of infection

(Figure 7). Recent work by Thaïss et al. has demonstrated that decreased barrier function induced by STZ increases susceptibility to *S. enterica* (Christopher A Thaïss et al., 2018). However, this study utilized a multiple-dose STZ model and did not begin the pathogen challenge until a few weeks after STZ treatment, thus these results may not translate to our study. For example, we found that, at low infection doses, STZ treatment had no impact on susceptibility in the absence of antibiotics. Thus, it is possible that the hyperglycemic and drug-treated microbiome is structurally, functionally, and metabolically perturbed in a way that promotes the colonization and expansion of *S. enterica*. For example, we observed enrichment of multiple ethanolamines, which are a carbon source that cannot be fermented by the microbiota but can be utilized by *Salmonella* (Christopher J Anderson, 2015; Srikumar and Fuchs, 2010; Thiennimitr et al., 2011b). *S. enterica* has notably flexible metabolism compared to the bulk of the microbiota (Savannah J Taylor, 2020), and can use non-accessible carbon sources like ethanolamines to promote both colonization and niche adaptation in the mammalian host (Christopher J Anderson, 2015). Other metabolites that may have impacted infection severity by *S. enterica* include acetyl-maltose, as *Salmonella* are equipped with tightly controlled maltose import systems that allow it to readily fuel this carbon source into its respiratory cycle (Erhardt and Dersch, 2015; Jain et al., 2020; Miller et al., 2013). Another elevated metabolite of interest was pantetheine, which *Salmonella* can also directly shunt into its CoA synthesis, potentially providing a fitness advantage through competitor exclusion (Ernst and Downs, 2015) (Table S1). An additive explanation for the increased expansion of *Salmonella* in our hyperglycemic and drug-treated mice is an overall increase in antibiotic-induced intestinal oxygenation. *Salmonella* are facultative anaerobes and can readily switch to

aerobic respiration when needed (Rhen, 2019). Additionally, *Salmonella* can use inflammation-related metabolites like tetrathionate as a terminal electron acceptor, and thus can coopt the oxygenated and inflamed gut to promote its own growth (Winter et al., 2010). Although more work is required to parse what components of the hyperglycemic microbiome provide *Salmonella* with a competitive advantage after AMX perturbation, our data provides strong preliminary evidence that host metabolism can also directly impact the acute consequences of antibiotic dysbiosis. Ultimately, our study demonstrates that host-related physiology and metabolic state must be a key consideration of any current and future therapeutic strategy aimed at mitigating antibiotic-induced microbiome damage.

Limitations. While our multi-omic approach provides a robust characterization of the murine cecal microbiome during dysglycemia and antibiotic perturbation, there are limitations in the study design and methodology that complicate the interpretation of the results. First, our study exclusively uses male mice. Female mice are partially resistant to STZ-induced hyperglycemia and require significantly higher doses and (or) repetitive dosing regimens compared to males to induce a metabolic phenotype (Deeds et al., 2011; Goyal et al., 2016). Key considerations of our metagenomic and metatranscriptomic analyses are both the dependence on existing databases that possess annotation-based limitations and the need for imperfect alignment algorithms (Consortium, 2012). About half of all genes within the microbiome have not been functionally characterized (Consortium, 2012), complicating the interpretation of any read assignments. Further,

WMGS data is also complicated by the fact that taxonomic levels are reported as relative abundance.

For untargeted metabolomics, ion annotation is still considered the primary bottleneck during analysis (Gertsman and Barshop, 2018; Schrimpe-Rutledge et al., 2016). Additionally, the diversity in chemical modification, polarity, solubility, and ionization of chemical structures from complex biological samples often requires multiple analytical modes (i.e. positive versus negative ion mode) to be run in order to characterize all structures, and that can subsequently complicate ion identification (Gertsman and Barshop, 2018; Lei et al., 2011; Luan et al., 2019). While metabolomics offers a robust and powerful examination of the small molecule repertoire of the cecum, it does not allow for us to distinguish between bacterially-derived, fungal-derived and host-derived metabolites (Gertsman and Barshop, 2018). Ultimately, further work will be required to correlate STZ and AMX-induced metabolomic changes with individual taxa, and greater annotation of metabolic syntrophy in the gut will aid in the biological interpretation of subsequent metabolomic analyses.

Acknowledgements

P.B. was supported by the U.S. Department of Defense through the Peer Reviewed Medical Research Program under award number W81XWH-18-1-0198, the National Institute of General Medical Sciences under the institutional development award P20GM121344, and the National Institute of Diabetes and Digestive and Kidney Diseases of the National Institutes of Health under award number R01DK125382. J.I.W. and S.P. were additionally supported by the Graduate Research Fellowship from the National

Science Foundation under award number 1644760. The funding agencies had no role in the design of the study, or the collection, analysis, and interpretation of data and the opinions and interpretations presented here are not representative of the standing of the funding agencies.

Part of this research was conducted using computational resources and services at the Center for Computation and Visualization at Brown University. The authors would additionally like to thank Jacqueline M. Howells for assistance in animal handling and Dr. Damien J. Cabral for computational training.

Author Contributions

Conceptualization: J.I.W and P.B.; Methodology: J.I.W. and P.B.; Formal Analysis: J.I.W., D.V.G., and K.N.; Investigation: J.I.W., R.L.P., D.V.G., K.N., S.P., C.E.B., and W.H.S.; Data Curation: J.I.W.; Writing- Original Draft: J.I.W., D.V.G., and P.B.; Writing- Review and Editing: J.I.W., R.L.P., S.P., D.V.G., R.A.Q., and P.B.; Visualization: J.I.W; Supervision: R.A.Q. and P.B.; Funding Acquisition: P.B.

Declarations of Interests

The authors declare no competing interests.

Main Figure Titles and Legends

Figure 1. The impact of streptozotocin and amoxicillin on the murine gut microbiome.

- A. Experimental design of this study. Figure was created with BioRender.com (BioRender, Toronto, Canada).
- B. Fasting blood glucose of individual mice before STZ injection (Day 0), 48 hours post-injection, and 96 hours post-injection. Only mice whose fasting blood glucose was ≥ 250 mg/dL were used in the antibiotic treatment experiment (N = 20 for controls, N = 24 for STZ-treated).
- C. Principal Coordinate Analysis of Bray-Curtis Dissimilarity between 16S rRNA amplicons from experimental groups.
- D. Average alpha diversity of experimental groups as measured by the Shannon diversity index of metagenomic samples.
- E. Average relative abundance of the five most-abundant bacterial phyla in our data set. Data are represented as mean \pm SEM for each phylum.
- F. Quantification of cecal glucose concentrations from experimental groups. Data represent averaged concentrations \pm SEM.
- G. Principal Coordinate Analysis of Bray-Curtis Dissimilarity between metabolome extracts from experimental groups.

For C-F: N = 5 to 8 per group

For G: N = 6 per group, 2 technical replicates per mouse

For C & G: (*, $P < 0.05$; **, $P < 0.01$; ***, $P < 0.001$, permutational ANOVA)

For D & F: (*, $P < 0.05$; **, $P < 0.01$; ***, $P < 0.001$; ****, $P < 0.0001$, Welch's ANOVA with Dunnet T3 test for multiple hypothesis testing)

Figure 2. Hyperglycemia modifies the cecal metabolome and metatranscriptome

- A. Differentially abundant bacterial species (from the 75 most-abundant taxa) detected following STZ treatment. Data represent log₂ fold change relative to normoglycemic controls \pm standard error (N = 5 to 8 per group).
- B. Differentially abundant (unpaired T-test with Welch's correction p value < 0.05) GNPS-annotated clusters that contain known metabolites within the cluster. Clusters were selected from the top-50 most relevant features via Random Forest Testing (Figure S2). See Table S2 for full results.
- C. Differentially abundant Q-TOF-MS metabolite features in the murine cecum following STZ treatment as represented by log₂ fold change \pm standard error. See Table S1 for full results.
- D. Linear discriminant analysis score of differentially expressed MetaCyc pathways following STZ treatment as calculated by LEfSe. See Table S6 for full pathway names and statistics.
- E. Differentially-abundant *B. thetaiotaomicron* transcripts after STZ treatment. Data represent log₂ fold change versus normoglycemic controls \pm standard error. See Table S5 for full results.

For B & C: N = 6 per group, 2 technical replicates per mouse

For D & E: N= 4 per group

For A, C & E: Differentially abundant = Benjamini-Hochberg adjusted p value < 0.05

Figure 3. Amoxicillin differentially alters the cecal metatranscriptome.

- A. Differentially-abundant CAZyme transcripts in control and STZ-treated mice, alongside their interaction value after AMX. Data represent \log_2 fold change relative to vehicle controls \pm standard error. See Table S4 for full results.
- B. Differentially-abundant level 2 SEED Subsystem transcripts in normoglycemic mice after AMX. Data represent \log_2 fold change relative to vehicle controls \pm standard error. See Table S7 for full results.
- C. Linear discriminant analysis score of differentially expressed MetaCyc pathways following AMX treatment in normoglycemic mice as calculated by LEfSe. See Table S6 for full pathway names and statistics.
- D. Differentially-abundant level 2 SEED Subsystem transcripts in hyperglycemic mice after AMX. Data represent \log_2 fold change relative to vehicle controls \pm standard error. See Table S7 for full results.
- E. Linear discriminant analysis score of differentially expressed MetaCyc pathways following AMX treatment in hyperglycemic mice as calculated by LEfSe. See Table S6 for full pathway names and statistics.

For all panels: N = 4 per group

For A, B, & D: Differentially abundant = Benjamini-Hochberg adjusted p value < 0.05

Figure 4. Amoxicillin differentially alters the cecal metabolome.

- A. Differentially-abundant (Benjamini-Hochberg adjusted p value < 0.05) Q-TOF-MS metabolite features normoglycemic (Control) and hyperglycemic (STZ) mice, alongside their interaction value after AMX treatment. Data represent log₂ fold change relative to vehicle controls \pm standard error. See Table S1 for full results.
- B. Differentially abundant GNPS-annotated clusters that contain known metabolites within the cluster. Clusters were selected from the top-50 most relevant features via Random Forest Testing (Figure S2). Comparison is between control mice receiving AMX versus vehicle. See Table S2 for full results.
- C. Differentially abundant GNPS-annotated clusters that contain known metabolites within the cluster. Clusters were selected from the top-50 most relevant features via Random Forest Testing (Figure S2). Comparison is between hyperglycemic mice receiving AMX versus vehicle. See Table S2 for full results.

For all panels, N = 6 per group with 2 technical replicates per mouse

For B & C: Differentially abundant = unpaired T-test with Welch's correction p value < 0.05

Figure 5. Hyperglycemia modifies the impact of amoxicillin on members of the *Bacteroides* genus.

A. Differentially abundant bacterial species (within the 75 most-abundant taxa) detected following AMX treatment in control and hyperglycemic mice, compared to their interaction value. Data represent log₂ fold change relative to vehicle-treated controls \pm standard error (N = 5 to 8 per group).

B. Differentially-abundant *B. thetaiotaomicron* transcripts after AMX treatment. Data represent log₂ fold change of hyperglycemic AMX-treated mice relative to vehicle controls \pm standard error. See Table S5 for full results (N = 4 per group).

For all panels: Differentially abundant = Benjamini-Hochberg adjusted p value < 0.05

Figure 6. Hyperglycemia and amoxicillin treatment modify the taxonomic composition of the murine cecal microbiome.

- A. Average relative abundance of the 25 most-abundant species in our data set. Data are represented as mean \pm SEM for each species.
- B. Average relative abundance of species from A after the removal of reads assigned to *B. thetaiotaomicron*. Data are represented as mean \pm SEM for each species.
- C. Average relative abundance of reads assigned to the Bacteroidetes phylum.
- D. Average relative abundance of reads assigned to the Actinobacteria phylum.
- E. Average relative abundance of reads assigned to the Firmicutes phylum.
- F. Average relative abundance of reads assigned to the Proteobacteria phylum.
- G. Average relative abundance of reads assigned to the Verrucomicrobia phylum.
- H. Average relative abundance of reads assigned to *Bacteroides thetaiotaomicron*.
- I. Average relative abundance of reads assigned to *Muribaculum intestinale*.
- J. Average relative abundance of reads assigned to *Acutalibacter muris*.
- K. Average relative abundance of reads assigned to *Clostridiales* bacterium CCNA10.
- L. Average relative abundance of reads assigned to *Flavonifractor plautii*.
- M. Average relative abundance of reads assigned to *Hungateiclostrideaceae* bacterium KB18.
- N. Average relative abundance of reads assigned to *Intestinimonas butyriciproducens*.
- O. Average relative abundance of reads assigned to *Oscillibacter* sp. PEA192.
- P. Average relative abundance of reads assigned to *Oscillibacter valericigenes*.
- Q. Average relative abundance of reads assigned to *Akkermansia muciniphila*.

For all panels, N = 5 to 8 per group.

For panels C-Q, (*, P < 0.05; **, P < 0.01; ***, P < 0.001; ****, P < 0.0001, Welch's ANOVA with Dunnet T3 test for multiple hypothesis testing).

Figure 7. Hyperglycemia and amoxicillin increase susceptibility to and worsen survival against *Salmonella enterica* infection.

A. Experimental design of pathogen challenge study. Figure was created with BioRender.com (BioRender, Toronto, Canada).

B. *Salmonella enterica* Typhimurium colony forming units (CFU) per gram of feces in control AMX(+/-), and hyperglycemic AMX(+/-) mice over the course of infection with an inoculum of 1×10^2 cells. Data represent mean CFU \pm standard error. (*, $P < 0.1$; **, $P < 0.05$ Mann-Whitney U test of STZ AMX(+) vs Control AMX(+)).

C. Kaplan Meier survival curve of normoglycemic mice after one week.

D. Kaplan Meier survival curve of hyperglycemic mice after one week.

For all panels N = 4 to 5 per group

STAR METHODS

Resource Availability

Lead Contact and Materials Availability

This study did not generate new, unique reagents. Further information and requests for resources and reagents should be directed to and will be fulfilled by the Lead Contact, Peter Belenky (peter_belenky@brown.edu).

Data and Code Availability

Raw 16S amplicon, metagenomic, and metatranscriptomic reads were submitted to the NCBI Short Read Archive (SRA) under the following BioProject numbers: PRJNA720755 for 16S rRNA reads, and PRJNA720712 for raw metagenomic and metatranscriptomic reads. Raw Q-TOF-MS Data and annotation guide are available within the supplementary data of Table S1. Raw LC-MS/MS files are available at massive.ucsd.edu under MassIVE ID MSV000087093. GNPS molecular networking is available at <https://gnps.ucsd.edu/ProteoSAFe/status.jsp?task=013901272f394a6f8fe94dc5d62df4e>. LC-MS/MS data and analysis scripts are available at <https://github.com/guziordo/Belenky-Brown-Diabetes-Antibiotics>.

Experimental Model and Subject Details

Mice

Experimental procedures involving mice were all approved by the Institutional Animal Care and Use Committee of Brown University. Five-week-old male C57BL/6J mice were purchased from the Jackson Laboratories (Bar Harbor, ME, USA) and given a two-week

697 habituation period immediately following their arrival at Brown University. All animals were
698 cohoused together in specific-pathogen-free (SPF), temperature controlled (21 ± 1.1 °C),
699 and 12-hour light/dark cycling conditions within Brown University's animal care facility,
700 while being fed a standard chow (Laboratory Rodent Diet 5001, LabDiet, St. Louis, MO,
701 USA). After habituation, mice were randomized into new cages to reduce potential cage
702 effects.

704 **Bacterial Strains**

705 *S. enterica* Typhimurium SL1344 (GFP+, AmpR) was generously donated by Dr. Venessa
706 Sperandio (University of Texas, Southwestern). Cells were grown at 37°C under shaking
707 aerobic conditions in Luria-Bertani (LB) broth containing ampicillin (100 µg/mL). Colony
708 forming units (CFU) were quantified on LB agar plates containing ampicillin (100 µg/mL).
709 Because *S. enterica* Typhimurium SL1344 constitutively expresses green-fluorescent
710 protein, CFU counts were confirmed by UV-imaging using the ChemiDoc Imaging System
711 (Bio-Rad, Hercules, CA, USA).

713 **Methods Details**

714 **Animal Experiments**

715 To induce hyperglycemia, 7-week-old male C57BL/6J mice were fasted for 4-6 hours,
716 then given an intraperitoneal injection of either streptozotocin (STZ) (150 mg/kg, pH 4.5)
717 or a Na-Citrate sham (pH 4.5). All mice were given overnight supplementation of 10%
718 sucrose water to avoid post-procedural hypoglycemia. Sucrose water was then replaced
719 with standard filter-sterilized water the following morning. Two days post-injection, fasting

blood glucose was assessed in all mice using the CONTOUR®NEXT blood glucose monitoring system (Bayer AG, Whippany, NJ, USA). Mice with hyperglycemia (fasting blood glucose \geq 250 mg/dL) were selected for subsequent antibiotic treatment along with normoglycemic controls. 24-hours after glycemic assessment, all mice were randomized again to reduced potential cage effects and given either amoxicillin (25 mg/kg/day) or a pH-adjusted vehicle via filter-sterilized drinking water *ad libitum* for 24 hours (Cabral et al., 2019). Mice were subsequently sacrificed and dissected to collect blood, tissues, and cecal contents. Cecal contents were weighed then divided to be processed according to their downstream application (nucleic acid extraction, Q-TOF-MS, or LC-MS/MS). Exact processing methods are described in each application section below.

Multi-omic Analysis: Pipelines, Purpose, and Scope

Our multi-omic approach to microbiome analysis features the combinatory usage of the *Kraken2* and *Bracken* annotation pipelines for whole metagenomic sequencing (WMGS) (Lu et al., 2017; Wood et al., 2019), and the *HMP Unified Metabolic Analysis Network* (HUMAN2) (Franzosa et al., 2018) and *Simple Annotation of Metatranscriptomes by Sequencing Analysis* (SAMSA2) pipelines for metatranscriptomics (Westreich et al., 2018). Combined utilization of these pipelines facilitates examination of species-level taxonomic shifts (*Kraken2/Bracken*), community-level changes in transcript abundances (*SAMSA2*) and community-level gene expression that is normalized to the abundance of each taxa (*HUMAN2*). We also used the pipeline developed by Deng et al. (Deng et al., 2018) to examine species-level transcriptional responses to STZ and amoxicillin challenge for high-abundance and transcriptionally active members of the microbiota.

Sequencing pipelines were used in conjunction with both *quadrupole flow injection electrospray time-of-flight mass spectrometry* (Q-TOF-MS) (Fuhrer et al., 2011) and *liquid chromatography tandem mass spectrometry* (LC-MS/MS) paired with spectral annotation and networking analysis via the *Global Natural Products Social Metabolic Network* (GNPS; <http://gnps.ucsd.edu>) (M. Wang et al., 2016) (Figure 1A). While recent advances in mass spectrometry methods have vastly increased the range and accuracy of metabolite detection, no single analytical method is currently capable of capturing the entirety of small molecules in a complex biological sample (Luan et al., 2019). Thus, we opted to increase our metabolite coverage through the combinatory use of a tandem (LC-MS/MS) and a high-resolution (Q-TOF-MS) method (M. X. Chen et al., 2019). The Q-TOF-MS data is presented at the metabolite level where unknown features are ignored. For pathway-level comparisons, available Kyoto Encyclopedia of Genes and Genomes compound identifiers were used to perform Pathway Activity Profiling (Aggio et al., 2010) of known features (Figure S1E, Table S3). A deeper metabolome analysis including unknown molecules or related metabolites to known compounds is presented with the and data originating from our LC-MS/MS dataset using GNPS cluster identification.

Nucleic Acid Extraction & Purification

For nucleic acid extraction, cecal contents were transferred to ZymoBIOMICS DNA/RNA Miniprep Kit (Zymo Research, Irvine, CA, USA) Collection Tubes containing DNA/RNA Shield. These tubes were then processed via vortex at maximum speed for 5 minutes to homogenize cecal contents, which were subsequently placed on ice until permanent storage at -80°C. Using the parallel extraction protocol as per the manufacturer's

instructions, the ZymoBIOMICS DNA/RNA Miniprep Kit was used to isolate total nucleic acids (DNA and RNA) from cecal slurry. Total DNA/RNA were eluted in nuclease-free water and quantified using the dsDNA-HS and RNA-HS kits on the Qubit™ 3.0 fluorometer (Thermo Fisher Scientific, Waltham, MA, USA).

16S rRNA Amplicon Generation and Sequencing

The V4 hypervariable region of the 16S ribosomal RNA was amplified from extracted total DNA using the 518F and 816R barcoded primers published under the Earth Microbiome Project (Thompson et al., 2017). Amplicons were generated using Phusion high-fidelity polymerase and the following cycling protocol: 98°C for 30 seconds initial denaturation, then 25 cycles of 98°C for 10 seconds (denaturation), 57°C for 30 seconds (annealing), and 72°C for 30 seconds (extension). This was followed by a final extension of 72°C for 5 minutes. Amplicon libraries were submitted to the Rhode Island Genomics and Sequencing Center at the University of Rhode Island (Kingston, RI, USA) for pair-end sequencing (2x250 bp) on the Illumina MiSeq platform using the 500-cycle kit with standard protocols. We obtained an average of $14,674 \pm 12,458$ reads per sample.

16S rRNA Read Processing & Analysis

Raw reads underwent quality filtering, trimming, de-noising and merging using the R (version 3.5.0) package implementation of DADA2 (version 1.8.0) (Cabral et al., 2020; 2019; Callahan et al., 2016). The resulting ribosomal sequence variants underwent taxonomic assignment by using the *assignTaxonomy* function in DADA2 with the RDP Classifier algorithm with RDP Training set 16. Both alpha (Shannon) and beta (Bray-

Curtis dissimilarity) diversity were calculated using the R package phyloseq (version 1.24.2) (McMurdie and Holmes, 2013).

Metagenomic & Metatranscriptomic Library Preparation

Libraries for metagenomics and metatranscriptomics were prepared as described in our recent work (Cabral et al., 2020). We prepared metagenomic libraries from DNA (100 ng) using the NEBNext® Ultra II FS DNA Library Prep Kit (New England BioLabs, Ipswich, MA, USA) and the > 100 ng input protocol as per the manufacturer's instructions, which generated a pool of fragments whose average size was between 250 and 500 bp. Meanwhile, we prepared metatranscriptomic libraries from total RNA (≤ 1 ug) using a combination of the MICROBExpress kit (Invitrogen, Carlsbad, CA, USA), NEBNext® rRNA Depletion Kit for Human/Mouse/Rat (New England BioLabs, Ipswich, MA, USA), and the NEBNext® Ultra II Direction RNA Sequencing Prep Kit as per the manufacturers' instructions. This generated a pool of fragments with an average size between 200 and 450 bp. Both metagenomic and metatranscriptomic libraries were pair-end sequenced (2x150 bp) on the Illumina HiSeq X Ten platform, yielding an average of $1,464,061 \pm 728,330$ reads per metagenomic sample and $35,884,874 \pm 27,059,402$ reads per metatranscriptomic sample.

Metagenomic & Metatranscriptomic Read Processing

Raw metagenomic and metatranscriptomic reads underwent trimming and decontamination using kneaddata (version 0.6.1) as previously described (Cabral et al., 2020; 2019; McIver et al., 2018). Illumina adapter sequences were removed using

Trimmomatic (version 0.36), then depleted of reads that mapped to C57BL/6J, murine mammary tumor virus (MMTV, accession NC_001503) and murine osteosarcoma virus (MOV, accession NC_001506.1) using bowtie2 (version 2.2) (Bolger et al., 2014; Cabral et al., 2020; Langmead and Salzberg, 2012). Metatranscriptomic reads were additionally depleted of sequences that aligned to the SILVA 128 LSU and SSU Parc ribosomal RNA databases as previously described (Cabral et al., 2020; 2019; Pruesse et al., 2007).

Taxonomic Classification of Reads

We taxonomically classified trimmed and decontaminated metagenomic reads against a database of all completed bacterial, archaeal, and viral genomes contained within NCBI RefSeq using Kraken2 (version 2.0.7-beta, “Kraken2 Standard Database”) with a k-mer length of 35 (Wood et al., 2019). Bracken (version 2.0.0) was then used to calculate phylum- and species-level abundances from Kraken2 reports, and the R package phyloseq (version 1.28.0) was used to calculate alpha and beta diversity metrics (Lu et al., 2017; McMurdie and Holmes, 2013).

We then performed differential abundance testing on species-level taxonomic assignments (Cabral et al., 2020; 2019). First, low-abundance taxa ($< 1,000$ reads in $\geq 20\%$ of samples) were removed, then differential abundance testing of filtered counts was performed with the DESeq2 package (version 1.24.0) using default parameters (Love et al., 2014). All p-values were corrected for multiple hypothesis testing using the Benjamini-Hochberg method (Benjamini and Hochberg, 1995). Features with an adjusted p-value of less than 0.05 were considered to be statistically significant.

Metatranscriptomic Read Annotation Using SAMSA2

We used a modified version of the Simple Annotation of Metatranscriptomes by Sequences Analysis 2 (SAMSA2) pipeline to annotate trimmed and decontaminated metatranscriptomics reads as previously described (Cabral et al., 2020; 2019; Westreich et al., 2018). This modified pipeline involves implementation of the Paired-End Read Merger (PEAR) utility to generate merged reads and DIAMOND (version 0.9.12) aligner algorithm (Buchfink et al., 2014; J. Zhang et al., 2014) to generate alignments against RefSeq, SEED Subsystem, and CAZyme databases (Cantarel et al., 2009; Overbeek et al., 2013). The resulting alignments were subjected to differential abundance testing using DESeq2 (version 1.24.0) with standard parameters and Benjamini-Hochberg multiple hypothesis testing correction (Benjamini and Hochberg, 1995; Love et al., 2014). Features with an adjusted p-value of less than 0.05 were considered to be statistically significant.

Metatranscriptomic Analysis Using HUMAnN2

We used the HMP Unified Metabolic Analysis Network 2 (HUMAnN2, version 0.11.1) pipeline to assess the impact of STZ-based hyperglycemia and amoxicillin treatment on gene expression within the gut microbiome (Franzosa et al., 2018). We supplied the taxonomic profiles generated for each sample into the HUMAnN2 algorithm in order to assure consistent taxonomic assignment between paired samples (Cabral et al., 2020; 2019). Then, using HUMAnN2, we generated MetaCyc pathway abundances and used these to estimate community-level gene expression and normalized this to metagenomic abundance using the Witten-Bell method (Witten and Bell, 1991). Unstratified smoothed

RPKM values were converted to relative abundances then analyzed using linear discriminant analysis as described (Cabral et al., 2020; 2019). This was performed with the LEfSe (version 1) toolkit hosted on the Huttenhower Galaxy server (Segata et al., 2011).

Single-species Transcriptomics

We performed transcriptional analysis at the individual species level using a modified version of the pipeline developed by Deng et al. (Deng et al., 2018). First, species whose metagenomic abundance was subjected to an interaction between host glycemia and antibiotic usage were selected. We then calculated total RNA read abundance for each of these species, and performed transcriptional analysis only on those with 500,000 or greater reads per sample (Table S5). First, reads that mapped to candidate taxa were extracted from our metatranscriptomes using the BBSplit utility within BBMap (version 37.96) (Bushnell, 2014). Reads from *B. thetaiotaomicron*, *O. valericigenes*, and *O. spp.* PEA192 were aligned to their corresponding reference genomes using BWA-MEM (version 0.7.15) (Cabral et al., 2020; H. Li and Durbin, 2010). Then, we used subread program (version 1.6.2) command *featureCounts* was used to generate a count table from alignments, and this count table was assessed for differential abundance using DESeq2 (Love et al., 2014). All p-values were corrected for multiple hypothesis testing using the Benjamini-Hochberg method (Benjamini and Hochberg, 1995). Features with an adjusted p-value of less than 0.05 were considered statistically significant.

Metabolite Extraction & Flow Injection Time-of-Flight Mass-Spectrometry

For untargeted Q-TOF-MS metabolomics, cecal samples were flash frozen upon collected and stored at -80°C until extraction. To extract metabolites, flash-frozen samples were removed from -80°C and placed on ice. A 10-20 mg sample was taken and submerged in 300 µl of fresh-made LC/MS-grade acetone:isopropanol (2:1) extraction solvent, then homogenized via vortex two times for 15 seconds each at 4°C. Supernatant extraction solvent was transferred to a new tube and was placed at -80°C temporarily. The 300 µl was and homogenization was repeated, and this supernatant was then added to the original solvent aliquot. Combined samples underwent centrifugation at 4°C for 10 minutes at 13,500 x G. After centrifugation, supernatant was moved to a fresh microcentrifuge tube, sealed with parafilm, and placed on dry ice before immediate delivery to General Metabolics Inc. (Boston, MA, USA) where samples were stored at -80°C.

Extracted metabolites were quantified as described in Fuhrer et al. (Fuhrer et al., 2011) using flow injection Time-of-Flight mass spectrometry on the Agilent G6550A iFunnel Quadrupole Time-of-Flight mass spectrometer (Agilent, Santa Clara, CA, USA) equipped with a dual AJS electrospray ionization source operated in negative ion mode. Samples were injected at a flow-rate of 0.15 mL/minute in a mobile phase containing isopropanol and water (60%:40% ratio) buffered in 1mM Ammonium Fluoride, 15nM HP-0921, and 5µM homotaurine. Mass spectra data was recorded in 4 GHz high-resolution Ms mode at a rate of 1.4 spectra/second. We detected 714.3 ms/spectra and 9652 transients/spectra between 50 and 1000 m/z. Source operating parameters included a temperature of 225°C, drying gas rate of 11 L/min, nebulizer pressure of 20 psi, sheath gas temperature of 350°C and flow of 10 L/min. The source Vcap and Nozzle voltage

were 3500V and 2000V. The ms TOF operating parameters include fragmentor, collision, RF peak-to-peak voltages of 350V, 0V, and 750V, respectively and the Skimmer was disabled.

Data processing and analysis was performed as described by Fuhrer et al. in Matlab (The Mathworks, Natick, MA, USA) using functions from the following toolkits: Bioinformatics, Statistics, Database, and Parallel Computing (Fuhrer et al., 2011). Ions were additionally referenced against the Human Metabolome Database in addition to KEGG. Data analyses were run on an automated embedded platform by General Metabolics Inc. then delivered upon run completion. Finally, principal coordinate analysis was performed on ion intensities by using Bray-Curtis dissimilarity paired with PERMANOVA analysis using the phyloseq (version 1.26.1) R package and subsequently visualized in Prism GraphPad (version 9.0.2) (McMurdie and Holmes, 2013).

Metabolite Extraction, Liquid Chromatography Tandem Mass Spectrometry, and GNPS Molecular Networking

For untargeted LC-MS/MS metabolomics, cecal samples were placed into 300 µl of LMCS-grade methanol then supplemented with 600 µl of 70% cold LC-MS-grade methanol. Samples were homogenized via vortex for 5 minutes, then placed at 4°C for an overnight incubation. Following incubation, samples were subjected to centrifugation at 1000 x G for 3 minutes. 500 µl of the supernatant was moved to a sterile microcentrifuge tube and stored at -80°C for long-term preservation.

Samples were thawed and diluted 1:1 (v/v) in 50% methanol prior to LC-MS/MS. Liquid chromatography was performed using a Vanquish Autosampler (Thermo Scientific,

Waltham, MA, USA) and an Acquity UPLC column (Waters, Milford, MA, USA). Mass spectrometry was performed using a Q Exactive® Hybrid Quadrupole-Orbitrap Mass Spectrometer (Thermo Scientific, Waltham, MA, USA) in positive ion mode. All analysis used a 5 µL injection volume. Samples were eluted via water-acetonitrile gradient (98:2 to 2:98) containing 0.1% formic acid at a 0.4 mL min⁻¹ flow rate. RAW files were converted via GNPS Vendor Conversion and mined with MZmine (ver. 2.52) prior to submission for feature based molecular networking (Pluskal et al., 2010; Nothias et al., 2020). Briefly, MS1 and MS2 feature extraction was performed for a centroid mass detector with a signal threshold of 5.0×10^5 and 5.0×10^4 respectively. Chromatogram builder was run with an *m/z* tolerance of 0.02 Da or 7 ppm and a minimum height of 1.0×10^5 . Then, chromatograms were deconvoluted utilizing a baseline cut-off algorithm of 1.0×10^5 and a peak duration range of 0 to 1.00 minutes. Following this, isotopic peaks were then grouped with an *m/z* tolerance of 0.02 Da or 7 ppm and a retention time percentage of 0.1. The Join Aligner Module was then utilized with a 0.02 Da or 7 ppm *m/z* tolerance and a retention time tolerance of 0.1 minutes. Feature-based molecular networking on GNPS was performed with the following parameters: precursor and fragment ion mass tolerance 0.02 Da; minimum cosine of 0.7 and minimum matched peaks of 4, all others were defaults. Library searching was performed with the same parameters as described above.

Differential Abundance Testing & Pathway Enrichment of Q-TOF-MS Metabolite Data

Differentially abundant metabolites were identified using the DESeq2 package (version 1.22.2) with standard parameters (Love et al., 2014). All p-values were corrected for

multiple hypothesis testing using the Benjamini-Hochberg method (Benjamini and Hochberg, 1995). Features with an adjusted p-value of less than 0.05 were considered to be statistically significant. KEGG compound identifiers that were feature-matched by the Bioinformatics MATLAB toolkit were used to create a list of all KEGG IDs associated with differentially abundant metabolites. This list (and associated ion intensities) were used to perform KEGG pathway enrichment analysis using the PAPI R package (version 1.22.1) with standard parameters (Aggio et al., 2010). Pathways with an adjusted p-value of less than 0.05 were considered statistically significant.

Random Forest Classification of LC-MS/MS Metabolite Data

First, principal coordinate analysis was performed on ion intensities by using Bray-Curtis dissimilarity paired with PERMANOVA analysis. These analyses were performed using the phyloseq (version 1.26.1) R package and subsequently visualized in Prism GraphPad (version 9.0.2) (McMurdie and Holmes, 2013). Random forest classification models on treatment mouse treatment group were then generated using the randomForest (version 4.6-16) R package (Breiman, 2001). Variable importance plots from the models were used to identify metabolites that best contributed to group classification. Each metabolite feature of interest was then checked for annotation in GNPS, if not directly annotated from MS/MS library searching, the node of interest was identified in the molecular network and assessed for spectral similarity to other annotated nodes. This provided a molecular family annotation of each unknown cluster. Models classifying hyperglycemic mice treated with amoxicillin and not treated with amoxicillin resulted in out-of-bag prediction error of 2.7%. Classification of nonhyperglycemic treated with amoxicillin and not treated

with amoxicillin resulted in out-of-bag prediction error of 6.25%. Classification of hyperglycemic mice and nonhyperglycemic mice, both treated with antibiotics, resulted in out-of-bag prediction error of 7.96%. Classification of hyperglycemic mice and nonhyperglycemic mice, neither treated with antibiotics, resulted in out-of-bag prediction error of 16.67%.

Cecal Glucose Assessment

Cecal glucose levels were assessed using the Abcam Glucose Detection Kit (cat. No. ab102517, Abcam, Cambridge, United Kingdom). First, cecal material was weighed out and resuspended in glucose assay buffer at a concentration of 100 mg material/mL of buffer, then homogenized via vortex until no visible clumps were present. Samples were spun at maximum speed for 1 minute to pellet any residual debris, and 500 µl of supernatant was transferred to a Corning Costar Spin-X 0.22 µm centrifuge tube filter (cat. No. CLS8160, Corning Brand, Corning, New York, USA). The costar tubes containing supernatant were spun via centrifugation at 15,000 x G for 10 minutes, after which up to 500 µl of flow-through was transferred to an abcam 10kD spin column in order to deproteinize the samples. Samples were again spun at 15,000 x G for 10 minutes and flow-through was quantified using the Abcam Glucose Assay kit as per the manufacturer's instructions.

Enteric Pathogen Challenge

Salmonella enterica serovar Typhimurium SL1344 was grown overnight in 5 mL Luria-Bertani (LB) broth supplemented with fresh-made ampicillin (100 µg/mL) and grown at

37°C. This culture was diluted 1:1000 into fresh LB+ampicillin (100 µg/mL) the morning of infections and grown until cells were approximately at mid-log phase (OD600 = 0.3-0.4).

Rather than sacrificing animals after the 24-hours of amoxicillin treatment as outlined above (See *Animal Procedures*), animals were given an additional 48 hours of *ad libitum* amoxicillin within their drinking water followed by antibiotic-free filter-sterilized water for 24 hours. Subsequently, animals were moved to clean cages and placed under a 4-hour fast, at which point they were infected with an inoculum between 10^2 and 10^6 cells/dose via oral gavage (volume ≤ 200 µl). Animals were transferred to clean cages and weighed daily throughout the course of pathogen challenge. Fecal samples were collected daily then resuspended in 1 mL of phosphate-buffered saline and homogenized via vortex at maximum speed for at least 5 minutes. Fecal slurry was then serially diluted and plates onto ampicillin-supplemented (100 µg/mL) LB agar plates and grown at 37°C for 24 hours. After growth, colonies were counted and the total colony forming units (CFU) were quantified per gram of feces to assess pathogen burden.

Quantification and Statistical Analysis

Specific details of the statistical analyses for all experiments are outlined in the figure legends and Results section. Sample numbers represent biological replicates, and instances of technical replicates are specifically stated in corresponding figure legends. LEfSe (version 1.0) was used to analyze MetaCyc pathway abundance data generated by HUMAnN2 on the Galaxy web server using default settings (<http://huttenhower.sph.harvard.edu/galaxy>). Metatranscriptomic outputs generated by

1019 SAMSA2 and single-species sequencing, along with Q-TOF-MS abundances were
1020 subjected to differential abundance testing using the DESeq2 package (1.24.0) in R
1021 (version 3.5.2) under default parameters and included contrast:interaction comparisons
1022 (Love et al., 2014). All DESeq2 results were corrected using the Benjamini-Hochberg
1023 method (Benjamini and Hochberg, 1995) to account for multiple hypothesis testing. LC-
1024 MS/MS Random Forest testing was conducted using the R package implementation
1025 (Breiman, 2001). Permutational ANOVA calculations were made using the vegan R
1026 package (version 2.5.2). ANOVA, unpaired T tests, and Mann-Whitney U tests were
1027 performed in Prism Graphpad (version 9.0) without sample size estimation.

1028

Supplementary Results

In addition to the results presented in the main-body text, we found that STZ treatment modified other significant macronutrient processing pathways that we will discuss here. In addition to the amino acid-related changes stated above, we found enrichment of metabolites like 6-methylnicotinamide along with pathway enrichment of AAA degradation and protein digestion, suggesting a shift towards AAA catabolism rather than *de novo* synthesis (Figure S1D, Figure S1E, Table S1, Table S3). We additionally identified perturbed amino acid pathways beyond AAA, including enrichment in 2-ketoisocaproate and α -ketovaline, which are metabolic intermediates of leucine and valine catabolism, respectively (Figure 2C, Figure S1D, Table S1). Glutamate, acetylornithine, and N-acetylornithine were also enriched after STZ treatment (Table S1). These changes were likely microbially-driven, as we observed increased expression of the arginine biosynthesis II pathway that generates arginine from glutamate and L-ornithine using an N-acetylornithine intermediate (Figure 2D, Table S6) (Sakanyan et al., 1992).

Our LC-MS/MS dataset showed STZ-specific enrichment of dipeptides containing either aliphatic or aromatic amino acids (Figure 2B: Cluster 713, Cluster 676, Figure S2, Table S2). STZ treatment reduced the abundance of amino acid-related SEED transcripts, specifically sarcosine oxidase (the generation of N-methylglycine from choline) and selenoprotein processing which are involved in glycine metabolism (Sliwowski and Stadtman, 1988) (Figure S1A, Table S7). We also observed changes in sulfated amino acid metabolism, specifically reduced sulfur assimilation transcripts (Figure S1A, Table S7) and pathway-level reductions in homoserine and methionine

1052 biosynthesis (Figure 2D, Table S6). Together, the enrichment of aliphatic amino acid
1053 catabolites and dipeptides, aromatic dipeptides, and arginine synthetic intermediates,
1054 coupled with reductions in transcripts related to glycine and sulfated amino acids
1055 suggests that STZ treatment shifts branched-chain amino acid metabolism by the gut
1056 microbiota (H. Zhang et al., 2018).

1057 A major signature of STZ-related perturbations to polysaccharide metabolism was
1058 the differential abundance of flavone compounds like apigenin and daidzein. The reason
1059 these particular metabolites are of importance is because aglycone compounds like
1060 apigenin and daidzein have glycoside residues that are liberated and likely metabolized
1061 by microbes (M. Wang et al., 2019; Lundgren and Christoph A Thaiss, 2020; Vollmer et
1062 al., 2018; M. Wang et al., 2019). Thus, their abundance can directly shift the composition
1063 of the local carbon pool.

1064 Beyond changes in carbon foraging and increased microbial metabolism, STZ
1065 treatment was also induced significant dyslipidemia, as characterized by reductions in
1066 multiple fatty acid synthetic pathways including sphingolipids (Figure 2B: Clusters 1703,
1067 30, and 2184, Table S2), linoleic, α -linoleic, arachidonic, and unsaturated fatty acids after
1068 STZ administration (Figure 2C, Figure S1D, Figure S1E, Table S1, Table S3). Our LC-
1069 MS/MS data indicated that STZ-treated communities are enriched for long-chain fatty acid
1070 alcohols, phospholipids, and epoxide derivatives of linoleic acid (Figure 2B: Clusters
1071 2803, 2721, 2851, 2759, Figure S2A, Table S2). Coupled with transcriptional reductions
1072 in the expression of unsaturated fatty acid biosynthesis pathways like cis-vaccenate
1073 (Figure 2D, Table S6), these data suggest that STZ hampers both host and microbial fatty
1074 acid processing, likely enriching for esterification reactions, although we are unable to

distinguish between dysregulation of fatty acid uptake and fatty acid storage based off our results (Johnson et al., 2020).

Prompted by the observed dyslipidemia, we additionally surveyed for changes in cecal bile acid metabolism. Metabolites involved in primary bile acid biosynthesis and secretion, as well as steroid metabolism (cholesterol sulfate), were depressed in STZ-treated communities (Figure S1D, Figure S1E, Table S1, Table S3). We observed a stark decrease in multiple bile acids including chenodeoxycholate, 7-sulfocholate, and sulfodeoxycholate (Figure S1D, Table S1). Overall, this paints a picture of reduced primary bile acid availability without a detectable change in secondary bile acids in the STZ-treated microbiome. At the species level we noticed that *B. thetaiotaomicron* had reduced expression of bile salt efflux systems (Figure 2E: BT2793-2795, Table S5) (H. Liu et al., 2019), perhaps due to overall systemic reductions in the bile acid pool. Both the concentration and composition of the bile acid pool has been demonstrated to exhibit control on the function of the colonic microbiome; bile acid transformations are executed by select community members, and primary bile acids can trigger spore induction in certain Clostridia (Quinn et al., 2020; Staley et al., 2016; Zheng et al., 2017). Thus, reductions in the overall bile acid pool may place the microbiota in a more susceptible state to antibiotic challenge by reducing sporulation capacity (Cabral et al., 2019). As with fatty acids, changes in bile acid metabolism have been reported in STZ-treated rodent models and are likely a major contributing factor to the larger set of metabolite changes in the cecum, given their involvement in both postprandial nutrient absorption and gut transit time (T. Li et al., 2012; Ugarte et al., 2012). Ultimately, STZ treatment dysregulated multiple macronutrient processing pathways, altered the available carbon pool and

appeared to shift the microbiome towards AAA catabolism. Altered amino acid acquisition in turn modified the generation of B-vitamins which increased glycolysis and TCA activity. Together these data suggest that STZ shifts the metabolic activity of the gut microbiome and impacts drug susceptibility, as stated above.

STZ and AMX co-treatment increased the abundance of multiple *Bacteroides* species relative to normoglycemic controls. This abundance change was also true for other Bacteroidetes including *Odoribacter splanchnicus*, *Parabacteroides* sp. CT06, and *Prevotella intermedia*. We observed a 2-fold and 4-fold increase in the abundances of the Bacteroidetes *Alistipes finegoldii* and *Alistipes shahii*, respectively, that were unique to STZ-treated mice. Interestingly, these species are heavily enriched for polysaccharide utilization loci, which may speak to a collective fitness advantage for these loci in STZ and AMX-treated communities (Grondin et al., 2017; Terrapon et al., 2015). Interestingly, in our WMGS dataset, we noticed that the taxa that were more reduced in STZ-treated mice have been correlated with lipid intake, cholesterol, and cholesterol metabolite abundance in other works (Clarke et al., 2014; Wohlgemuth et al., 2014). For example, some species of *Erysipelotrichaceae* are auxotrophic for lipid biosynthesis; thus, the combination of STZ- and AMX-induced dyslipidemia may provide an explanation for the differential abundance of these taxa under hyperglycemic conditions (Kaakoush, 2015; Martínez et al., 2012).

Despite significant glycemia-dependent differences in the impact of AMX, we observed some common antibiotic responses from the gut microbiota. First, we observed that drug treatment caused enrichment of numerous monosaccharides including deoxyribose, hexose, triose, and pentoses, regardless of host phenotype (Table S1). The

availability of these monosaccharides resulted in respiratory microbial metabolism, as indicated by increases in fructose biphosphate aldolase, succinate dehydrogenase, and ATP synthase transcripts (Table S8). Concurrently, regardless of host glycemia, AMX treatment increased the expression of chorismate synthesis (Figure 3C, Figure 3E, Table S6), which likely resulted in elevated production of electron carriers (Boersch et al., 2018). For example, the GNPS Clusters 1020, 883, and 886 which are related to valeryl, palmitoyl, and lauroyl-conjugated carnitine species were elevated (Figure 4B, Figure 4C, Figure S2B, Figure S2C, Table S3). Carnitines have been identified as possible alternative final electron acceptors in obligate anaerobes (including the *Enterobacteriaceae*), suggesting an increased capacity for anaerobic respiratory activity as a common response to drug challenge (Bernal et al., 2007; Meadows and Wargo, 2015). This respiratory increase is consistent with the model of bactericidal antibiotic toxicity in which a lethal respiratory burst is a significant contribution to drug susceptibility (Belenky et al., 2015; Cabral et al., 2019; Lobritz et al., 2015).

Antibiotic-induced dysbiosis has been associated with changes in bile acids (Theriot et al., 2015), as well as dyslipidemia in multiple animal models (Sato et al., 2016; Yan et al., 2020) and microbes (Belenky et al., 2015). Thus, we anticipated that signatures of dyslipidemia and bile acid dysregulation would occur in our datasets. AMX reduced the abundance of metabolites involved in primary and secondary bile acid synthesis as well as bile secretion pathways irrespective of host glycemia (Table S3). Specifically, the primary bile acid metabolites 3 α ,7 α -dihydroxycoprostanic acid, cholate, chenodeoxycholate (Figure 4B, Figure 4C: Cluster 376, Table S2), the related GNPS Clusters 915 and 380 (Figure 4B, Figure 4C, Table S2), as well as bile acid alcohols like

1144 6-deoxodolichosterone, 5 β -Cholestane-3 α ,7 α ,12 α ,23S,25-pentol, and 27-
1145 norcholestanehexol were all reduced after antibiotic administration (Table S1). We also
1146 observed that STZ-treated communities exhibited typical signatures of antibiotic stress
1147 including increased transcripts related to stress responses, iron metabolism, translation,
1148 and quorum sensing/biofilms (Figure 3D, Table S7) (Cabral et al., 2020; 2019). Together
1149 these data suggest that AMX-induced bile acid dysregulation is not host dependent, while
1150 dyslipidemia is, and that STZ-treatment increases the abundance of pro-inflammatory
1151 intestinal metabolites and antibiotic-stress related transcripts.

1152 The observed reduction of polysaccharide utilization in STZ and AMX co-treated
1153 hosts held true at the species level. Specifically, *B. thetaiotaomicron* uniquely
1154 downregulated the expression of multiple polysaccharide PULs (BT4293-BT4299,
1155 BT4296-4298, BT3025), including those targeted at fructose (BT1759-1763, and
1156 BT1759), ribose (BT2804), levan (BT1761, BT1762), and fucose substrates (BT3665)
1157 (Figure 5B, Table S5) (Lynch and Sonnenburg, 2012; Mardo et al., 2017; Mimee et al.,
1158 2015; Townsend et al., 2020). Simultaneously, the combination of STZ and AMX
1159 treatment coincided with significant upregulation of one of *B. thetaiotaomicron*'s primary
1160 redox balance loci, specifically the NADH dehydrogenase complex spanning positions
1161 BT4058-4067 (Fischbach and Sonnenburg, 2011). We additionally observed increased
1162 activity in another NADH ubiquinone reductase operon (BT0616) (Goodman et al., 2009),
1163 ATPase (BT1746) (Figure 5B, Table S5). Our community-level metabolomics indicated
1164 STZ-specific loss of phosphoenolpyruvate (Table S1), which is likely related to the
1165 differential regulation of the NADH complex that modifies respiratory activity in *B.*
1166 *thetaiotaomicron*.

Supplementary Discussion

When evaluating data that examine host-microbe interactions it is important to acknowledge the influence of host physiology on the system. It is known that proper endocrine function is required for intestinal glucose uptake, and endocrine disruption can result in perturbed host monosaccharide metabolism. This in turn can modify the carbohydrate pool that reaches the colon. Specifically streptozotocin (STZ)-mediated insulin dysfunction, has been shown to directly modulate intestinal glucose absorption by rapidly increased expression of SI glucose transporters (Koepsell, 2020). Some have suggested that genetic disruption of intestinal insulin signaling increases glucose release from enteroendocrine cells (Ussar et al., 2017). A common clinical feature of metabolic disturbances is delayed gastric transit time, which is intrinsically linked with proper intestinal glucose absorption (Rayner and Horowitz, 2006). This phenotype has been recapitulated in multiple rodent models, including STZ-treated rats that have significant delays in stomach-to-cecal transit time (Chesta et al., 1990). Delays in gut transit and altered expression of intestinal glucose uptake likely impacts the carbohydrate pool that reaches the cecum, and might explain some of the microbiome disturbances seen in metabolic diseases (Dabke et al., 2019).

Ultimately, we found that host-hyperglycemia had relatively little impact on taxonomic composition but greatly perturbed glycan foraging and amino acid catabolism in the gut. This, in turn, increased the generation of B-vitamin species, energy carrier abundance, and respiratory rate by the microbiota. These changes may have subsequently created an environment that enhanced the toxicity of AMX in metabolically permissive taxa, which may have directly modified the post-antibiotic transcriptome and

metabolome at the community and species level. While we did detect common antibiotic responses, most of the drug-induced changes we observed were divergent and influenced by host glycemia. Specifically, hyperglycemia exacerbated the AMX-induced collapse of Clostridial Firmicutes and the expansion of *Bacteroides* species. These taxonomic shifts were correlated with reductions in fiber, polyphenol, and mucus utilization and a simultaneous increase in PTS system activity and catabolism at the community level. At the species level we observed that *B. thetaiotaomicron* had increased expression of its NADH dehydrogenase locus and ATP synthesis, suggesting increased respiratory activity in response to elevated cecal glucose levels when compared to normoglycemic controls. Finally, we observed that STZ- and AMX-treated mice had increased susceptibility to *S. enterica* and reduced survival after pathogen challenge when compared to normoglycemic controls. Together, these data demonstrate that changes in host metabolism are sufficient to modify microbial metabolism and worsen the severity of antibiotic-induced dysbiosis, and contributes to high pathogen susceptibility.

We found that a hallmark feature of STZ-induced hyperglycemia was significant dysregulation of cecal lipid metabolism in both the pre- and post-antibiotic treatment groups. This finding is in line with existing studies on serum metabolomics in rats, which find perturbation in fatty acid metabolism as a reliable biomarker of STZ-treatment (Fernández-Ochoa et al., 2020; Ugarte et al., 2012). While the host executes significant control of lipid processing via pancreaticobiliary secretions, there is evidence from germ-free animal studies that implicates the gut microbiome as an integral component of fatty acid metabolism, and suggests that microbial dyslipidemia results in negative metabolic phenotypes (Schoeler and Caesar, 2019). Microbial lipid processing (for example the

conjugation of linoleic acid) has also been implicated in the generation of metabolite intermediates that increase the integrity of gut epithelial barrier function (Schoeler and Caesar, 2019) . Thus, it stands to reason that disruption of lipid homeostasis within the gut, as observed in our datasets, has downstream consequences to gut barrier function and places the cecal microbiota in a more delicate state prior to antibiotic challenge. Decreases in gut barrier function have also been directly implicated in the susceptibility of the microbiome to enteric pathogen challenge (Christopher A Thaiss et al., 2018), and we observed that the enteric pathogen *S. enterica* was able to infect hyperglycemic drug-treated animals more readily and caused more lethal disease. These data indicate a potential link between perturbed lipid metabolism and pathogen colonization, but more work is required to elucidate specific mechanisms.

Beyond disruption to lipid homeostasis, a novel finding in our datasets was that both STZ and AMX treatment reduced the abundance of primary bile acids within the cecum. The microbiota executes a large portion of bile acid conjugation reactions and cross-talks with the host to regulate primary bile acid secretion (Ridlon et al., 2014). Thus, antibiotic-induced changes were anticipated and were in agreeance with an existing body of work that indicates antibiotic administration modifies the abundance and composition of the bile acid pool (Ridlon et al., 2014; Sayin et al., 2013; Vrieze et al., 2014). Interestingly, other beta-lactam antibiotics have been shown to increase the total bile acid abundance within the colon (Kuribayashi et al., 2012). Meanwhile, vancomycin, clindamycin, cefoperazone, polymyxin B, and the combinatory cocktail of vancomycin/metronidazole/kanamycin/clindamycin reduce the abundance of secondary bile acids but do not modify the primary bile acid pool (Kuno et al., 2018; Theriot et al.,

2015). Thus, our data may represent a novel, STZ- and AMX-specific bile acid dysregulation.

We previously identified that polysaccharide fermentation by *B. thetaiotaomicron* functions as an AMX tolerance response in normoglycemic animals (Cabral et al., 2019). However, this study complicates that understanding, as STZ-specific reductions in *B. thetaiotaomicron*'s polysaccharide and mucus foraging suggests that these may not be universal AMX tolerance responses. There may be non-mucosal or non-polysaccharide metabolite species that induce a protective phenotype to members of the *Bacteroides* genus and might explain their relative fitness advantage in STZ and AMX dual treatment. Alternatively, members of the *Bacteroides* genus possess beta-lactamases within their genomes, and differences in the expression of these resistance genes may be involved in the observed enrichment of *Bacteroides* in STZ and AMX-treated samples (Edwards, 1997). Regardless, reduction in polysaccharide fermentation by *Bacteroides* disrupts the balance of nutrients available for syntrophic metabolism with Firmicutes and Actinobacteria (Fischbach and Sonnenburg, 2011). These changes may induce a proinflammatory state in the gut through reduced SCFA production and contribute to the increased dysbiosis experienced by STZ-treated animals during drug challenge. Given the total ecological complexity of the gut microbiome, gleaning a more complete understanding of cross-feeding networks will be integral to the full characterization of a given perturbation's impact on the microbiome.

References

- Adolfsen, K.J., Brynildsen, M.P., 2015. Futile cycling increases sensitivity toward oxidative stress in *Escherichia coli* 29, 26–35. doi:10.1016/j.ymben.2015.02.006
- Aggio, R.B.M., Ruggiero, K., Villas-Bôas, S.G., 2010. Pathway Activity Profiling (PAPi): from the metabolite profile to the metabolic pathway activity. *Bioinformatics* 26, 2969–2976. doi:10.1093/bioinformatics/btq567
- Ahn, S., Jung, J., Jang, I.-A., Madsen, E.L., Park, W., 2016. Role of Glyoxylate Shunt in Oxidative Stress Response. *J. Biol. Chem.* 291, 11928–11938. doi:10.1074/jbc.M115.708149
- Albenberg, L.G., Wu, G.D., 2014. Diet and the Intestinal Microbiome: Associations, Functions, and Implications for Health and Disease. *Gastroenterology* 146, 1564–1572. doi:10.1053/j.gastro.2014.01.058
- Allaway, D., Haydock, R., Lonsdale, Z.N., Deusch, O.D., O’Flynn, C., Hughes, K.R., 2020. Rapid Reconstitution of the Fecal Microbiome after Extended Diet-Induced Changes Indicates a Stable Gut Microbiome in Healthy Adult Dogs. *Applied and Environmental Microbiology* 86, 2889–13. doi:10.1128/AEM.00562-20
- Andersen, L.W., Liu, X., Peng, T.J., Giberson, T.A., Khabbaz, K.R., Donnino, M.W., 2015. Pyruvate Dehydrogenase Activity and Quantity Decreases After Coronary Artery Bypass Grafting. *Shock* 43, 250–254. doi:10.1097/SHK.0000000000000306
- Anderson, C.J., Kendall, M.M., 2016. Location, location, location. *Salmonella* senses ethanolamine to gauge distinct host environments and coordinate gene expression. *Microbial Cell* 3, 1–3. doi:10.1371/journal.ppat.1005278
- Anderson, C.J., Satkovich, J., Lu, V.K.K., Agaisse, H., Kendall, M.M., 2018. The Ethanolamine Permease EutH Promotes Vacuole Adaptation of *Salmonella enterica* and *Listeria monocytogenes* during Macrophage Infection. *Infection and Immunity* 86, 1–12. doi:10.1128/IAI.00172-18
- Bäumler, A.J., Sperandio, V., 2016. Interactions between the microbiota and pathogenic bacteria in the gut. *Nature* 535, 85–93.
- Belenky, P., Bogan, K.L., Brenner, C., 2007. NAD⁺ metabolism in health and disease 1–8. doi:10.1016/j.tibs.2006.11.006
- Belenky, P., Ye, J.D., Porter, C.B.M., Cohen, N.R., Lobritz, M.A., Ferrante, T., Jain, S., Korry, B.J., Schwarz, E.G., Walker, G.C., Collins, J.J., 2015. Bactericidal Antibiotics Induce Toxic Metabolic Perturbations that Lead to Cellular Damage. *CellReports* 13, 968–980. doi:10.1016/j.celrep.2015.09.059
- Belzer, C., Chia, L.W., Aalvink, S., Chamlagain, B., Piironen, V., Knol, J., De Vos, W.M., 2017. Microbial Metabolic Networks at the Mucus Layer Lead to Diet-Independent Butyrate and Vitamin B12 Production by Intestinal Symbionts. *mBio* 8, 776–14. doi:10.1128/mBio.00770-17
- Benjamini, Y., Hochberg, Y., 1995. Controlling the False Discovery Rate: A Practical and Powerful Approach to Multiple Testing. *Journal of the Royal Statistical Society* 57, 289–300.
- Bernal, V., Sevilla, Á., Cánovas, M., Iborra, J.L., 2007. Production of L-carnitine by secondary metabolism of bacteria. *Microb Cell Fact* 6, 31–17. doi:10.1186/1475-2859-6-31

- Bisanz, J.E., Upadhyay, V., Turnbaugh, J.A., Ly, K., Turnbaugh, P.J., 2019. Meta-Analysis Reveals Reproducible Gut Microbiome Alterations in Response to a High-Fat Diet. *Cell Host & Microbe* 26, 265–272. doi:10.1016/j.chom.2019.06.013
- Boersch, M., Rudrawar, S., Grant, G., Zunk, M., 2018. Menaquinone biosynthesis inhibition: a review of advancements toward a new antibiotic mechanism 1–7. doi:10.1039/C7RA12950E
- Bolger, A.M., Lohse, M., Usadel, B., 2014. Trimmomatic: a flexible trimmer for Illumina sequence data. *Bioinformatics* 30, 2114–2120. doi:10.1093/bioinformatics/btu170
- Boon, E., Meehan, C.J., Whidden, C., Wong, D.H.-J., Langille, M.G.I., Beiko, R.G., 2014. Interactions in the microbiome: communities of organisms and communities of genes. *FEMS Microbiology Reviews* 38, 90–118. doi:10.1111/1574-6976.12035
- Böttcher, C., Chapman, A., Fellermeier, F., Choudhary, M., Scheel, D., Glawischnig, E., 2014. The Biosynthetic Pathway of Indole-3-Carbaldehyde and Indole-3-Carboxylic Acid Derivatives in *Arabidopsis*. *Plant Physiol.* 165, 841–853. doi:10.1104/pp.114.235630
- Braune, A., Blaut, M., 2016. Bacterial species involved in the conversion of dietary flavonoids in the human gut. *Gut Microbes* 7, 216–234. doi:10.1080/19490976.2016.1158395
- Breiman, L., 2001. Random Forests. *Machine Learning* 45, 5-32. doi:10.1023/A:1010933404324
- Brestoff, J.R., Artis, D., 2013. Commensal bacteria at the interface of host metabolism and the immune system. *Nat Immunol* 14, 676–684. doi:10.1038/ni.2640
- Buchfink, B., Xie, C., Huson, D.H., 2014. Fast and sensitive protein alignment using DIAMOND. *Nat Methods* 12, 59–60. doi:10.1038/nmeth.3176
- Buffie, C.G., Jarchum, I., Equinda, M., Lipuma, L., Gobourne, A., Viale, A., Ubeda, C., Xavier, J., Pamer, E.G., 2012. Profound alterations of intestinal microbiota following a single dose of clindamycin results in sustained susceptibility to *Clostridium difficile*-induced colitis. *Infection and Immunity* 80, 62–73. doi:10.1128/IAI.05496-11
- Bui, T.P.N., Schols, H.A., Jonathan, M., Stams, A.J.M., de Vos, W.M., Plugge, C.M., 2019. Mutual Metabolic Interactions in Co-cultures of the Intestinal Anaerostipes rhamnosivorans With an Acetogen, Methanogen, or Pectin-Degrader Affecting Butyrate Production. *Front Microbiol* 10, 1–12. doi:10.3389/fmicb.2019.02449
- Bui, T.P.N., Shetty, S.A., Lagkouravdos, I., Ritari, J., Chamlagain, B., Douillard, F.P., Paulin, L., Piironen, V., Clavel, T., Plugge, C.M., De Vos, W.M., 2016a. Comparative genomics and physiology of the butyrate-producing bacterium *Intestinimonas butyriciproducens*. *Environmental Microbiology Reports* 8, 1024–1037. doi:10.1111/1758-2229.12483
- Bui, T.P.N., Shetty, S.A., Lagkouravdos, I., Ritari, J., Chamlagain, B., Douillard, F.P., Paulin, L., Piironen, V., Clavel, T., Plugge, C.M., De Vos, W.M., 2016b. Comparative genomics and physiology of the butyrate-producing bacterium *Intestinimonas butyriciproducens*. *Environmental Microbiology Reports* 8, 1024–1037. doi:10.1111/1758-2229.12483
- Burlingame, R., Chapman, P.J., 1983. Catabolism of Phenylpropionic Acid and Its 3-Hydroxy Derivative by *Escherichia coli*. *Journal of Bacteriology* 155, 1–9.
- Bushnell, B., 2014. BBMap: A Fast, Accurate, Splice-Aware Aligner, in: Presented at the 14th Annual Genomics of Energy Environment Meeting, Walnut Creek, CA.

- Cabral, D.J., Penumutchu, S., Reinhart, E.M., Zhang, C., Korry, B.J., Wurster, J.I., Nilson, R., Guang, A., Sano, W.H., Rowan-Nash, A.D., Li, H., Belenky, P., 2019. Microbial Metabolism Modulates Antibiotic Susceptibility within the Murine Gut Microbiome. *Cell Metabolism* 30, 800–823.e7. doi:10.1016/j.cmet.2019.08.020
- Cabral, D.J., Wurster, J.I., Korry, B.J., Penumutchu, S., Belenky, P., 2020. Consumption of a Western-Style Diet Modulates the Response of the Murine Gut Microbiome to Ciprofloxacin. *mSystems* 5, 51–19. doi:10.1128/mSystems.00317-20
- Callahan, B.J., McMurdie, P.J., Rosen, M.J., Han, A.W., Johnson, A.J.A., Holmes, S.P., 2016. DADA2: High-resolution sample inference from Illumina amplicon data. *Nat Methods* 13, 581–583. doi:10.1038/nmeth.3869
- Cantarel, B.L., Coutinho, P.M., Rancurel, C., Bernard, T., Lombard, V., Henrissat, B., 2009. The Carbohydrate-Active EnZymes database (CAZy): an expert resource for Glycogenomics. *Nucleic Acids Research* 37, D233–D238. doi:10.1093/nar/gkn663
- Chang, J.Y., Antonopoulos, D.A., Kalra, A., Tonelli, A., Khalife, W.T., Schmidt, T.M., Young, V.B., 2008. Decreased Diversity of the Fecal Microbiome in Recurrent *Clostridium difficile*–Associated Diarrhea. *J INFECT DIS* 197, 435–438. doi:10.1086/525047
- Chassaing, B., Raja, S.M., Lewis, J.D., Srinivasan, S., Gewirtz, A.T., 2017. Colonic Microbiota Encroachment Correlates With Dysglycemia in Humans. *Cellular and Molecular Gastroenterology and Hepatology* 4, 205–221. doi:10.1016/j.jcmgh.2017.04.001
- Chávez-Talavera, O., Tailleux, A., Lefebvre, P., Staels, B., 2017. Bile Acid Control of Metabolism and Inflammation in Obesity, Type 2 Diabetes, Dyslipidemia, and Nonalcoholic Fatty Liver Disease. *Gastroenterology* 152, 1–19. doi:10.1053/j.gastro.2017.01.055
- Chen, L., Tuo, B., Dong, H., 2016. Regulation of Intestinal Glucose Absorption by Ion Channels and Transporters. *Nutrients* 8, 43–11. doi:10.3390/nu8010043
- Chen, M.X., Wang, S.-Y., Kuo, C.-H., Tsai, I.-L., 2019. Metabolome analysis for investigating host-gut microbiota interactions. *Journal of the Formosan Medical Association* 118, S10–S22. doi:10.1016/j.jfma.2018.09.007
- Chesta, J., Debnam, E.S., Srai, S.K.S., Epstein, O., 1990. Delayed stomach to caecum transit time in the diabetic rat. Possible role of hyperglucagonaemia. *Gut* 31, 660–662.
- Christopher J Anderson, D.E.C.M.A.M.M.K., 2015. Ethanolamine Signaling Promotes *Salmonella* Niche Recognition and Adaptation during Infection. *PLoS Pathog* 11, 1–20. doi:10.1371/journal.ppat.1005278&domain=pdf
- Clarke, S.F., Murphy, E.F., Nilaweera, K., Ross, P.R., Shanahan, F., O’Toole, P.W., Cotter, P.D., 2014. The gut microbiota and its relationship to diet and obesity. *Gut Microbes* 3, 186–202. doi:10.4161/gmic.20168
- Clooney, A.G., Fouhy, F., Sleator, R.D., O’ Driscoll, A., Stanton, C., Cotter, P.D., Claesson, M.J., 2016. Comparing Apples and Oranges?: Next Generation Sequencing and Its Impact on Microbiome Analysis. *PLoS ONE* 11, e0148028–16. doi:10.1371/journal.pone.0148028
- Collins, J., Robinson, C., Danhof, H., Knetsch, C.W., van Leeuwen, H.C., Lawley, T.D., Auchtung, J.M., Britton, R.A., 2018. Dietary trehalose enhances virulence of epidemic

1393 *Clostridium difficile*. Nature Publishing Group 553, 291–294.
 1394 doi:10.1038/nature25178
 1395 Conlon, B.P., Rowe, S.E., Gandt, A.B., Nuxoll, A.S., Donegan, N.P., Zalis, E.A., Clair, G.,
 1396 Adkins, J.N., Cheung, A.L., Lewis, K., 2016. Persister formation in *Staphylococcus*
 1397 *aureus* is associated with ATP depletion. *Nat. Microbiol* 1, 16051–16.
 1398 doi:10.1038/nmicrobiol.2016.51
 1399 Consortium, T.H.M.P., 2012. A framework for human microbiome research. *Nature* 486,
 1400 215–221. doi:10.1038/nature11209
 1401 Coyte, K.Z., Rakoff-Nahoum, S., 2019. Understanding Competition and Cooperation
 1402 within the Mammalian Gut Microbiome. *Current Biology* 29, R583–R544.
 1403 doi:10.1016/j.cub.2019.04.017
 1404 Crost, E.H., Tailford, L.E., Monestier, M., Swarbreck, D., Henrissat, B., Crossman, L.C.,
 1405 Juge, N., 2016. The mucin-degradation strategy of *Ruminococcus gnavus*: The
 1406 importance of intramolecular trans-sialidases. *Gut Microbes* 7, 302–312.
 1407 doi:10.1080/19490976.2016.1186334
 1408 Crowell, A., Amir, E., Tegatz, P., Barman, M., Salzman, N.H., 2009. Prolonged Impact
 1409 of Antibiotics on Intestinal Microbial Ecology and Susceptibility to Enteric *Salmonella*
 1410 Infection. *Infection and Immunity* 77, 2741–2753. doi:10.1128/IAI.00006-09
 1411 Dabke, K., Hendrick, G., Devkota, S., 2019. The gut microbiome and metabolic
 1412 syndrome. *Journal of Clinical Investigation* 129, 4050–4057. doi:10.1172/JCI129194
 1413 Đanic, M., Stanimirov, B., Pavlovic, N., Golocorbin-Kon, S., Al-Salami, H., Stankov, K.,
 1414 Mikov, M., 2018. Pharmacological Applications of Bile Acids and Their Derivatives in
 1415 the Treatment of Metabolic Syndrome. *Front. Pharmacol.* 9, 1–20.
 1416 doi:10.3389/fphar.2018.01382
 1417 David, L.A., Maurice, C.F., Carmody, R.N., Gootenberg, D.B., Button, J.E., Wolfe, B.E.,
 1418 Ling, A.V., Devlin, A.S., Varma, Y., Fischbach, M.A., Biddinger, S.B., Dutton, R.J.,
 1419 Turnbaugh, P.J., 2014. Diet rapidly and reproducibly alters the human gut
 1420 microbiome. *Nature* 505, 559–563. doi:10.1038/nature12820
 1421 Deeds, M.C., Anderson, J.M., Armstrong, A.S., Gastineau, D.A., Hiddinga, H.J., Jahangir,
 1422 A., Eberhardt, N.L., Kudva, Y.C., 2011. Single dose streptozotocin-induced diabetes:
 1423 considerations for study design in islet transplantation models. *Lab Anim* 45, 131–
 1424 140. doi:10.1258/la.2010.010090
 1425 Deng, Z.-L., Sztajer, H., Jarek, M., Bhujju, S., Wagner-Döbler, I., 2018. Worlds Apart –
 1426 Transcriptome Profiles of Key Oral Microbes in the Periodontal Pocket Compared to
 1427 Single Laboratory Culture Reflect Synergistic Interactions. *Front Microbiol* 9, 15–15.
 1428 doi:10.3389/fmicb.2018.00124
 1429 Desai, M.S., Seekatz, A.M., Koropatkin, N.M., Kamada, N., Hickey, C.A., Wolter, M.,
 1430 Pudlo, N.A., Kitamoto, S., Terrapon, N., Muller, A., Young, V.B., Henrissat, B.,
 1431 Wilmes, P., Stappenbeck, T.S., Núñez, G., Martens, E.C., 2016. A Dietary Fiber-
 1432 Deprived Gut Microbiota Degrades the Colonic Mucus Barrier and Enhances
 1433 Pathogen Susceptibility. *Cell* 167, 1339–1353.e1321.
 1434 Dethlefsen, L., Relman, D.A., 2011. Incomplete recovery and individualized responses of
 1435 the human distal gut microbiota to repeated antibiotic perturbation. *Proc. Natl. Acad.*
 1436 *Sci. U.S.A.* 108, 4551–4561. doi:10.1073/pnas.1000087107/-
 1437 /DCSupplemental/pnas.201000087SI.pdf

1438 Dwyer, D.J., Belenky, P.A., Yang, J.H., MacDonald, I.C., Martell, J.D., Takahashi, N.,
 1439 Chan, C.T.Y., Lobritz, M.A., Braff, D., Schwarz, E.G., Ye, J.D., Pati, M., Vercruysse,
 1440 M., Ralifo, P.S., Allison, K.R., Khalil, A.S., Ting, A.Y., Walker, G.C., Collins, J.J., 2014.
 1441 Antibiotics induce redox-related physiological alterations as part of their lethality.
 1442 Proc. Natl. Acad. Sci. U.S.A. 111, E2100–E2109. doi:10.1073/pnas.1401876111
 1443 Edwards, R., 1997. Resistance to *B*-lactam antibiotics in *Bacteroides* spp. Journal of
 1444 Medical Microbiology 46, 979–986.
 1445 Erhardt, M., Dersch, P., 2015. Regulatory principles governing Salmonella and Yersinia
 1446 virulence. Front Microbiol 6, 1–20. doi:10.3389/fmicb.2015.00949
 1447 Ernst, D.C., Downs, D.M., 2015. The STM4195 Gene Product (PanS) Transports
 1448 Coenzyme A Precursors in *Salmonella enterica*. Journal of Bacteriology 197, 1–10.
 1449 doi:10.1128/JB.02506-14
 1450 Fernández-Ochoa, Á., Cázares-Camacho, R., Borrás-Linares, I., Domínguez-Avila, J.A.,
 1451 Segura-Carretero, A., González-Aguilar, G.A., 2020. Evaluation of metabolic changes
 1452 in liver and serum of streptozotocin-induced diabetic rats after Mango diet
 1453 supplementation. Journal of Functional Foods 64, 103695.
 1454 doi:10.1016/j.jff.2019.103695
 1455 Fischbach, M.A., Sonnenburg, J.L., 2011. Eating For Two: How Metabolism Establishes
 1456 Interspecies Interactions in the Gut. Cell Host & Microbe 10, 336–347.
 1457 doi:10.1016/j.chom.2011.10.002
 1458 Franzosa, E.A., McIver, L.J., Rahnnavard, G., Thompson, L.R., Schirmer, M., Weingart,
 1459 G., Lipson, K.S., Knight, R., Caporaso, J.G., Segata, N., Huttenhower, C., 2018.
 1460 Species-level functional profiling of metagenomes and metatranscriptomes. Nat
 1461 Methods 15, 962–968. doi:10.1038/s41592-018-0176-y
 1462 Fraser, C.M., Chapple, C., 2011. The Phenylpropanoid Pathway in Arabidopsis. The
 1463 Arabidopsis Book 9, e0152–19. doi:10.1199/tab.0152
 1464 Fuhrer, T., Heer, D., Begemann, B., Zamboni, N., 2011. High-Throughput, Accurate Mass
 1465 Metabolome Profiling of Cellular Extracts by Flow Injection–Time-of-Flight Mass
 1466 Spectrometry. Anal. Chem. 83, 7074–7080. doi:10.1021/ac201267k
 1467 Fujisaka, S., Ussar, S., Clish, C., Devkota, S., Dreyfuss, J.M., Sakaguchi, M., Soto, M.,
 1468 Konishi, M., Softic, S., Altindis, E., Li, N., Gerber, G., Bry, L., Kahn, C.R., 2016.
 1469 Antibiotic effects on gut microbiota and metabolism are host dependent. Journal of
 1470 Clinical Investigation 126, 4430–4443. doi:10.1172/JCI86674
 1471 Gao, J., Xu, K., Liu, H., Liu, G., Bai, M., Peng, C., Li, T., Yin, Y., 2018. Impact of the Gut
 1472 Microbiota on Intestinal Immunity Mediated by Tryptophan Metabolism. Front. Cell.
 1473 Infect. Microbiol. 8, 1010–22. doi:10.3389/fcimb.2018.00013
 1474 Garsin, D.A., 2010. Ethanolamine Utilization in Bacterial Pathogens: Roles and
 1475 Regulation. Nat Rev Micro 8, 290–295. doi:10.1038/nrmicro2334
 1476 Gertsman, I., Barshop, B.A., 2018. Promises and pitfalls of untargeted metabolomics. J
 1477 Inherit Metab Dis 41, 355–366. doi:10.1007/s10545-017-0130-7
 1478 Goodman, A.L., McNulty, N.P., Zhao, Y., Leip, D., Mitra, R.D., Lozupone, C.A., Knight,
 1479 R., Gordon, J.I., 2009. Identifying Genetic Determinants Needed to Establish a
 1480 Human Gut Symbiont in Its Habitat. Cell Host & Microbe 6, 279–289.
 1481 doi:10.1016/j.chom.2009.08.003
 1482 Goyal, S.N., Reddy, N.M., Patil, K.R., Nakhate, K.T., Ojha, S., Patil, C.R., Agrawal, Y.O.,
 1483 2016. Challenges and issues with streptozotocin-induced diabetes - A clinically

- relevant animal model to understand the diabetes pathogenesis and evaluate
therapeutics. *Chemico-Biological Interactions* 244, 49–63.
doi:10.1016/j.cbi.2015.11.032
- Grondin, J.M., Tamura, K., Déjean, G., Abbott, D.W., Brumer, H., 2017. Polysaccharide
Utilization Loci: Fueling Microbial Communities. *Journal of Bacteriology* 199, 237–15.
doi:10.1128/JB.00860-16
- Holst, J.J., Gribble, F., Horowitz, M., Rayner, C.K., 2016. Roles of the Gut in Glucose
Homeostasis. *Dia Care* 39, 884–892. doi:10.2337/dc16-0351
- Iino, T., Mori, K., Tanaka, K., Suzuki, K.-I., Harayama, S., 2007. *Oscillibacter*
valericigenes gen. nov., sp. nov., a valerate-producing anaerobic bacterium isolated
from the alimentary canal of a Japanese corbicula clam. *International Journal of*
Systematic and Evolutionary Microbiology 57, 1840–1845. doi:10.1099/ij.s.0.64717-0
- Jain, N., Mishra, S.K., Shankar, U., Jaiswal, A., Sharma, T.K., Kodgire, P., Kumar, A.,
2020. G-quadruplex stabilization in the ions and maltose transporters gene inhibit
Salmonella enterica growth and virulence. *Genomics* 11, 4863–4874.
doi:10.1016/j.ygeno.2020.09.010
- Johnson, E.L., Heaver, S.L., Waters, J.L., Kim, B.I., Bretin, A., Goodman, A.L., Gewirtz,
A.T., Worgall, T.S., Ley, R.E., 2020. Sphingolipids produced by gut bacteria enter
host metabolic pathways impacting ceramide levels. *Nature Communications* 11, 1–
11. doi:10.1038/s41467-020-16274-w
- Kaakoush, N.O., 2015. Insights into the Role of *Erysipelotrichaceae* in the Human Host.
Front. Cell. Infect. Microbiol. 5, 181–4. doi:10.3389/fcimb.2015.00084
- Kaiko, G.E., Stappenbeck, T.S., 2014. Host–microbe interactions shaping the
gastrointestinal environment. *Trends in Immunology* 35, 538–548.
doi:10.1016/j.it.2014.08.002
- Kazemian, N., Ramezankhani, M., Sehgal, A., Khalid, F.M., Kalkhoran, A.H.Z., Narayan,
A., Wong, G.K.-S., Kao, D., Pakpour, S., 2020. The trans-kingdom battle between
donor and recipient gut microbiome influences fecal microbiota transplantation
outcome. *Sci Rep* 1–10. doi:10.1038/s41598-020-75162-x
- Kobayashi, K., Forte, T.M., Taniguchi, S., Ishida, B.Y., Oka, K., Chan, L., 2000. The *db/db*
Mouse, a Model for Diabetic Dyslipidemia: Molecular Characterization and Effect of
Western Diet Feeding. *Metabolism* 49, 22–31.
- Koepsell, H., 2020. Glucose transporters in the small intestine in health and disease 1–
42. doi:10.1007/s00424-020-02439-5
- Kohanski, M.A., Dwyer, D.J., Hayete, B., Lawrence, C.A., Collins, J.J., 2007. A Common
Mechanism of Cellular Death Induced by Bactericidal Antibiotics. *Cell* 130, 797–810.
doi:10.1016/j.cell.2007.06.049
- Kuno, T., Hirayama-Kurogi, M., Ito, S., Ohtsuki, S., 2018. Reduction in hepatic secondary
bile acids caused by short-term antibiotic-induced dysbiosis decreases mouse serum
glucose and triglyceride levels. *Sci Rep* 1–15. doi:10.1038/s41598-018-19545-1
- Kuribayashi, H., Miyata, M., Yamakawa, H., Yoshinari, K., Yamazoe, Y., 2012.
Enterobacteria-mediated deconjugation of taurocholic acid enhances ileal farnesoid
X receptor signaling. *European Journal of Pharmacology* 697, 132–138.
doi:10.1016/j.ejphar.2012.09.048
- Lam, P.L., Wong, R.S.M., Lam, K.H., Hung, L.K., Wong, M.M., Yung, L.H., Ho, Y.W.,
Wong, W.Y., Hau, D.K.P., Gambari, R., Chui, C.H., 2020. The role of reactive oxygen

species in the biological activity of antimicrobial agents_ An updated mini review. *Chemico-Biological Interactions* 320, 109023. doi:10.1016/j.cbi.2020.109023

Langmead, B., Salzberg, S.L., 2012. Fast gapped-read alignment with Bowtie 2. *Nat Methods* 9, 357–359. doi:10.1038/nmeth.1923

Layeghifard, M., Hwang, D.M., Guttman, D.S., 2017. Disentangling Interactions in the Microbiome: A Network Perspective. *Trends in Microbiology* 25, 217–228. doi:10.1016/j.tim.2016.11.008

Lei, Z., Huhman, D.V., Sumner, L.W., 2011. Mass Spectrometry Strategies in Metabolomics. *J. Biol. Chem.* 286, 25435–25422. doi:10.1074/jbc.R111.238691

Ley, R.E., 2014. Harnessing Microbiota to Kill a Pathogen: The sweet tooth of *Clostridium difficile*. *Nat Med* 20, 248–249. doi:10.1038/nm.3494

Li, H., Durbin, R., 2010. Fast and accurate long-read alignment with Burrows–Wheeler transform. *Bioinformatics* 26, 589–595. doi:10.1093/bioinformatics/btp698

Li, T., Francl, J.M., Boehme, S., Ochoa, A., Zhang, Y., Klaassen, C.D., Erickson, S.K., Chiang, J.Y.L., 2012. Glucose and Insulin Induction of Bile Acid Synthesis. *J. Biol. Chem.* 287, 1861–1873. doi:10.1074/jbc.M111.305789

Liu, H., Price, M.N., Carlson, H.K., Chen, Y., Ray, J., Shiver, A.L., Petzold, C.J., Huang, K.C., Arkin, A.P., Deutschbauer, A.M., 2019. Large-scale chemical-genetics of the human gut bacterium *Bacteroides thetaiotaomicron*. *bioRxiv* 26, 563–35. doi:10.1101/573055

Liu, S., Qin, P., Wang, J., 2019. High-Fat Diet Alters the Intestinal Microbiota in Streptozotocin-Induced Type 2 Diabetic Mice. *Microorganisms* 7, 1–12. doi:10.3390/microorganisms7060176

Lobritz, M.A., Belenky, P., Porter, C.B.M., Gutierrez, A., Yang, J.H., Schwarz, E.G., Dwyer, D.J., Khalil, A.S., Collins, J.J., 2015. Antibiotic efficacy is linked to bacterial cellular respiration. *Proc. Natl. Acad. Sci. U.S.A.* 112, 8173–8180.

Love, M.I., Huber, W., Anders, S., 2014. Moderated estimation of fold change and dispersion for RNA-seq data with DESeq2. *Genome Biol.* 15, 31–21. doi:10.1186/s13059-014-0550-8

Lu, J., Breitwieser, F.P., Thielen, P., Salzberg, S.L., 2017. Bracken: estimating species abundance in metagenomics data. *PeerJ Computer Science* 3, 1–17. doi:10.7717/peerj-cs.104

Luan, H., Wang, X., Cai, Z., 2019. Mass spectrometry-based metabolomics: Targeting the crosstalk between gut microbiota and brain in neurodegenerative disorders. *Mass Spectrometry Reviews* 38, 22–33. doi:10.1002/mas.21553

Lundgren, P., Thaïs, Christoph A, 2020. The microbiome-adipose tissue axis in systemic metabolism. *American Journal of Physiology-Gastrointestinal and Liver Physiology* 318, G717–G724. doi:10.1152/ajpgi.00304.2019

Lynch, J.B., Sonnenburg, J.L., 2012. Prioritization of a plant polysaccharide over a mucus carbohydrate is enforced by a *Bacteroides* hybrid two-component system. *Mol. Microbiol.* 85, 478–491. doi:10.1111/j.1365-2958.2012.08123.x

Ma, Q., Li, Y., Wang, J., Li, P., Duan, Y., Dai, H., An, Y., Cheng, L., Wang, T., Wang, C., Wang, T., Zhao, B., 2020. Investigation of gut microbiome changes in type 1 diabetic mellitus rats based on high-throughput sequencing. *Biomedicine & Pharmacotherapy* 124, 109873. doi:10.1016/j.biopha.2020.109873

- Makki, K., Deehan, E.C., Walter, J., Bäckhed, F., 2018. The Impact of Dietary Fiber on Gut Microbiota in Host Health and Disease. *Cell Host & Microbe* 23, 705–715. doi:10.1016/j.chom.2018.05.012
- Mardo, K., Visnapuu, T., Vija, H., Aasamets, A., Viigand, K., Alamäe, T., 2017. A Highly Active Endo-Levanase BT1760 of a Dominant Mammalian Gut Commensal *Bacteroides thetaiotaomicron* Cleaves Not Only Various Bacterial Levans, but Also Levan of Timothy Grass. *PLoS ONE* 12, e0169989–25. doi:10.1371/journal.pone.0169989
- Martens, E.C., Chiang, H.C., Gordon, J.I., 2008. Mucosal Glycan Foraging Enhances Fitness and Transmission of a Saccharolytic Human Gut Bacterial Symbiont. *Cell Host & Microbe* 4, 447–457. doi:10.1016/j.chom.2008.09.007
- Martínez, I., Perdicaro, D.J., Brown, A.W., Hammons, S., Carden, T.J., Carr, T.P., Eskridge, K.M., Walter, J., 2012. Diet-Induced Alterations of Host Cholesterol Metabolism Are Likely To Affect the Gut Microbiota Composition in Hamsters. *Applied and Environmental Microbiology* 79, 516–524. doi:10.1128/AEM.03046-12
- McIver, L.J., Abu-Ali, G., Franzosa, E.A., Schwager, R., Morgan, X.C., Waldron, L., Segata, N., Huttenhower, C., 2018. bioBakery: a meta'omic analysis environment. *Bioinformatics* 34, 1235–1237. doi:10.1093/bioinformatics/btx754#supplementary-data
- McMurdie, P.J., Holmes, S., 2013. phyloseq: An R Package for Reproducible Interactive Analysis and Graphics of Microbiome Census Data. *PLoS ONE* 8, e61217–11. doi:10.1371/journal.pone.0061217
- Meadows, J.A., Wargo, M.J., 2015. Carnitine in bacterial physiology and metabolism. *Microbiology* 161, 1161–1174. doi:10.1099/mic.0.000080
- Mewis, K., Lenfant, N., Lombard, V., Henrissat, B., 2016. Dividing the Large Glycoside Hydrolase Family 43 into Subfamilies: a Motivation for Detailed Enzyme Characterization. *Applied and Environmental Microbiology* 82, 1686–1692. doi:10.1128/AEM.03453-15
- Meylan, S., Porter, C.B.M., Yang, J.H., Belenky, P., Gutierrez, A., Lobritz, M.A., Park, J., Kim, S.H., Moskowitz, S.M., Collins, J.J., 2017. Carbon Sources Tune Antibiotic Susceptibility in *Pseudomonas aeruginosa* via Tricarboxylic Acid Cycle Control. *Cell Chem Biol* 24, 195–206. doi:10.1016/j.chembiol.2016.12.015
- Miller, K.A., Phillips, R.S., Mrazek, J., Hoover, T.R., 2013. *Salmonella* Utilizes D-Glucosamine via a Mannose Family Phosphotransferase System Permease and Associated Enzymes. *Journal of Bacteriology* 195, 4057–4066. doi:10.1128/JB.00290-13
- Mimee, M., Tucker, A.C., Voigt, C.A., Lu, T.K., 2015. Programming a Human Commensal Bacterium, *Bacteroides thetaiotaomicron*, to Sense and Respond to Stimuli in the Murine Gut Microbiota. *Cell Systems* 1, 62–71. doi:10.1016/j.cels.2015.06.001
- Molinero, N., Ruiz, L., Sanchez, B., Margolles, A., Delgado, S., 2019. Intestinal Bacteria Interplay With Bile and Cholesterol Metabolism: Implications on Host Physiology. *fphys-10-00185.tex* 1–10. doi:10.3389/fphys.2019.00185
- Moore, B.S., Hertweck, C., Hopke, J.N., Izumikawa, M., Kalaitzis, J.A., Nilsen, G., O'Hare, T., Piel, J., Shipley, P.R., Xiang, L., Austin, M.B., Noel, J.P., 2002. Plant-like Biosynthetic Pathways in Bacteria: From Benzoic Acid to Chalcone 1. *J. Nat. Prod.* 65, 1956–1962. doi:10.1021/np020230m

- Motyl, K., McCabe, L.R., 2009. Streptozotocin, Type I Diabetes Severity and Bone. *Biological Procedures Online* 11, 296–315. doi:10.1007/s12575-009-9000-5
- Nawrocki, K.L., Wetzel, D., Jones, J.B., Woods, E.C., McBride, S.M., 2018. Ethanolamine is a Valuable Nutrient Source that Impacts *Clostridium difficile* Pathogenesis. *Environmental Microbiology* 20, 1419–1435. doi:10.1111/1462-2920.14048
- Neis, E., Dejong, C., Rensen, S., 2015. The Role of Microbial Amino Acid Metabolism in Host Metabolism. *Nutrients* 7, 2930–2946. doi:10.3390/nu7042930
- Newman, M.A., Petri, R.M., Grüll, D., Zebeli, Q., Metzler-Zebeli, B.U., 2018. Transglycosylated Starch Modulates the Gut Microbiome and Expression of Genes Related to Lipid Synthesis in Liver and Adipose Tissue of Pigs. *Front Microbiol* 9, 5245–17. doi:10.3389/fmicb.2018.00224
- Ng, K.M., Aranda-Díaz, A., Tropini, C., Frankel, M.R., Van Treuren, W., O’Loughlin, C.T., Merrill, B.D., Yu, F.B., Pruss, K.M., Oliveira, R.A., Higginbottom, S.K., Neff, N.F., Fischbach, M.A., Xavier, K.B., Sonnenburg, J.L., Huang, K.C., 2019. Recovery of the Gut Microbiota after Antibiotics Depends on Host Diet, Community Context, and Environmental Reservoirs. *Cell Host & Microbe* 26, 650–665.e4. doi:10.1016/j.chom.2019.10.011
- Nikita Lomis, S.W., 2015. The Gut Microflora and its Metabolites Regulate the Molecular Crosstalk between Diabetes and Neurodegeneration. *J Diabetes Metab* 06, 1–17. doi:10.4172/2155-6156.1000577
- Nothias, L.-F., Petras, D., Schmid, R., Dührkop, K., Rainer, J., Sarvepalli, A., Protsyuk, I., Ernst, M., Tsugawa, H., Fleischauer, M., Aicheler, F., Aksenov, A.A., Alka, O., Allard, P.-M., Barsch, A., Cachet, X., Caraballo-Rodriguez, A.M., Da Silva, R.R., Dang, T., Garg, N., Gauglitz, J.M., Gurevich, A., Isaac, G., Jarmusch, A.K., Kameník, Z., Kang, K.B., Kessler, N., Koester, I., Korf, A., Le Gouellec, A., Ludwig, M., Martin, C.H., McCall, L.-I., McSayles, J., Meyer, S.W., Mohimani, H., Morsy, M., Moyne, O., Neumann, S., Neuweiger, H., Nguyen, N.H., Nothias-Esposito, M., Paolini, J., Phelan, V.V., Pluskal, T., Quinn, R.A., Rogers, S., Shrestha, B., Tripathi, A., van der Hooft, J.J.J., Vargas, F., Weldon, K.C., Witting, M., Yang, H., Zhang, Z., Zubeil, F., Kohlbacher, O., Böcker, S., Alexandrov, T., Bandeira, N., Wang, M., Dorrestein, P.C., 2020. Feature-based molecular networking in the GNPS analysis environment. *Nature Methods* 17, 905-908. doi:10.1038/s41592-020-0933-6
- Noor, S., Khan, R.U., Ahmad, J., 2017. Diabetes & Metabolic Syndrome: Clinical Research & Reviews. *Diabetes & Metabolic Syndrome: Clinical Research & Reviews* 11, 149–156. doi:10.1016/j.dsx.2016.06.023
- Oliphant, K., Allen-Vercoe, E., 2019. Macronutrient metabolism by the human gut microbiome: major fermentation by- products and their impact on host health. *Microbiome* 7, 1–15. doi:10.1186/s40168-019-0704-8
- Ormsby, M.J., Logan, M., le A Johnson, S.Ã., McIntosh, A., Fallata, G., Papadopoulou, R., Papachristou, E., Hold, G.L., Hansen, R., Ijaz, U.Z., Russell, R.K., Gerasimidis, K., Wall, D.M., 2019. Inflammation associated ethanolamine facilitates infection by Crohn's disease-linked adherent-invasive *Escherichia coli*. *EBioMedicine* 43, 325–332. doi:10.1016/j.ebiom.2019.03.071
- Overbeek, R., Olson, R., Pusch, G.D., Olsen, G.J., Davis, J.J., Disz, T., Edwards, R.A., Gerdes, S., Parrello, B., Shukla, M., Vonstein, V., Wattam, A.R., Xia, F., Stevens, R., 2013. The SEED and the Rapid Annotation of microbial genomes using Subsystems

Technology (RAST). *Nucleic Acids Research* 42, D206–D214. doi:10.1093/nar/gkt1226

Patterson, E., Marques, T.M., O’Sullivan, O., Fitzgerald, P., Fitzgerald, G.F., Cotter, P.D., Dinan, T.G., Cryan, J.F., Stanton, C., Ross, R.P., 2014. Streptozotocin-induced type-1-diabetes disease onset in Sprague–Dawley rats is associated with an altered intestinal microbiota composition and decreased diversity. *Microbiology* 161, 182–193. doi:10.1099/mic.0.082610-0

Pluskal, T., Castillo, S., Villar-Briones, A., Orešič, M., 2010. MZmine 2: Modular framework for processing, visualizing, and analyzing mass spectrometry-based molecular profile data. *BMC Bioinformatics* 11, 1–11. doi:10.1186/1471-2105-11-395

Poretzky, R., Rodriguez-R, L.M., Luo, C., Tsementzi, D., Konstantinidis, K.T., 2014. Strengths and Limitations of 16S rRNA Gene Amplicon Sequencing in Revealing Temporal Microbial Community Dynamics. *PLoS ONE* 9, e93827–12. doi:10.1371/journal.pone.0093827

Pruesse, E., Quast, C., Knittel, K., Fuchs, B.M., Ludwig, W., Peplies, J., Glockner, F.O., 2007. SILVA: a comprehensive online resource for quality checked and aligned ribosomal RNA sequence data compatible with ARB. *Nucleic Acids Research* 35, 7188–7196. doi:10.1093/nar/gkm864

Qin, J., Li, Y., Cai, Z., Li, S., Zhu, J., Zhang, F., Liang, S., Zhang, W., Guan, Y., Shen, D., Peng, Y., Zhang, D., Jie, Z., Wu, W., Qin, Y., Xue, W., Li, J., Han, L., Lu, D., Wu, P., Dai, Y., Sun, X., Li, Z., Tang, A., Zhong, S., Li, X., Chen, W., Xu, R., Wang, M., Feng, Q., Gong, M., Yu, J., Zhang, Y., Zhang, M., Hansen, T., Sanchez, G., Raes, J., Falony, G., Okuda, S., Almeida, M., LeChatelier, E., Renault, P., Pons, N., Batto, J.-M., Zhang, Z., Chen, H., Yang, R., Zheng, W., Li, S., Yang, H., Wang, J., Ehrlich, S.D., Nielsen, R., Pedersen, O., Kristiansen, K., Wang, J., 2012. A metagenome-wide association study of gut microbiota in type 2 diabetes. *Nature* 490, 55–60. doi:10.1038/nature11450

Quinn, R.A., Melnik, A.V., Vrbancac, A., Fu, T., Patras, K.A., Christy, M.P., Bodai, Z., Belda-Ferre, P., Tripathi, A., Chung, L.K., Downes, M., Welch, R.D., Quinn, M., Humphrey, G., Panitchpakdi, M., Weldon, K.C., Aksenov, A., Silva, R., Avila-Pacheco, J., Clish, C., Bae, S., Mallick, H., Franzosa, E.A., Lloyd-Price, J., Bussell, R., Thron, T., Nelson, A.T., Wang, M., Leszczynski, E., Vargas, F., Gauglitz, J.M., Meehan, M.J., Gentry, E., Arthur, T.D., Komor, A.C., Poulsen, O., Boland, B.S., Chang, J.T., Sandborn, W.J., Lim, M., Garg, N., Lumeng, J.C., Xavier, R.J., Kazmierczak, B.I., Jain, R., Egan, M., Rhee, K.E., Ferguson, D., Raffatellu, M., Vlamakis, H., Haddad, G.G., Siegel, D., Huttenhower, C., Mazmanian, S.K., Evans, R.M., Nizet, V., Knight, R., Dorrestein, P.C., 2020. Global chemical effects of the microbiome include new bile-acid conjugations. *Nature* 579, 123–129. doi:10.1038/s41586-020-2047-9

Ranjan, R., Rani, A., Metwally, A., McGee, H.S., Perkins, D.L., 2016. Analysis of the microbiome: Advantages of whole genome shotgun versus 16S amplicon sequencing. *Biochem. Biophys. Res. Commun.* 469, 967–977. doi:10.1016/j.bbrc.2015.12.083

Rayner, C.K., Horowitz, M., 2006. Gastrointestinal motility and glycemic control in diabetes: the chicken and the egg revisited? *Journal of Clinical Investigation* 116, 299–302. doi:10.1172/JCI25618

- Rey, F.E., Faith, J.J., Bain, J., Muehlbauer, M.J., Stevens, R.D., Newgard, C.B., Gordon, J.I., 2010. Dissecting the *in Vivo* Metabolic Potential of Two Human Gut Acetogens. *J. Biol. Chem.* 285, 22082–22090. doi:10.1074/jbc.M110.117713
- Rhen, M., 2019. *Salmonella* and Reactive Oxygen Species: A Love-Hate Relationship. *Journal of Innate Immunity* 11, 216–226. doi:10.1159/000496370
- Ridlon, J.M., Kang, D.J., Hylemon, P.B., Bajaj, J.S., 2014. Bile acids and the gut microbiome. *Current Opinion in Gastroenterology* 30, 332–338. doi:10.1097/MOG.0000000000000057
- Rivera-Chávez, F., Zhang, L.F., Faber, F., Lopez, C.A., Byndloss, M.X., Olsan, E.E., Xu, G., Velazquez, E.M., Lebrilla, C.B., Winter, S.E., Bäuml, A.J., 2016. Depletion of Butyrate-Producing Clostridia from the Gut Microbiota Drives an Aerobic Luminal Expansion of *Salmonella*. *Cell Host & Microbe* 19, 443–454. doi:10.1016/j.chom.2016.03.004
- Rowley, C.A., Anderson, C.J., Kendall, M.M., 2018. Ethanolamine Influences Human Commensal *Escherichia coli* Growth, Gene Expression, and Competition with Enterohemorrhagic *E. coli* O157:H7. *mBio* 9, 1–5. doi:10.1128/mBio.01429-18
- Sabatino, A., Regolisti, G., Cosola, C., Gesualdo, L., Fiaccadori, E., 2017. Intestinal Microbiota in Type 2 Diabetes and Chronic Kidney Disease 1–9. doi:10.1007/s11892-017-0841-z
- Saeedi, P., Petersohn, I., Salpea, P., Malanda, B., Karuranga, S., Unwin, N., Colagiuri, S., Guariguata, L., Motala, A.A., Ogurtsova, K., Shaw, J.E., Bright, D., Williams, R., 2019. Global and regional diabetes prevalence estimates for 2019 and projections for 2030 and 2045: Results from the International Diabetes Federation Diabetes Atlas, 9th edition. *Diabetes Research and Clinical Practice* 157, 107843–27. doi:10.1016/j.diabres.2019.107843
- Sakanyan, V., Kochikyan, A., Mett, I., Legrain, C., Charlier, D., Pierard, A., Glansdorff, N., 1992. A re-examination of the pathway for ornithine biosynthesis in a thermophilic and two mesophilic *Bacillus* species. *Journal of General Microbiology* 138, 125–130.
- Sato, H., Zhang, L.S., Martinez, K., Chang, E.B., Yang, Q., Wang, F., Howles, P.N., Hokari, R., Miura, S., Tso, P., 2016. Antibiotics Suppress Activation of Intestinal Mucosal Mast Cells and Reduce Dietary Lipid Absorption in Sprague-Dawley Rats. *Gastroenterology* 151, 923–932. doi:10.1053/j.gastro.2016.07.009
- Savannah J Taylor, S.E.W., 2020. *Salmonella* finds a way: Metabolic versatility of *Salmonella enterica* serovar Typhimurium in diverse host environments. *PLoS Pathog* 16. doi:10.1371/journal.ppat.1008540
- Sayin, S.I., Wahlström, A., Felin, J., Jäntti, S., Marschall, H.-U., Bamberg, K., Angelin, B., Hyötyläinen, T., Orešič, M., Bäckhed, F., 2013. Gut Microbiota Regulates Bile Acid Metabolism by Reducing the Levels of Tauro-beta-muricholic Acid, a Naturally Occurring FXR Antagonist. *Cell Metabolism* 17, 225–235. doi:10.1016/j.cmet.2013.01.003
- Schoeler, M., Caesar, R., 2019. Dietary lipids, gut microbiota and lipid metabolism. *Reviews in Endocrine and Metabolic Disorders* 20, 461–472. doi:10.1007/s11154-019-09512-0
- Schrimpe-Rutledge, A.C., Codreanu, S.G., Sherrod, S.D., McLean, J.A., 2016. Untargeted Metabolomics Strategies—Challenges and Emerging Directions. *J. Am. Soc. Mass Spectrom.* 27, 1897–1905. doi:10.1007/s13361-016-1469-y

- Segata, N., Izard, J., Waldron, L., Gevers, D., Miropolsky, L., Garrett, W.S., Huttenhower, C., 2011. Metagenomic biomarker discovery and explanation. *Genome Biol.* 12, R60. doi:10.1186/gb-2011-12-6-r60
- Shin, A., Preidis, G.A., Shulman, R., Kashyap, P.C., 2019. The Gut Microbiome in Adult and Pediatric Functional Gastrointestinal Disorders. *Clinical Gastroenterology and Hepatology* 17, 256–274. doi:10.1016/j.cgh.2018.08.054
- Sliwkowski, M.X., Stadtman, T.C., 1988. Selenoprotein A of the clostridial glycine reductase complex: Purification and amino acid sequence of the selenocysteine-containing peptide. *Proc. Natl. Acad. Sci. U.S.A.* 85, 368–371.
- Smits, S.A., Leach, J., Sonnenburg, E.D., Gonzalez, C.G., Lichtman, J.S., Reid, G., Knight, R., Manjurano, A., Chagalucha, J., Elias, J.E., Dominguez-Bello, M.G., Sonnenburg, J.L., 2017. Seasonal cycling in the gut microbiome of the Hadza hunter-gatherers of Tanzania. *Science* 357, 802–806. doi:10.1126/science.aan4834
- Sonnenburg, J.L., Xu, J., Leip, D.D., Chen, C.-H., Westover, B.P., Weatherford, J., Buhler, J.D., Gordon, J.I., 2005. Glycan Foraging in vivo by an Intestine-Adapted Bacterial Symbiont. *Science* 307, 1952–1955. doi:10.1126/science.1108397
- Srikumar, S., Fuchs, T.M., 2010. Ethanolamine Utilization Contributes to Proliferation of *Salmonella enterica* Serovar Typhimurium in Food and in Nematodes. *Applied and Environmental Microbiology* 77, 1–10. doi:10.1128/AEM.01403-10
- Staley, C., Weingarden, A.R., Khoruts, A., Sadowsky, M.J., 2016. Interaction of gut microbiota with bile acid metabolism and its influence on disease states. *Appl Microbiol Biotechnol* 101, 47–64. doi:10.1007/s00253-016-8006-6
- Steinert, R.E., Lee, Y.-K., Sybesma, W., 2020. Vitamins for the Gut Microbiome. *Trends in Molecular Medicine* 26, 137–140. doi:10.1016/j.molmed.2019.11.005
- Stokes, J.M., Lopatkin, A.J., Lobritz, M.A., Collins, J.J., 2019a. Bacterial Metabolism and Antibiotic Efficacy. *Cell Metabolism*.
- Stokes, J.M., Lopatkin, A.J., Lobritz, M.A., Collins, J.J., 2019b. Bacterial Metabolism and Antibiotic Efficacy. *Cell Metabolism* 30, 251–259. doi:10.1016/j.cmet.2019.06.009
- Šarenac, T.M., Mikov, M., 2018. Bile Acid Synthesis: From Nature to the Chemical Modification and Synthesis and Their Applications as Drugs and Nutrients. *Front. Pharmacol.* 9, 5–22. doi:10.3389/fphar.2018.00939
- Tanes, C., Bittinger, K., Gao, Y., Friedman, E.S., Nessel, L., Paladhi, U.R., Chau, L., Panfen, E., Fischbach, M.A., Braun, J., Xavier, R.J., Clish, C.B., Li, H., Bushman, F.D., Lewis, J.D., Wu, G.D., 2021. Role of dietary fiber in the recovery of the human gut microbiome and its metabolome. *Cell Host & Microbe* 1–20. doi:10.1016/j.chom.2020.12.012
- Tang, M., Etokidem, E., Lai, K., 2016. The Leloir Pathway of Galactose Metabolism – A Novel Therapeutic Target for Hepatocellular Carcinoma. *AR* 36, 6265–6272. doi:10.21873/anticancerres.11221
- Terrapon, N., Lombard, V., Gilbert, H.J., Henrissat, B., 2015. Automatic prediction of polysaccharide utilization loci in Bacteroidetes species. *Bioinformatics* 31, 647–655. doi:10.1093/bioinformatics/btu716/-/DC1
- Thaiss, Christopher A, Levy, M., Grosheva, I., Zheng, D., Soffer, E., Blacher, E., Braverman, S., Tengeler, A.C., Barak, O., Elazar, M., Ben-Zeev, R., Lehavi-Regev, D., Katz, M.N., Pevsner-Fischer, M., Gertler, A., Halpern, Z., Harmelin, A., Aamar, S., Serradas, P., Grosfeld, A., Shapiro, H., Geiger, B., Elinav, E., 2018. Hyperglycemia

drives intestinal barrier dysfunction and risk for enteric infection. *Science* 359, 1376–1383.

Theriot, C.M., Bowman, A.A., Young, V.B., 2015. Antibiotic-Induced Alterations of the Gut Microbiota Alter Secondary Bile Acid Production and Allow for *Clostridium difficile* Spore Germination and Outgrowth in the Large Intestine. *mSphere* 1, e00045–15–16. doi:10.1128/mSphere.00045-15

Theriot, C.M., Young, V.B., 2015. Interactions Between the Gastrointestinal Microbiome and *Clostridium difficile*. *Annu. Rev. Microbiol.* 69, 445–461. doi:10.1146/annurev-micro-091014-104115

Thiennimitr, P., Winter, S.E., Winter, M.G., Xavier, M.N., Tolstikov, V., Huseby, D.L., Sterzenbach, T., Tsois, R.M., Roth, J.R., Bäuml, A.J., 2011a. Intestinal inflammation allows *Salmonella* to use ethanolamine to compete with the microbiota. *Proc. Natl. Acad. Sci. U.S.A.* 108, 17480–17485. doi:10.1073/pnas.1107857108/-/DCSupplemental/pnas.201107857SI.pdf

Thiennimitr, P., Winter, S.E., Winter, M.G., Xavier, M.N., Tolstikov, V., Huseby, D.L., Sterzenbach, T., Tsois, R.M., Roth, J.R., Bäuml, A.J., 2011b. Intestinal inflammation allows *Salmonella* to use ethanolamine to compete with the microbiota. *Proc. Natl. Acad. Sci. U.S.A.* 108, 1–6. doi:10.1073/pnas.1107857108/-/DCSupplemental/pnas.201107857SI.pdf

Thomas, V.C., Kinkead, L.C., Janssen, A., Schaeffer, C.R., Woods, K.M., Lindgren, J.K., Peaster, J.M., Chaudhari, S.S., Sadykov, M., Jones, J., Mohamadi AbdelGhani, S.M., Zimmerman, M.C., Bayles, K.W., Somerville, G.A., Fey, P.D., 2013. A Dysfunctional Tricarboxylic Acid Cycle Enhances Fitness of *Staphylococcus epidermidis* During Lactam Stress. *mBio* 4, e00437–13. doi:10.1128/mBio.00437-13

Thompson, L.R., Sanders, J.G., McDonald, D., Amir, A., Ladau, J., Locey, K.J., Prill, R.J., Tripathi, A., Gibbons, S.M., Ackermann, G., Navas-Molina, J.A., Janssen, S., Kopylova, E., Vázquez-Baeza, Y., González, A., Morton, J.T., Mirarab, S., Zech Xu, Z., Jiang, L., Haroon, M.F., Kanbar, J., Zhu, Q., Jin Song, S., Kosciolk, T., Bokulich, N.A., Lefler, J., Brislawn, C.J., Humphrey, G., Owens, S.M., Hampton-Marcell, J., Berg-lyons, D., McKenzie, V., Fierer, N., Fuhrman, J.A., Clauset, A., Stevens, R.L., Shade, A., Pollard, K.S., Goodwin, K.D., Jansson, J.K., Gilbert, J.A., Knight, R., The Earth Microbiome Project Consortium, 2017. A communal catalogue reveals Earth’s multiscale microbial diversity. *Nature* 551, 457–463. doi:10.1038/nature24621

Tian, L., Wang, X.-W., Wu, A.-K., Fan, Y., Friedman, J., Dahlin, A., Waldor, M.K., Weinstock, G.M., Weiss, S.T., Liu, Y.-Y., 2020. Deciphering functional redundancy in the human microbiome. *Nature Communications* 1–11. doi:10.1038/s41467-020-19940-1

Townsend, G.E., II, Han, W., Schwalm, N.D., III, Hong, X., Bencivenga-Barry, N.A., Goodman, A.L., Groisman, E.A., 2020. A Master Regulator of *Bacteroides thetaiotaomicron* Gut Colonization Controls Carbohydrate Utilization and an Alternative Protein Synthesis Factor. *mBio* 11, 34–15. doi:10.1128/mBio.03221-19

Tzin, V., Galili, G., 2010. The Biosynthetic Pathways for Shikimate and Aromatic Amino Acids in *Arabidopsis thaliana*, *The Arabidopsis Book*. doi:10.1199/tab.0132

Ugarte, M., Brown, M., Hollywood, K.A., Cooper, G.J., Bishop, P.N., Dunn, W.B., 2012. Metabolomic analysis of rat serum in streptozotocin-induced diabetes and after treatment with oral triethylenetetramine (TETA). *Genome Medicine* 4, AA.

1850 Ussar, S., Haering, M.-F., Fujisaka, S., Lutter, D., Lee, K.Y., Li, N., Gerber, G.K., Bry, L.,
 1851 Kahn, C.R., 2017. Regulation of Glucose Uptake and Enteroendocrine Function by
 1852 the Intestinal Epithelial Insulin Receptor. *Diabetes* 66, 886–896. doi:10.2337/db15-
 1853 1349
 1854 Vacca, M., Celano, G., Calabrese, F.M., Portincasa, P., Gobbetti, M., De Angelis, M.,
 1855 2020. The Controversial Role of Human Gut Lachnospiraceae. *Microorganisms* 8,
 1856 573–25. doi:10.3390/microorganisms8040573
 1857 Vollmer, M., Esders, S., Farquharson, F.M., Neugart, S., Duncan, S.H., Schreiner, M.,
 1858 Louis, P., Maul, R., Rohn, S., 2018. Mutual Interaction of Phenolic Compounds and
 1859 Microbiota: Metabolism of Complex Phenolic Apigenin- C- and Kaempferol- O-
 1860 Derivatives by Human Fecal Samples. *J. Agric. Food Chem.* 66, 485–497.
 1861 doi:10.1021/acs.jafc.7b04842
 1862 Vrieze, A., Out, C., Fuentes, S., Jonker, L., Reuling, I., Kootte, R.S., van Nood, E.,
 1863 Holleman, F., Knaapen, M., Romijn, J.A., Soeters, M.R., Blaak, E.E., Dallinga-Thie,
 1864 G.M., Reijnders, D., Ackermans, M.T., Serlie, M.J., Knop, F.K., Holst, J.J., van der
 1865 Ley, C., Kema, I.P., Zoetendal, E.G., De Vos, W.M., Hoekstra, J.B.L., Stroes, E.S.,
 1866 Groen, A.K., Nieuwdorp, M., 2014. Impact of oral vancomycin on gut microbiota, bile
 1867 acid metabolism, and insulin sensitivity. *Journal of Hepatology* 60, 824–831.
 1868 doi:10.1016/j.jhep.2013.11.034
 1869 Wang, C.-Y., Liao, J.K., 2011. A Mouse Model of Diet-Induced Obesity and Insulin
 1870 Resistance, in: Allen, I.C. (Ed.), *Mouse Models of Innate Immunity, Methods in*
 1871 *Molecular Biology*. Humana Press, Totowa, NJ, pp. 421–433. doi:10.1007/978-1-
 1872 61779-430-8_27
 1873 Wang, M., Carver, J.J., Phelan, V.V., Sanchez, L.M., Garg, N., Peng, Y., Nguyen, D.D.,
 1874 Watrous, J., Kapon, C.A., Luzzatto-Knaan, T., Porto, C., Bouslimani, A., Melnik,
 1875 A.V., Meehan, M.J., Liu, W.-T., Crusemann, M., Boudreau, P.D., Esquenazi, E.,
 1876 Sandoval-Calderón, M., Kersten, R.D., Pace, L.A., Quinn, R.A., Duncan, K.R., Hsu,
 1877 C.-C., Floros, D.J., Gavilan, R.G., Kleigrewe, K., Northen, T., Dutton, R.J., Parrot, D.,
 1878 Carlson, E.E., Aigle, B., Michelsen, C.F., Jelsbak, L., Sohlenkamp, C., Pevzner, P.,
 1879 Edlund, A., McLean, J., Piel, J., Murphy, B.T., Gerwick, L., Liaw, C.-C., Yang, Y.-L.,
 1880 Humpf, H.-U., Maansson, M., Keyzers, R.A., Sims, A.C., Johnson, A.R., Sidebottom,
 1881 A.M., Sedio, B.E., Klitgaard, A., Larson, C.B., Boya P, C.A., Torres-Mendoza, D.,
 1882 Gonzalez, D.J., Silva, D.B., Marques, L.M., Demarque, D.P., Pociute, E., O'Neill, E.C.,
 1883 Briand, E., Helfrich, E.J.N., Granatosky, E.A., Glukhov, E., Ryffel, F., Houson, H.,
 1884 Mohimani, H., Kharbush, J.J., Zeng, Y., Vorholt, J.A., Kurita, K.L., Charusanti, P.,
 1885 McPhail, K.L., Nielsen, K.F., Vuong, L., Elfeki, M., Traxler, M.F., Engene, N., Koyama,
 1886 N., Vining, O.B., Baric, R., Silva, R.R., Mascuch, S.J., Tomasi, S., Jenkins, S.,
 1887 Macherla, V., Hoffman, T., Agarwal, V., Williams, P.G., Dai, J., Neupane, R., Gurr, J.,
 1888 Rodríguez, A.M.C., Lamsa, A., Zhang, C., Dorrestein, K., Duggan, B.M., Almaliti, J.,
 1889 Allard, P.-M., Phapale, P., Nothias, L.-F., Alexandrov, T., Litaudon, M., Wolfender, J.-
 1890 L., Kyle, J.E., Metz, T.O., Peryea, T., Nguyen, D.-T., VanLeer, D., Shinn, P., Jadhav,
 1891 A., Müller, R., Waters, K.M., Shi, W., Liu, X., Zhang, L., Knight, R., Jensen, P.R.,
 1892 Palsson, B.O., Poglian, K., Linington, R.G., Gutiérrez, M., Lopes, N.P., Gerwick,
 1893 W.H., Moore, B.S., Dorrestein, P.C., Bandeira, N., 2016. Sharing and community
 1894 curation of mass spectrometry data with Global Natural Products Social Molecular
 1895 Networking. *Nature Biotechnology* 34, 828–837. doi:10.1038/nbt.3597

1896 Wang, M., Firman, J., Liu, L., Yam, K., 2019. Review Article A Review on Flavonoid
 1897 Apigenin: Dietary Intake, ADME, Antimicrobial Effects, and Interactions with Human
 1898 Gut Microbiota. *BioMed Research International* 2019, 1–18.
 1899 doi:10.1155/2019/7010467
 1900 Wang, X., Xia, K., Yang, X., Tang, C., 2019. Growth strategy of microbes on mixed carbon
 1901 sources. *Nature Communications* 1–7. doi:10.1038/s41467-019-09261-3
 1902 Westreich, S.T., Treiber, M.L., Mills, D.A., Korf, I., Lemay, D.G., 2018. SAMSA2: a
 1903 standalone metatranscriptome analysis pipeline. *BMC Bioinformatics* 19, 1–11.
 1904 doi:10.1186/s12859-018-2189-z
 1905 Winter, S.E., Thiennimitr, P., Winter, M.G., Butler, B.P., Huseby, D.L., Crawford, R.W.,
 1906 Russell, J.M., Bevins, C.L., Adams, L.G., Tsolis, R.M., Roth, J.R., Bäumler, A.J.,
 1907 2010. Gut inflammation provides a respiratory electron acceptor for *Salmonella*.
 1908 *Nature* 467, 426–429. doi:10.1038/nature09415
 1909 Witten, I.H., Bell, T.C., 1991. The Zero-Frequency Problem: Estimating the Probabilities
 1910 of Novel Events in Adaptive Text Compression. *IEEE Transactions of Information*
 1911 *Theory* 137, 1–10.
 1912 Wohlgemuth, S., Keller, S., Kertscher, R., Stadion, M., Haller, D., Kisling, S., Jahreis, G.,
 1913 Blaut, M., Loh, G., 2014. Intestinal steroid profiles and microbiota composition in
 1914 colitic mice. *Gut Microbes* 2, 159–166. doi:10.4161/gmic.2.3.16104
 1915 Wood, D.E., Lu, J., Ben Langmead, 2019. Improved metagenomic analysis with Kraken
 1916 2. *Genome Biol.* 20, 1–13. doi:10.1186/s13059-019-1891-0
 1917 Xiao, L., Sonne, S.B., Feng, Q., Chen, N., Xia, Z., Li, X., Fang, Z., Zhang, D., Fjære, E.,
 1918 Midtbø, L.K., Derrien, M., Hugenholtz, F., Tang, L., Li, J., Zhang, J., Liu, C., Hao, Q.,
 1919 Vogel, U.B., Mortensen, A., Kleerebezem, M., Licht, T.R., Yang, H., Wang, J., Li, Y.,
 1920 Arumugam, M., Wang, J., Madsen, L., Kristiansen, K., 2017. High-fat feeding rather
 1921 than obesity drives taxonomical and functional changes in the gut microbiota in mice.
 1922 *Microbiome* 5, 1–12. doi:10.1186/s40168-017-0258-6
 1923 Yan, H., Yu, B., Degroote, J., Sprangers, T., Noten, N., Majdeddin, M., Poucke, M.,
 1924 Peelman, L., Vrieze, J., Boon, N., Gielen, I., De Smet, S., Chen, D., Michiels, J., 2020.
 1925 Antibiotic affects the gut microbiota composition and expression of genes related to
 1926 lipid metabolism and myofiber types in skeletal muscle of piglets 1–12.
 1927 doi:10.1186/s12917-020-02592-0
 1928 Yang, M., Liu, Y., Xie, H., Wen, Z., Zhang, Y., Wu, C., Huang, L., Wu, J., Xie, C., Wang,
 1929 T., Peng, W., Liu, S., Chen, L., Liu, X., 2019. Gut Microbiota Composition and
 1930 Structure of the Ob/Ob and Db/Db Mice. *International Journal of Endocrinology* 2019,
 1931 1–9. doi:10.1155/2019/1394097
 1932 Yin, R., Xue, Y., Hu, J., Hu, X., Shen, Q., 2020. The effects of diet and streptozotocin on
 1933 metabolism and gut microbiota in a type 2 diabetes mellitus mouse model. *Food and*
 1934 *Agricultural Immunology* 31, 723–739. doi:10.1080/09540105.2020.1761302
 1935 Yoon, M.Y., Yoon, S.S., 2018. Disruption of the Gut Ecosystem by Antibiotics. *Yonsei*
 1936 *Med J* 59, 4–12. doi:10.3349/ymj.2018.59.1.4
 1937 Yoshii, K., Hosomi, K., Sawane, K., Kunisawa, J., 2019. Metabolism of Dietary and
 1938 Microbial Vitamin B Family in the Regulation of Host Immunity. *Front. Nutr.* 6, 562–
 1939 12. doi:10.3389/fnut.2019.00048
 1940 Zeng, M.Y., Inohara, N., (null), G.N., 2017. Mechanisms of inflammation-driven bacterial
 1941 dysbiosis in the gut. *Mucosal Immunology* 10, 18–26. doi:10.1038/mi.2016.75

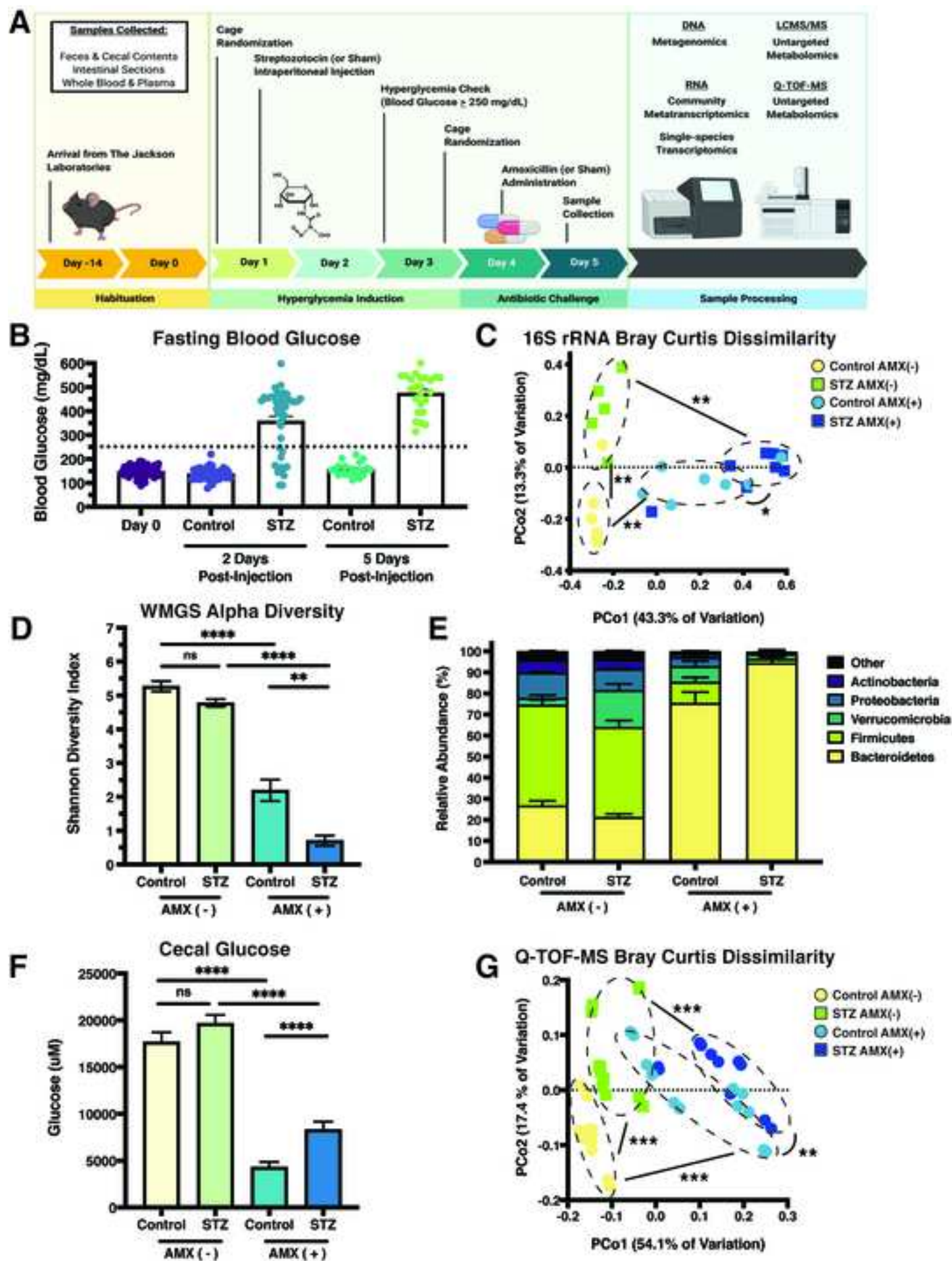
1942 Zhang, H., Li, Y., Wang, C., Wang, X., 2018. Understanding the high l-valine production
 1943 in *Corynebacterium glutamicum* VWB-1 using transcriptomics and proteomics. *Sci*
 1944 *Rep* 1–18. doi:10.1038/s41598-018-21926-5

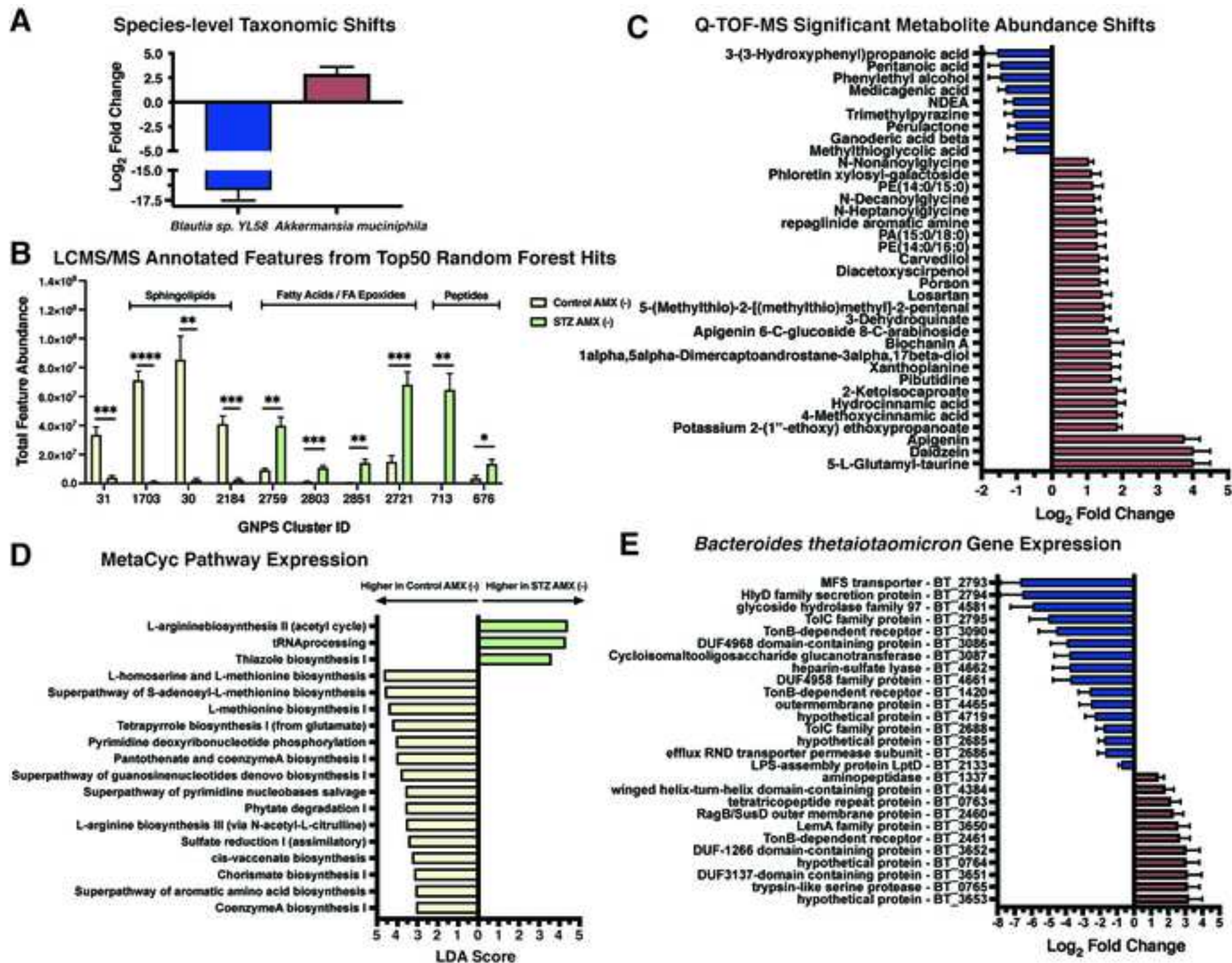
1945 Zhang, J., Kobert, K., Flouri, T., Stamatakis, A., 2014. PEAR: a fast and accurate Illumina
 1946 Paired-End reAd mergeR. *Bioinformatics* 30, 614–620.
 1947 doi:10.1093/bioinformatics/btt593

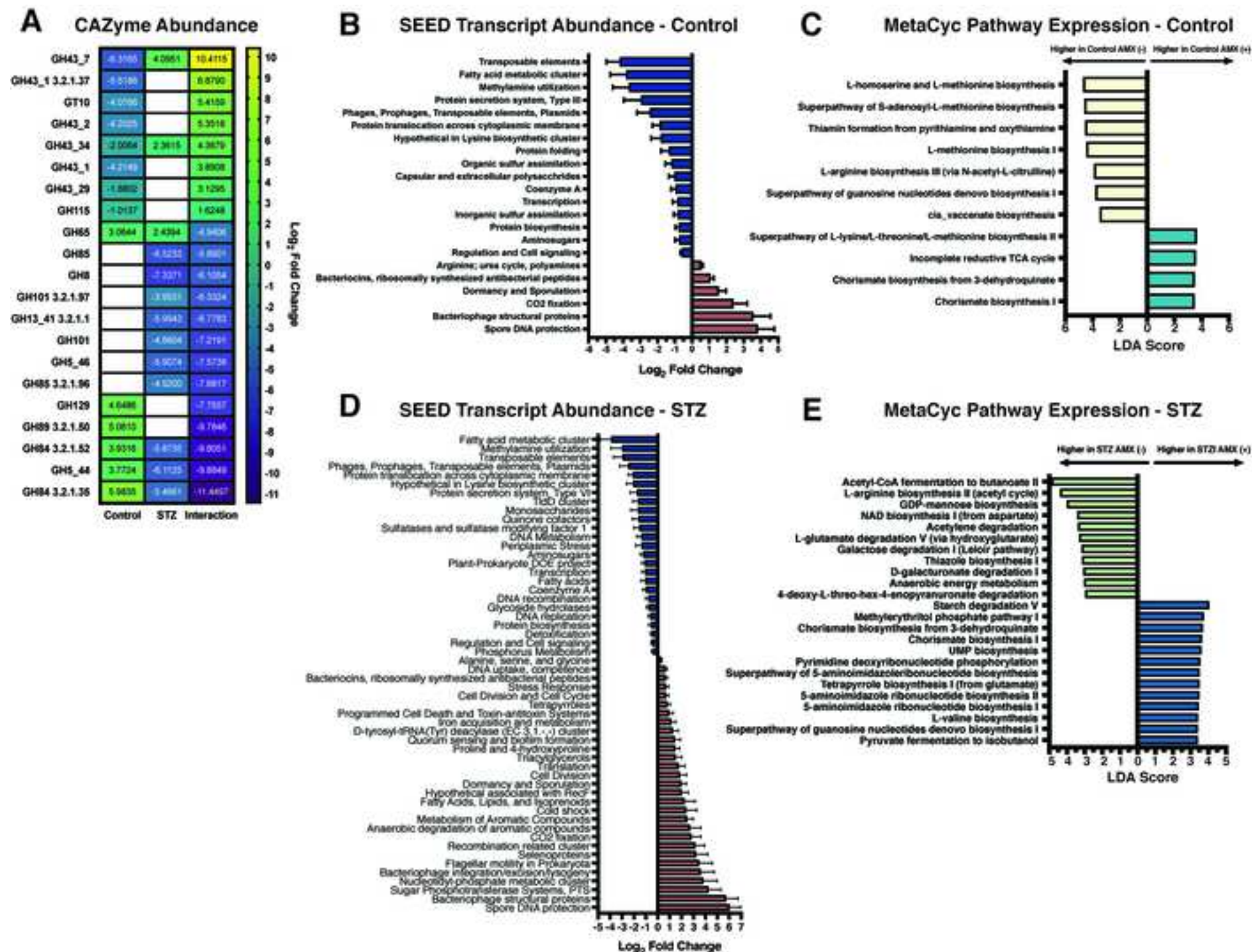
1948 Zhang, M., Lv, X.-Y., Xu, Z.-G., Chen, L., 2008. The Characterization of High-Fat Diet
 1949 and Multiple Low-Dose Streptozotocin Induced Type 2 Diabetes Rat Model.
 1950 *Experimental Diabetes Reserach* 2008, 1–9. doi:10.1155/2008/704045

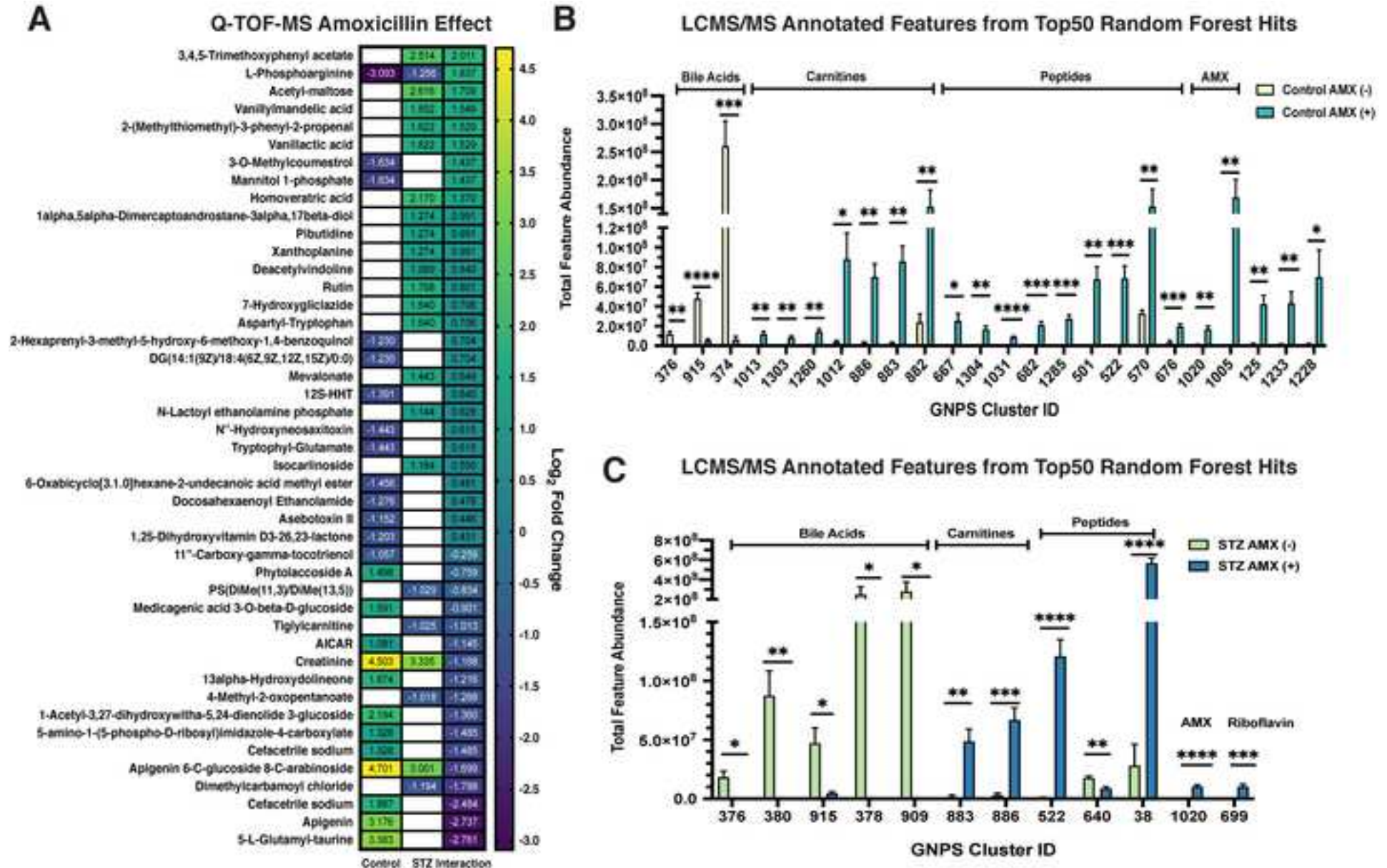
1951 Zhang, T., Li, Q., Cheng, L., Buch, H., Zhang, F., 2019. *Akkermansia muciniphila* is a
 1952 promising probiotic. *Microbial Biotechnology* 12, 1109–1125. doi:10.1111/1751-
 1953 7915.13410

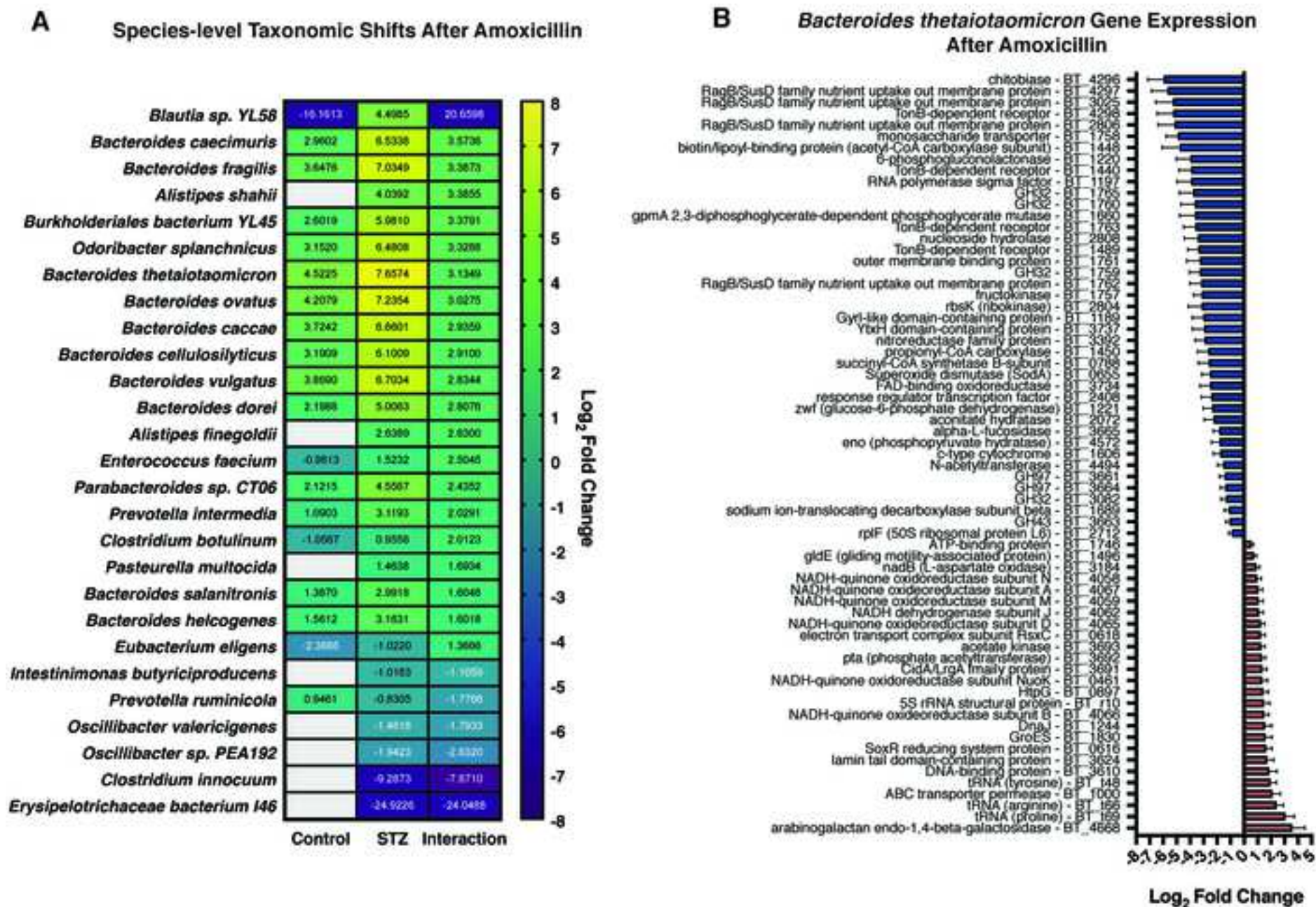
1954 Zheng, X., Huang, F., Zhao, A., Lei, S., Zhang, Y., Xie, G., Chen, T., Qu, C., Rajani, C.,
 1955 Dong, B., Li, D., Jia, W., 2017. Bile acid is a significant host factor shaping the gut
 1956 microbiome of diet-induced obese mice. *BMC Biology* 15, 1–15. doi:10.1186/s12915-
 1957 017-0462-7

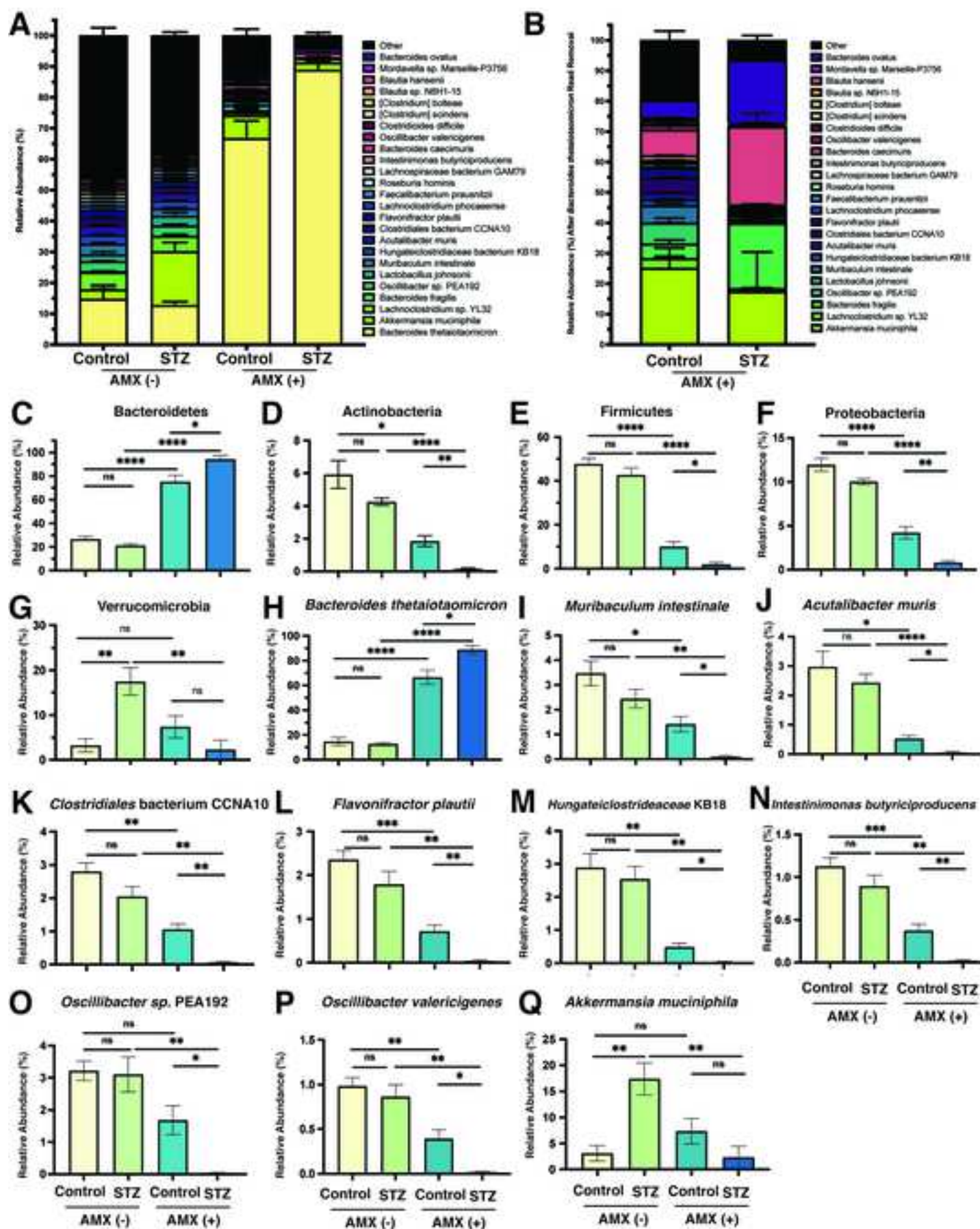


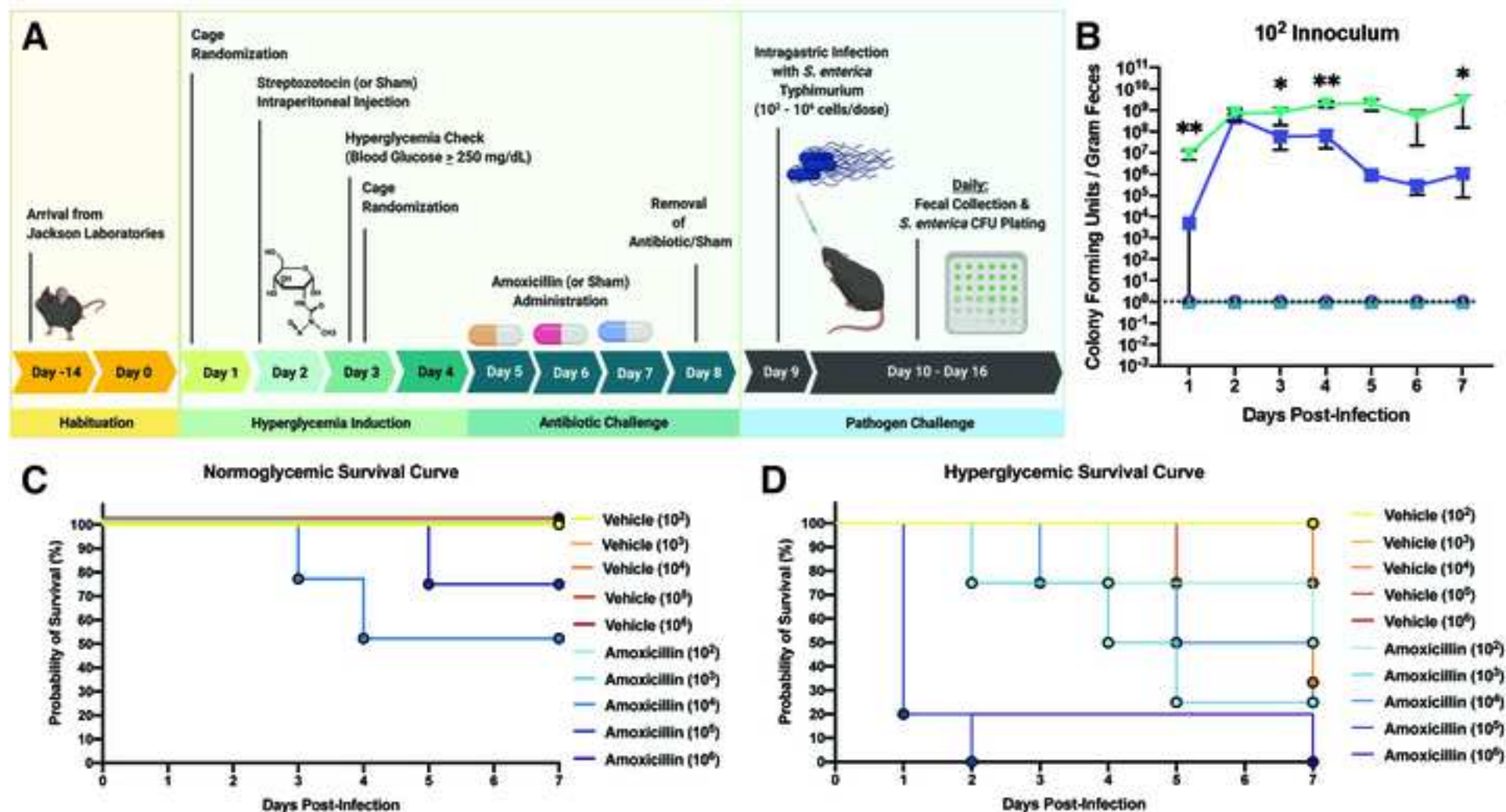












Supplemental Data/Video/Table Title and Legends

Figure S1. STZ-induced hyperglycemia modifies both the cecal metabolome and metatranscriptome. Related to Figure 2.

- A. Differentially-abundant (Benjamini-Hochberg adjusted p value < 0.05) level 2 SEED Subsystem transcripts in STZ-induced hyperglycemic mice. Data represent log₂ fold change relative to normoglycemic controls \pm standard error. See Table S7 for full results (N = 4 per group).
- B. Differentially-abundant (Benjamini-Hochberg adjusted p value < 0.05) CAZyme transcripts in STZ-induced hyperglycemic mice. Data represent log₂ fold change relative to normoglycemic controls \pm standard error. See Table S4 for full results (N = 4 per group).
- C. Volcano plot of the cecal metatranscriptome following streptozotocin treatment. Purple points represent differentially-abundant (Benjamini-Hochberg adjusted p value < 0.05) transcripts. Transcripts of features are labeled. See Table S8 for full results. (N = 4 per group).
- D. Volcano plot of the cecal metabolome in STZ-induced hyperglycemic mice relative to normoglycemic controls. Purple points represent differentially-abundant (Benjamini-Hochberg adjusted p value < 0.05) metabolite features. Metabolites of interest are labeled. See Table S1 for full results (N = 6 per group, 2 technical replicates per mouse)
- A. KEGG Pathway Assignments for enriched (red) and depleted (blue) metabolites within the cecum following streptozotocin treatment. Significant pathways (unpaired t-test p value < 0.05) were calculated using the Pathway Activity Profiling pipeline (see methods). See Table S3 for full results (N = 6 per group, 2 technical replicates per mouse)

Figure S2. Streptozotocin and amoxicillin treatment differentially impact the cecal metabolome as determined by LC-MS/MS. Related to Figure 2 and Figure 4.

- A. Top-50 most relevant metabolite features detected via Random Forest Classification between normoglycemic and STZ-treated cecal LC-MS/MS metabolomes. Colored diamonds indicate GNPS clusters that contain known/annotated metabolites.
- B. Top-50 most relevant metabolite features detected via Random Forest Classification between vehicle and amoxicillin-treated cecal LC-MS/MS metabolomes from normoglycemic mice. Colored diamonds indicate GNPS clusters that contain known/annotated metabolites.
- C. Top-50 most relevant metabolite features detected via Random Forest Classification between vehicle and amoxicillin-treated cecal LC-MS/MS metabolomes from hyperglycemic mice. Colored diamonds indicate GNPS clusters that contain known/annotated metabolites.

For all panels, N = 6 per group (2 technical replicates per mouse)

Figure S3. The amoxicillin treated metabolome differs between normoglycemic and hyperglycemic mice. Related to Figure 7.

- A. Differentially abundant (Benjamini-Hochberg adjusted p value < 0.05) Q-TOF-MS metabolite features in the murine cecum following amoxicillin treatment between hyperglycemic and normoglycemic mice. Data represented by log₂ fold change \pm standard error of hyperglycemic amoxicillin-treated mice versus normoglycemic amoxicillin-treated mice. See Table S1 for full results
- B. Differentially abundant (unpaired T-test with Welch's correction p value < 0.05) GNPS-annotated clusters that contain known metabolites within the cluster. Clusters were selected from the top-50 most relevant features via Random Forest Testing. Comparison is between hyperglycemic mice receiving amoxicillin versus normoglycemic mice receiving amoxicillin. See Table S2 for full results.
- C. KEGG Pathway Assignments for enriched (red) and depleted (blue) metabolites within the cecum of hyperglycemic amoxicillin-treated mice compared to normoglycemic amoxicillin-treated controls. Significant pathways (unpaired t-test p value < 0.05) were calculated using the Pathway Activity Profiling pipeline (see methods).

For all panels, N = 6 per group with 2 technical replicates per mouse

Table S1: Raw Q-TOF-MS Ion Intensities, annotation guide, and full DESeq2 results of Q-TOF-MS data. Related to Figure 1G, Figure 2C, Figure 4A, Figure S1D, and Figure S3A.

- A. Raw Q-TOF-MS ion intensities generated by General Metabolics Inc. (Boston, MA, USA)
- B. Annotation guide for Q-TOF-MS ion intensities generated by General Metabolics Inc. (Boston, MA, USA)
- C. Differential abundance testing of the impact of streptozotocin treatment on the abundance of Q-TOF-MS metabolites in the murine cecal microbiome prior to antibiotic administration. Log₂ fold change values were calculated relative to normoglycemic controls samples (STZ AMX - vs Control AMX -)
- D. Differential abundance testing of the impact of amoxicillin treatment on the abundance of Q-TOF-MS metabolites in the normoglycemic murine cecal microbiome. Log₂ fold change values were calculated relative to normoglycemic vehicle-treated controls samples (Control AMX - vs Control AMX +)
- E. Differential abundance testing of the impact of amoxicillin treatment on the abundance of Q-TOF-MS metabolites in the hyperglycemic murine cecal microbiome. Log₂ fold change values were calculated relative to hyperglycemic vehicle-treated controls samples (STZ AMX - vs STZ AMX +)
- F. Differential abundance testing of the impact of streptozotocin treatment on the abundance of Q-TOF-MS metabolites in the murine cecal microbiome after amoxicillin treatment. Log₂ fold change values were calculated relative to normoglycemic amoxicillin-treated controls samples (Control AMX + vs STZ AMX +)
- G. Interaction term analysis generated by DESeq2 for the impact of host glycemia on changes in metabolite abundance following amoxicillin therapy. Log₂ fold change values were calculated relative to normoglycemic vehicle-treated samples (Control AMX -)

Table S2: Random Forest Classification of GNPS-annotated LC-MS/MS Clusters. Related to Figure 2B, Figure 4B, Figure 4C, Figure S2, and Figure S3B.

- A. Full Random Forest results of feature importance distinguishing normoglycemic and hyperglycemic cecal metabolomes before antibiotic treatment (i.e. STZ AMX - vs. Control AMX -)
- B. Full Random Forest results of feature importance distinguishing vehicle-treated and amoxicillin-treated cecal metabolomes in normoglycemic mice (i.e. Control AMX - vs. Control AMX +)
- C. Full Random Forest results of feature importance distinguishing vehicle-treated and amoxicillin-treated cecal metabolomes in hyperglycemic mice (i.e. STZ AMX - vs. STZ AMX +)
- D. Full Random Forest results of feature importance distinguishing normoglycemic and hyperglycemic cecal metabolomes after antibiotic treatment (i.e. STZ AMX + vs. Control AMX +)

Table S3: Full KEGG-based Pathway Activity Profiling of enriched and depleted cecal Q-TOF-MS metabolites. Related to Figure S1E and Figure S3C.

- A. Combined results from Pathway Activity Profiling of metabolites that are differentially abundant during streptozotocin treatment (Table S1C).
- B. Combined results from Pathway Activity Profiling of metabolites that are differentially abundant during amoxicillin treatment in normoglycemic mice (Table S1D).
- C. Combined results from Pathway Activity Profiling of metabolites that are differentially abundant during amoxicillin treatment in hyperglycemic mice (Table S1E).
- D. Combined results from Pathway Activity Profiling of metabolites that are differentially abundant after amoxicillin treatment between normo- and hyperglycemic mice (Table S1F).

Table S4: Full DESeq2 results of CAZyme transcript abundance generated by SAMSA2. Related to Figure 3A and Figure S1B.

- A. Differential abundance testing of the impact of streptozotocin treatment on the abundance of CAZyme transcripts in the murine cecal metatranscriptome. Log₂ fold change values were calculated relative to normoglycemic controls (STZ AMX - vs Control AMX -)
- B. Differential abundance testing of the impact of amoxicillin treatment on the abundance of CAZyme transcripts in the murine cecal metatranscriptome in normoglycemic animals. Log₂ fold change values were calculated relative to normoglycemic vehicle-treated samples (Control AMX - vs Control AMX +)
- C. Differential abundance testing of the impact of amoxicillin treatment on the abundance of CAZyme transcripts in the murine cecal metatranscriptome in hyperglycemic animals. Log₂ fold change values were calculated relative to hyperglycemic vehicle-treated samples (STZ AMX - vs STZ AMX +)
- D. Interaction term analysis generated by DESeq2 for the impact of host glycemia on changes in CAZyme transcripts abundance after amoxicillin treatment. Log₂ fold change values were calculated relative to normoglycemic vehicle-treated samples (Control AMX-).

Table S5: Full DESeq2 results of transcript abundance analysis of *A. muciniphila* and *B. thetaiotaomicron* during dietary intervention and ciprofloxacin treatment and dietary formulation. Related to Figure 2E and Figure 5B.

- A. Total and average counts for Kraken2-generated metatranscriptomic read assignments.
- B. Differential abundance testing of the impact of hyperglycemia on the abundance of *B. thetaiotaomicron* transcripts within the murine cecal metatranscriptome. Log₂ fold change values were calculated relative to normoglycemic controls (STZ AMX - vs Control AMX -)
- C. Differential abundance testing of the impact of amoxicillin treatment on the abundance of *B. thetaiotaomicron* transcripts within the normoglycemic murine cecal metatranscriptome. Log₂ fold change values were calculated relative to normoglycemic vehicle-treated controls (Control AMX - vs Control AMX +)
- D. Differential abundance testing of the impact of amoxicillin treatment on the abundance of *B. thetaiotaomicron* transcripts within the hyperglycemic murine

- cecal metatranscriptome. Log₂ fold change values were calculated relative to hyperglycemic vehicle-treated controls (STZ AMX - vs STZ AMX +)
- E. Interaction term analysis generated by DESeq2 for the impact of host glycemia on changes in *B. thetaiotaomicron* transcripts abundance after amoxicillin treatment. Log₂ fold change values were calculated relative to normoglycemic vehicle-treated samples (Control AMX-).
 - F. Differential abundance testing of the impact of hyperglycemia on the abundance of *O. valericigenes* transcripts within the murine cecal metatranscriptome. Log₂ fold change values were calculated relative to normoglycemic controls (STZ AMX - vs Control AMX -)
 - G. Differential abundance testing of the impact of amoxicillin treatment on the abundance of *O. valericigenes* transcripts within the normoglycemic murine cecal metatranscriptome. Log₂ fold change values were calculated relative to normoglycemic vehicle-treated controls (Control AMX - vs Control AMX +)
 - H. Differential abundance testing of the impact of amoxicillin treatment on the abundance of *O. valericigenes* transcripts within the hyperglycemic murine cecal metatranscriptome. Log₂ fold change values were calculated relative to hyperglycemic vehicle-treated controls (STZ AMX - vs STZ AMX +)
 - I. Interaction term analysis generated by DESeq2 for the impact of host glycemia on changes in *O. valericigenes* transcripts abundance after amoxicillin treatment. Log₂ fold change values were calculated relative to normoglycemic vehicle-treated samples (Control AMX-).
 - J. Differential abundance testing of the impact of hyperglycemia on the abundance of *O. sp. PEA192* transcripts within the murine cecal metatranscriptome. Log₂ fold change values were calculated relative to normoglycemic controls (STZ AMX - vs Control AMX -)
 - K. Differential abundance testing of the impact of amoxicillin treatment on the abundance of *O. sp. PEA192* transcripts within the normoglycemic murine cecal metatranscriptome. Log₂ fold change values were calculated relative to normoglycemic vehicle-treated controls (Control AMX - vs Control AMX +)
 - L. Differential abundance testing of the impact of amoxicillin treatment on the abundance of *O. sp. PEA192* transcripts within the hyperglycemic murine cecal metatranscriptome. Log₂ fold change values were calculated relative to hyperglycemic vehicle-treated controls (STZ AMX - vs STZ AMX +)
 - M. Interaction term analysis generated by DESeq2 for the impact of host glycemia on changes in *O. sp. PEA192* transcripts abundance after amoxicillin treatment. Log₂ fold change values were calculated relative to normoglycemic vehicle-treated samples (Control AMX-).

Table S6: Full LEfSe results from the analysis of MetaCyc pathway abundance generated by HUMAnN2. “Class” denotes the experimental group a particular pathway was associated with. Related to Figure 2D, Figure 3C, and Figure 3E.

- A. Pairwise LEfSe analysis of normoglycemic and hyperglycemic samples prior to antibiotic treatment (STZ AMX - vs Control AMX -)
- B. Pairwise LEfSe analysis of amoxicillin- and vehicle-treated samples from normoglycemic mice (Control AMX - vs Control AMX +)

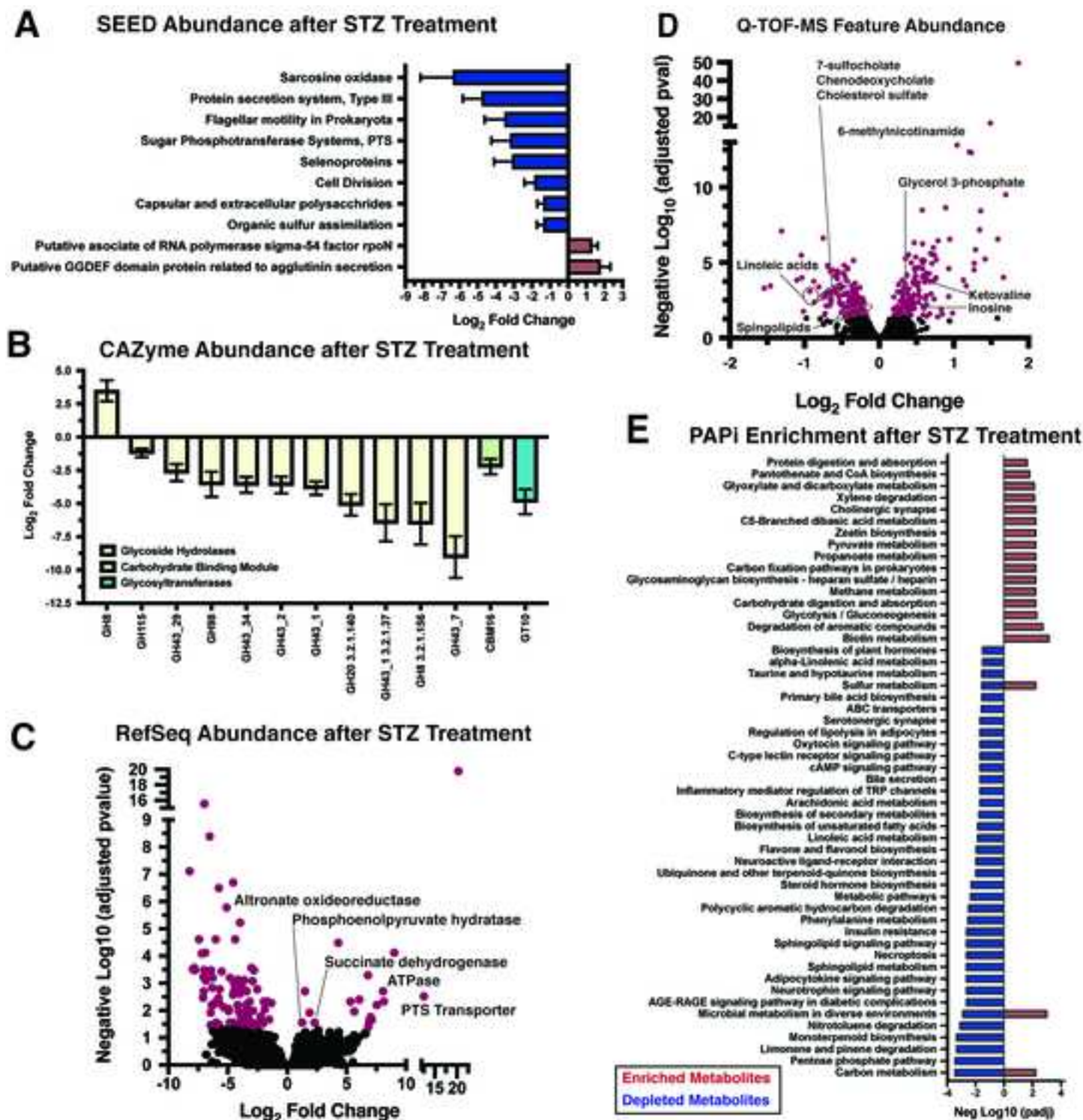
- C. Pairwise LEfSe analysis of amoxicillin- and vehicle-treated samples from hyperglycemic mice (STZ AMX - vs STZ AMX +)

Table S7: Full DESeq2 results of SEED subsystem abundance generated by SAMSA2. Related to Figure 3B, Figure 3D, and Figure S1A.

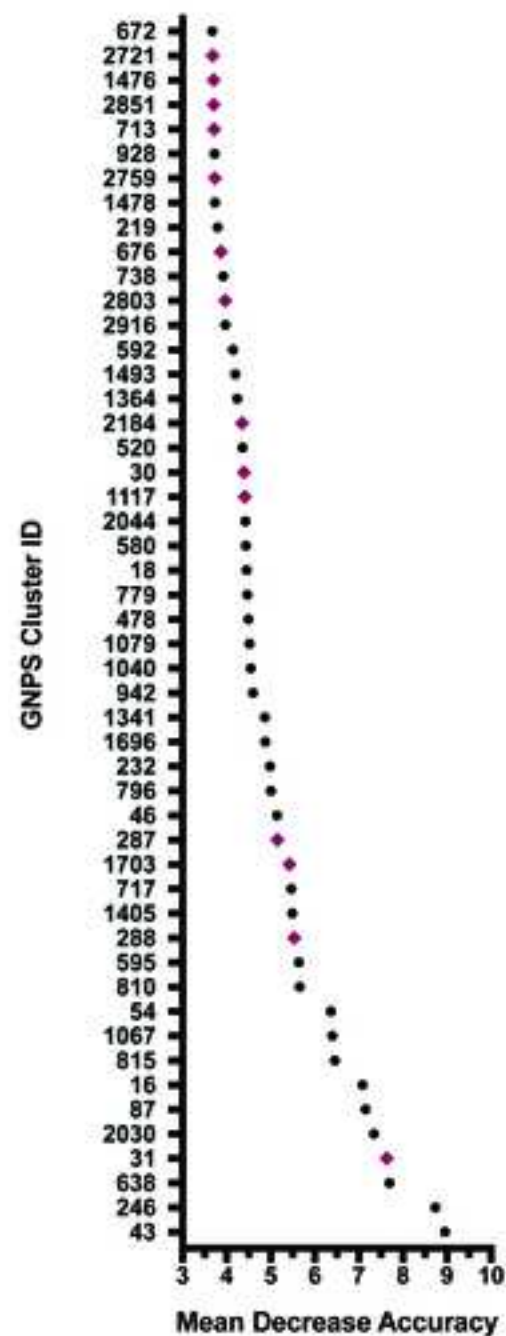
- A. Differential abundance testing of the impact of streptozotocin treatment on the abundance of SEED subsystem transcripts in the murine cecal metatranscriptome. Log₂ fold change values were calculated relative to normoglycemic controls (STZ AMX- vs Control AMX-)
- B. Differential abundance testing of the impact of amoxicillin treatment on the abundance of SEED subsystem transcripts in the murine cecal metatranscriptome in normoglycemic animals. Log₂ fold change values were calculated relative to normoglycemic vehicle-treated samples (Control AMX - vs Control AMX +)
- C. Differential abundance testing of the impact of amoxicillin treatment on the abundance of SEED subsystem transcripts in the murine cecal metatranscriptome in hyperglycemic animals. Log₂ fold change values were calculated relative to hyperglycemic vehicle-treated samples (STZ AMX - vs STZ AMX +)
- D. Interaction term analysis generated by DESeq2 for the impact of host glycemia on changes in SEED subsystem transcript abundance after amoxicillin treatment. Log₂ fold change values were calculated relative to normoglycemic vehicle-treated samples on the (Control AMX-).

Table S8: Full DESeq2 results of RefSeq transcript abundance generated by SAMSA2. Related to Figure S1C.

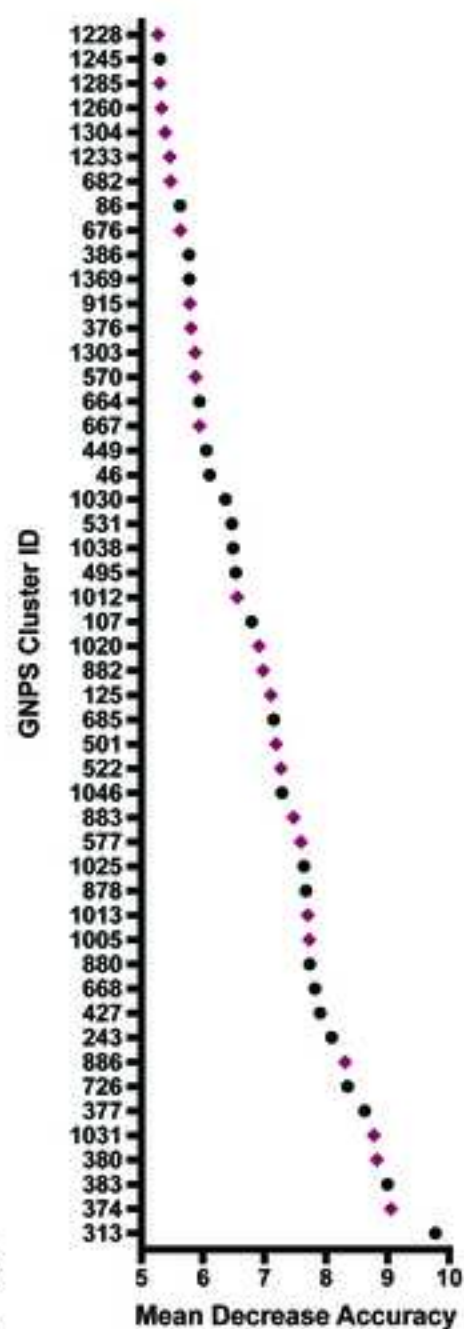
- A. Differential abundance testing of the impact of streptozotocin treatment on the abundance of RefSeq transcripts in the murine cecal metatranscriptome. Log₂ fold change values were calculated relative to normoglycemic controls (STZ AMX- vs Control AMX-)
- B. Differential abundance testing of the impact of amoxicillin treatment on the abundance of RefSeq transcripts in the murine cecal metatranscriptome in normoglycemic animals. Log₂ fold change values were calculated relative to normoglycemic vehicle-treated samples (Control AMX - vs Control AMX +)
- C. Differential abundance testing of the impact of amoxicillin treatment on the abundance of RefSeq transcripts in the murine cecal metatranscriptome in hyperglycemic animals. Log₂ fold change values were calculated relative to hyperglycemic vehicle-treated samples (STZ AMX - vs STZ AMX +)
- D. Interaction term analysis generated by DESeq2 for the impact of host glycemia on changes in RefSeq transcript abundance after amoxicillin treatment. Log₂ fold change values were calculated relative to normoglycemic vehicle-treated samples on the (Control AMX-).



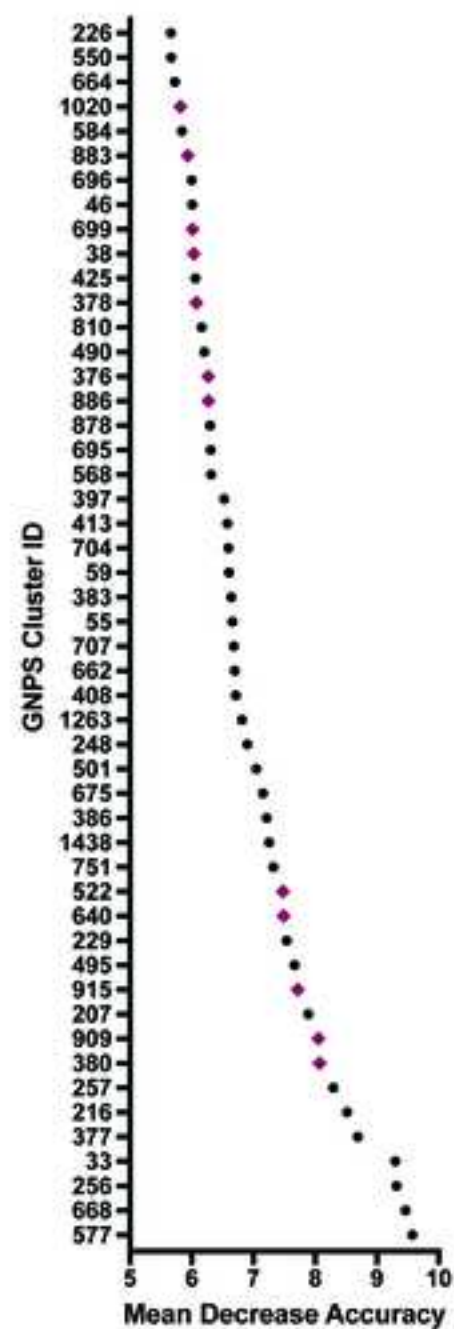
A LCMS/MS Top-50 Features
after STZ Treatment

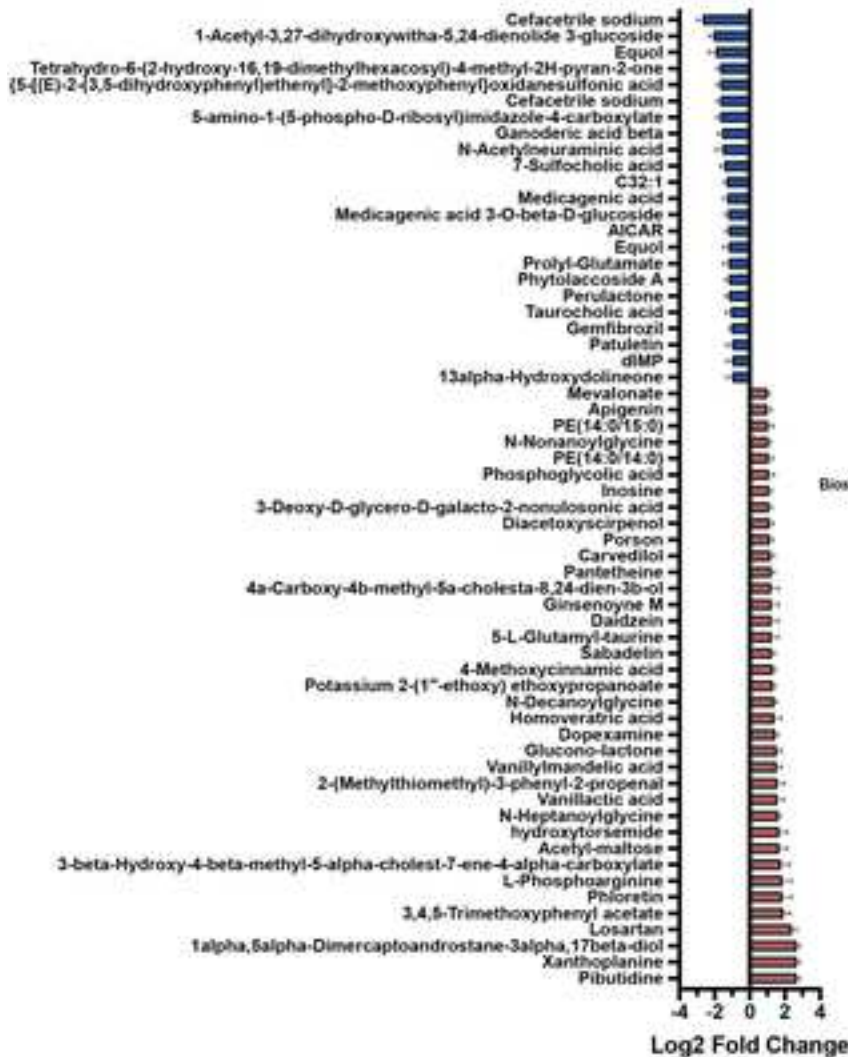


B LCMS/MS Top-50 Features
after AMX (Control)

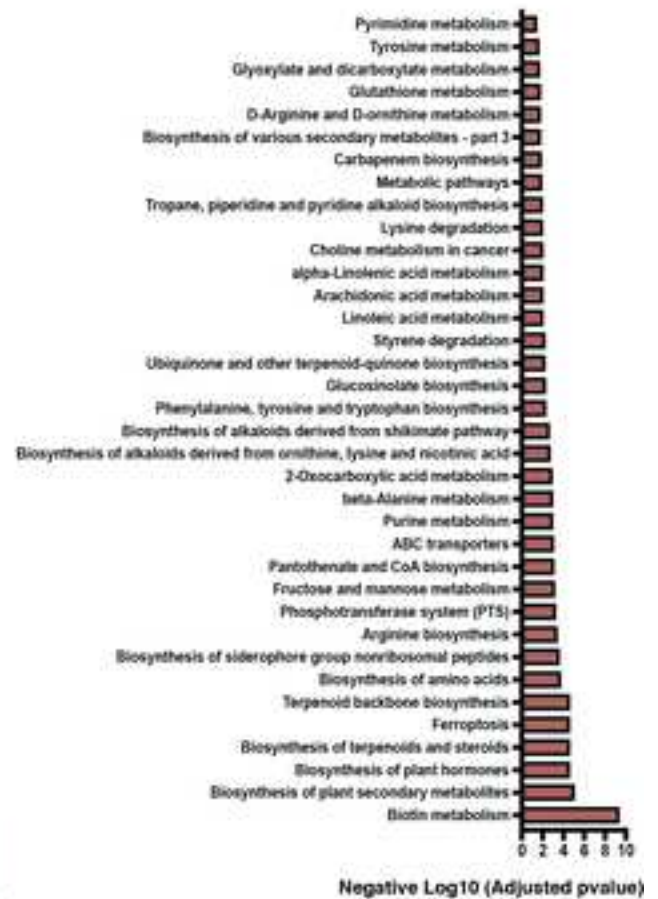
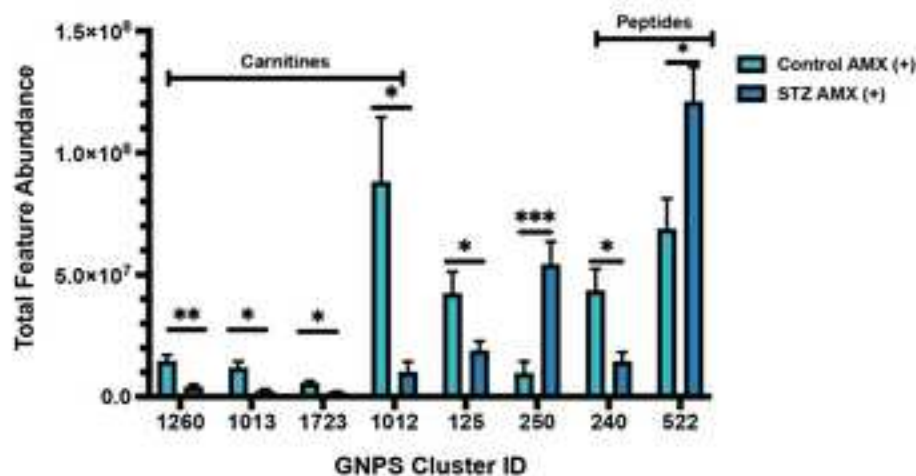


C LCMS/MS Top-50 Features
after AMX (STZ)



A Q-TOF-MS Significant Feature Abundance Shifts**C**

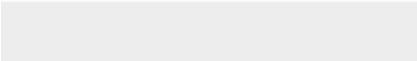
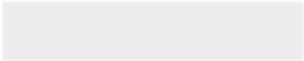
Metabolomic Pathway Enrichment

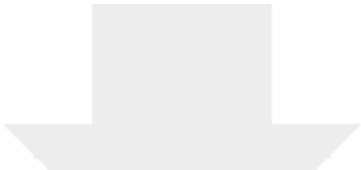
**B** LCMS/MS Annotated Features from Top50 Random Forest Hits



[Click here to access/download](#)

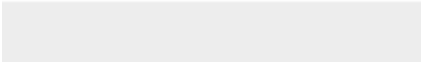
Supplemental Videos and Spreadsheets
TableS1.xlsx

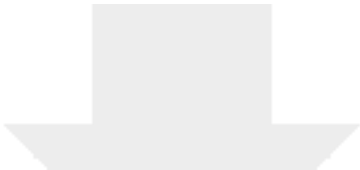




[Click here to access/download](#)

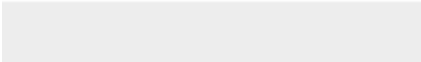
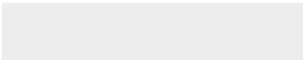
Supplemental Videos and Spreadsheets
TableS2.xlsx

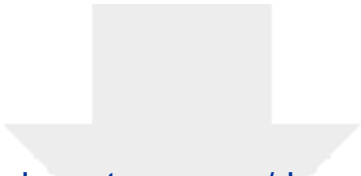




[Click here to access/download](#)

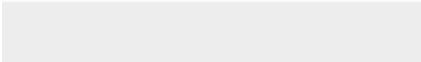
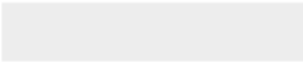
Supplemental Videos and Spreadsheets
TableS3.xlsx

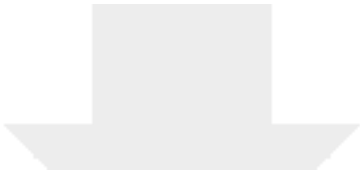




[Click here to access/download](#)

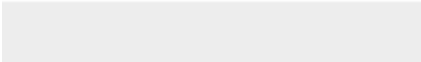
Supplemental Videos and Spreadsheets
TableS4.xlsx

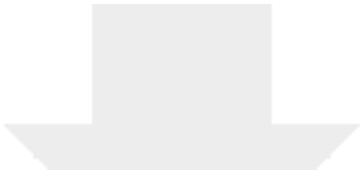




[Click here to access/download](#)

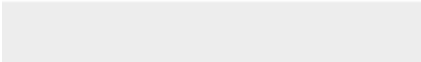
Supplemental Videos and Spreadsheets
TableS5.xlsx

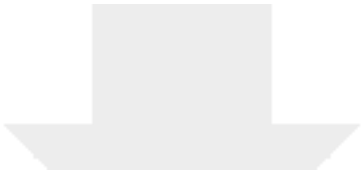




[Click here to access/download](#)

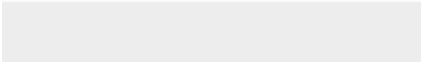
Supplemental Videos and Spreadsheets
TableS6.xlsx

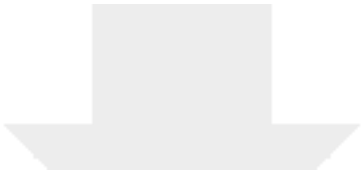




[Click here to access/download](#)

Supplemental Videos and Spreadsheets
TableS7.xlsx





[Click here to access/download](#)

Supplemental Videos and Spreadsheets
TableS8.xlsx

